Numerical Modelling of Mesoscale Eddies in the Tasman Sea

Author:
Macdonald, Helen

Publication Date:
2013

DOI:
https://doi.org/10.26190/unsworks/16063

Numerical Modelling of Mesoscale Eddies in the Tasman Sea

by

Helen Macdonald

A thesis submitted for the degree of Doctor of Philosophy
at
The University of New South Wales
Australia

April, 2013

PLEASE TYPE

THE UNIVERSITY OF NEW SOUTH WALES
Thesis/Dissertation Sheet

Surname or Family name: **Macdonald**

First name: **Helen** Other name/s: **Skye**

Abbreviation for degree as given in the University calendar: **PhD**

School: **Mathematics and Statistics** Faculty: **Science**

Title:**Numerical modelling of mesoscale eddies in the Tasman Sea**

Abstract 350 words maximum: (PLEASE TYPE)

Western boundary currents (WBC), such as the East Australian Current (EAC), are some of the world's strongest currents. Mesoscale eddies are a common feature in WBCs and can be important for the transport of heat, vertical mixing and retention of larval species. To better understand the physical processes which create differences between eddies the Regional Ocean Modeling System is used to investigate the ocean state during the formation of a warm-core eddy (WCE) in the EAC during October of 2008 and a cold-core eddy (CCE) during October of 2009.

The WCE formed from a retroflexion of the EAC. Lagrangian particle tracks are used and some passive tracers are introduced into the model to investigate this eddy. There are two distinct stages in the eddy's development. The first where the EAC encircles the eddy; the second where the EAC overwashes the eddy. The water entrained into the WCE comes from the EAC during overwashing. Overwashing submerges the original eddy, creating a two-layered system with interesting dynamical consequences.

Potential drivers of the formation of the CCE, such as gradients in temperature and velocity, along with the impact of 3 wind forcing scenarios (upwelling, downwelling and realistic winds) are investigated. In all three cases a CCE formed, although the location, size and isotherm uplift varies. Counter-intuitively, the strongest upwelling eddy forms with downwelling winds. Analysis of energy transformation shows the prevailing source of eddy kinetic energy to the CCE was the EAC.

Particle release experiments are used to investigate the eddy's source waters. Nearly all of the surface waters within the eddy originate from the continental shelf. Water entrained into the eddy came from both north, due to the southward flowing EAC, and, unexpectedly, from south of the eddy. Particles that come from south of the eddy do so due to a northward flow on the continental shelf just prior to the eddy's formation.

The results show that mesoscale eddies within the western Tasman Sea, while generally following simple models for eddies, also display more complex physical interactions. This has implications in understanding how eddies can influence distribution of heat, energy and biological production in WBC regions.

FOR OFFICE USE ONLY Date of completion of requirements for Award:

THIS SHEET IS TO BE GLUED TO THE INSIDE FRONT COVER OF THE THESIS

ORIGINALITY STATEMENT 'I hereby declare that this submission is my own work and to the best of my knowledge it contains no materials previously published or written by another person, or substantial proportions of material which have been accepted for the award of any other degree or diploma at UNSW or any other educational institution, except where due acknowledgement is made in the thesis. Any contribution made to the research by others, with whom I have worked at UNSW or elsewhere, is explicitly acknowledged in the thesis. I also declare that the intellectual content of this thesis is the product of my own work, except to the extent that assistance from others in the project's design and conception or in style, presentation and linguistic expression is acknowledged.'

Signed .....

Date .....

Abstract

Western boundary currents (WBC), such as the East Australian Current (EAC), are some of the world's strongest currents. Mesoscale eddies are a common feature in WBCs and can be important for the transport of heat, vertical mixing and the retention of larval species. To better understand the physical processes that drive eddy formation in the Tasman Sea, The Regional Ocean Modelling System is used to investigate the ocean state during the formation of a warm-core eddy (WCE) in the EAC during October of 2008 and a cold-core eddy (CCE) during October of 2009.

The WCE formed from a retroflexion of the EAC. Lagrangian particle tracks are used and some passive tracers are introduced into the model to investigate this eddy. There are two distinct stages in the eddy's development. The first where the EAC encircles the eddy; the second where the EAC overwashes the eddy. The water entrained into the WCE comes from the EAC during overwashing. Overwashing submerges the original eddy, creating a two-layered system with interesting dynamical consequences.

Potential drivers of the formation of the CCE, such as gradients in temperature and velocity, along with the impact of 3 wind forcing scenarios (upwelling, downwelling and realistic winds) are investigated. In all three cases a CCE formed, although the location, size and isotherm uplift varies. Counter-intuitively, the strongest upwelling eddy forms with downwelling winds. Analysis of energy transformation shows the prevailing source of eddy kinetic energy to the CCE was the EAC.

Particle release experiments are used to investigate the cold-core eddy's source

waters. Nearly all of the surface waters within the eddy originate from the continental shelf. Water entrained into the eddy came from both north, due to the southward flowing EAC, and, unexpectedly, from south of the eddy. Particles that come from south of the eddy do so due to a northward flow on the continental shelf just prior to the eddy's formation.

The results show that mesoscale eddies within the western Tasman Sea, while generally following simple models for eddies, also display more complex physical interactions. This has implications in understanding how eddies can influence distribution of heat, energy and biological production in WBC regions.

Acknowledgements

A thesis is not an endeavour to be completed on one's own and, as such, there are many people that I would like to acknowledge for their support. First and foremost, I would like to thank my supervisors, Moninya Roughan, Mark Baird and John Wilkin for their guidance, insight and encouragement during my candidature. I am deeply appreciative of the time and effort that they have put into advising me.

I am also grateful to my flatmate, David Hay; my parents, Jane and Ewen Macdonald; and my brother in law, James Shadlow, for the time and effort that they have invested into proof reading this thesis. I would also like to thank my sister, Catherine Shadlow, for her amazing baked goods and meals that sustained me through the end of this thesis.

I would also like to thank the scientists and crew aboard the research cruises SS2008/10, SS2009/5 and SS2009/6. In particular, I would like to thank Iain Suthers and Jason Everett who were always happy to discuss research and data sets arising from these cruises.

I will always be grateful for the support, encouragement and friendship that I have gained from my fellow PhD students and the oceanography staff, Julie Wood, Amirah Rahman, Josh Capel, Michelle Dunbar, Natasha Henschke, Amandine Schaeffer, Vincent Rossi, Brad Morris, Tim Austin, Stuart Mills and Gordon MacDonald.

I would like to thank the ROMS developers for the free use of their code. I am also indebted to the computing staff here at UNSW, particularly Martin Thompson, for setting up and maintaining the High Performance Computing

Facilities that were greatly utilised during the making of this thesis.

Supporting Publications

Journal Articles

Macdonald HS, Roughan M, Baird ME and Wilkin J (2013). A numerical modelling study of the East Australian Current encircling and overwashing a warm-core eddy. *J. Geophys. Res. Vol 118, doi:10.1029/2012JC008386*

Macdonald HS, Roughan M, Baird ME and Wilkin J. The formation of a cold-core eddy in a western boundary current submitted to *Ocean Modelling*

Conference Proceedings

Macdonald HS, Roughan M, Baird ME and Wilkin J (2012). The evolution of a Cold-Core Eddy in a Western Boundary Current. In proceedings, Australian Marine Science Association Annual Conference, Hobart.

Macdonald HS, Roughan M, Baird ME and Wilkin J (2012). Anatomy of a submerging warm-core eddy. In proceedings, Australian Meteorology and Oceanographic Society Annual Conference, Sydney.

Macdonald HS, Roughan M, Baird ME and Wilkin J (2011). Surface flooding of a warm-core eddy. In proceedings, Gordon Research Conference in Ocean Modelling, South Hadley.

Macdonald HS, Roughan M, Baird ME and Wilkin J (2010). Surface flooding of a warm-core eddy. In proceedings, Australian Marine Science Association An-

nual Conference, Wollongong.

Contents

List of Figures

List of Tables

Chapter 1

Introduction

1.1 Motivation

1.1.1 Western Boundary Currents

Western boundary currents (WBCs) such as the Kuroshio Current (Barkley, 1970), the Gulf stream (Fuglister and Worthington, 1951), the East Australian Current (Hamon, 1965) and the Aghulus Current (Pearce, 1977) form on the western side of oceanic basins. WBCs tend to be deep, narrow and are some of the world's strongest currents with the velocity exceeding 1 m s^{-1}. WBCs flow northward in the Northern Hemisphere and southward in the Southern Hemisphere transporting heat and energy from the equator towards the poles. As WBCs flow along the eastern side of land masses, they affect the weather and climate of the adjacent continent, generating a warmer climate than average for a given latitude (Minobe et al., 2008).

Mesoscale eddies are a common feature in WBCs and can be important for

the transport of heat, energy and vertical mixing in the ocean (Parker, 1971; Yang et al., 1999; Hamon, 1965; Rossby, T., 1987; Oort, 1964; Duncan, 1968; Yaochu and Jilan, 1988; Didden and Schott, 1993). Additionally, eddies are important for marine biological processes such as the retention of larval species (Kasai et al., 2002; Henschke et al., 2011; Sponaugle et al., 2005; Kimura et al., 1997). WBC eddies frequently form near the coast and can entrain waters from the coastal zone.

1.1.2 Mesoscale eddies

Simple models of eddies suggest that cold-core eddies (CCEs) upwell water in the centre of the eddy (Bakun, 2006). The upwelled water comes from deeper in the ocean and, hence, is cooler and contains nutrients sourced from falling, decaying biota. In nutrient poor regions, upwelled nutrients can result in algal blooms. Algal blooms form the base of the food chain and, as such, cold-core eddies tend to enhance biomass throughout the food chain, resulting in increased fish stock (Logerwell and Smith, 2001). On the other hand, simple models of warm-core eddies (WCEs) predict that they downwell water in the centre (Bakun, 2006) resulting in warmer temperature anomalies and less surface nutrients. As such, they are thought of as less biologically productive (Bakun, 2006).

WBC eddies are more complex than these simple models and their physical processes vary, yielding different and important responses (Baird et al., 2010; Cresswell, 1982; Bakun, 2006; Nilsson and Cresswell, 1980; Tranter et al., 1982). The simple conceptual models described above only hold true for the eddies while they are in a "spin up" stage. When eddies are decaying the vertical mo-

tion is reversed and CCEs will downwell in the centre while WCEs will upwell (Bakun, 2006). In addition to this, interactions on a smaller scale can create upwelling/downwelling cells at the front between these eddies and the surrounding ocean (frontogenesis) (Capet et al., 2008). These processes become more complicated when eddies start to interact with the current (Baird et al., 2010), other eddies (Cresswell, 1982) or the bathymetry (Oke and Griffin, 2010). Therefore, understanding the physical processes which create differences between eddies becomes important in understanding how WBC eddies can influence distribution of heat, energy and biological production in WBC regions.

1.1.3 The study area

For this thesis a WCE and a CCE will be studied in the ocean off southeast Australia. Physical and biological processes on the southeast Australian continental shelf are dominated by the presence of the East Australian Current (EAC), a poleward flowing western boundary current (WBC) (Godfrey et al., 1980b). The evolution of the EAC has been described by Ridgway and Dunn (2003): The EAC forms between 15^oS and 25^oS, fed from the bifurcation of the South Equatorial current (Church, 1987). It extends along the east Australian coast, intensifying as the shelf narrows. The EAC has been observed to travel faster than 1 m s^{-1} (Godfrey et al., 1980a; Nilsson and Cresswell, 1980; Everett et al., 2011) and can extend to depths of 2000 m. The EAC undergoes bifurcation between 30^0S and 31.5^0S. Part of the bifurcated current extends eastwards, forming the Tasman front and an intense eddy field. This current then attaches itself to the east of New Zealand, forming the East Auckland current. The other

branch of the bifurcated current remains attached to the east coast of Australia and is observed in declining strength as far south as Tasmania. The region of bifurcation and separation of the EAC from the coast is a very energetic and variable area, producing many eddies (Ridgway and Godfrey, 1997; Wilkin and Zhang, 2007; Everett et al., 2012).

1.1.4 Eddies in the East Australian Current

The eddy field associated with the EAC separation zone can be larger than the current itself. As a result, the EAC is not always distinguishable as a current (Godfrey et al., 1980b). While the EAC has little transport in comparison to other WBCs the variability caused by these eddies is comparable. The EAC separation zone (also called "Eddy Avenue") has a high concentration of eddies with an average of 75 cyclonic and 74 anticyclonic eddies per 10 000 km^2 (Everett et al., 2012). These eddies are energetic compared to global and Tasman sea averages (Everett et al., 2012). They often have sea-level anomalies and rotational speeds in excess of 0.15 m and 0.3 m s^{-1} respectively (Everett et al., 2012). WCEs, due to their size, tend to dominate the region (Marchesiello and Middleton, 2000). CCEs tend to be smaller and form slightly inshore when compared to the larger WCEs. WCEs move southwards creating sharp temperature fronts. Both CCE and WCE fields influence the flow, temperature fronts and biological interactions along the continental shelf off southeast Australia.

WCEs are shed from the energetic separation zone of the EAC 1 to 4 times a year (Bowen et al., 2005; Mata et al., 2006). They can persist for periods of months to years, transporting heat, salt and energy through the Tasman Sea.

Therefore, understanding the dynamics behind the transfer of heat and energy from the EAC to these eddies is important in explaining heat and energy budgets for the EAC and Tasman Sea. WCEs are well studied for the EAC region (Oke and Griffin, 2010; Cresswell, 1982; Bowen et al., 2005; Mata et al., 2006; Nilsson and Cresswell, 1980; Tranter et al., 1980; Baird et al., 2010). As these eddies form at the front between the warmer EAC waters and the cooler Tasman waters, cold water can be entrained into the centre of a 'warm-core' eddy (Nilsson and Cresswell, 1980). To complicate this further there is a heat loss over winter in (warm core) eddies which can be accounted for by atmospheric forcing. The cooling causes a winter core formation whereby the surface signal of the 'warm core' eddy is cooler than the surrounding waters (Nilsson and Cresswell, 1980). In this case the sea surface elevation can be a better guide to the location of eddies.

One interesting dynamic of WCEs in the EAC region is a process called overwashing, or flooding (Nof and Dewar, 1994; Baird et al., 2010; Tranter et al., 1982). In this process the WCE sinks, or is pushed under, warmer, less dense waters. For EAC WCEs this water can be sourced from the EAC itself (Baird et al., 2010). The mechanisms for overwashing or, indeed, the mechanisms which prevent this overwashing have not been explored. As overwashing could be a mechanism for transferring heat, salt and energy properties from the EAC to the eddies and eventually to the Tasman sea an understanding of the processes driving this overwashing is important.

Less is known about CCEs than their WCE counterparts. In the energetic EAC region 65 % of CCEs have positive surface chlorophyll anomalies, suggesting

that they are more biologically productive than the mean ocean state (Everett et al., 2012). If the CCEs entrain coastal waters they can have a significant impact on coastal marine ecosystems. Therefore, it is important to understand the source of the seeding populations into CCEs and the physical dynamics within CCEs that supply food to the entrained population.

1.2 Scope of study

The purpose of this study is to gain a better understanding of the physical oceanography of the EAC separation region and, in particular, knowledge of the processes involved in the formation of mesoscale eddies, transfer of energy and heat to eddies and vertical movement. To this end a case study of a WCE that formed in 2008 and a CCE that formed during 2009 are investigated. The CCE is studied in more detail as less is known about CCEs in the EAC region. In addition to this, CCEs tend to be more biologically productive than WCEs and, hence, the CCEs will have important biological implications. There is also evidence in satellite derived surface chlorophyll that the October CCE is more biologically productive than the October 2008 WCE (Fig 1.1).

This modelling study compliments the works of Everett et al. (2011); Baird et al. (2010) and Henschke et al. (2011). These studies were primarily observational and, with the exception of Baird et al. (2010), focused on biological processes. The study here adds temporal and spatial resolution to these observational studies and adds knowledge of physical processes to aid in the interpretations of the biological interactions.

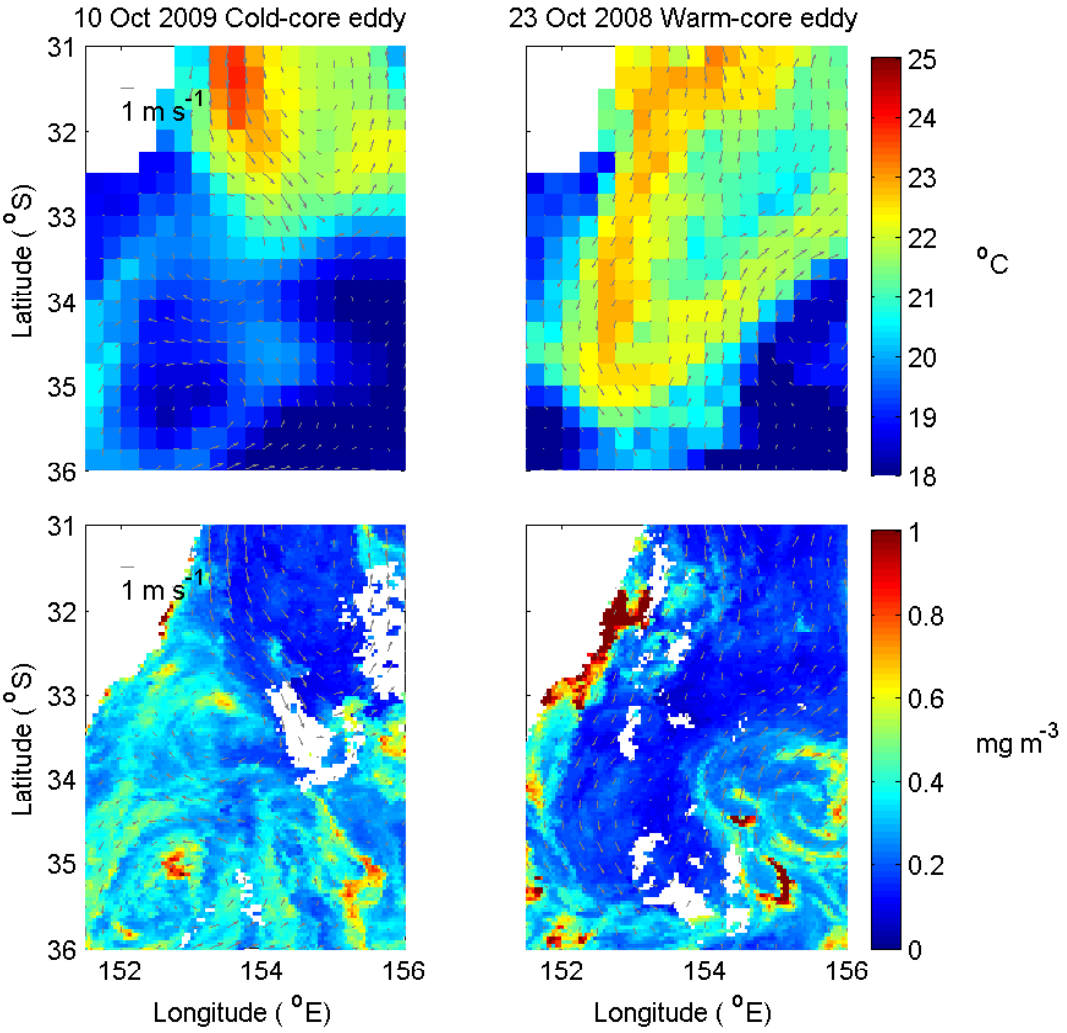

Figure 1.1: SynTS sea-surface temperature (top) and Chlorophyll a concentrations from NASA Ocean Colour L3 mapped HDF product (bottom) coinciding with the October 2009 cold-core eddy (left) and the October 2008 warm-core eddy (right).

1.3 Objectives

The main objectives of this study are:

1. *To understand dynamics within an East Australian Current warm-core eddy, particularly when it is being overwashed by East Australian Current waters.*

2. *To examine the dynamics within an East Australian Current cold-core eddy and suggest possible mechanisms for eddy formation.*

3. *To investigate the source waters for an East Australian Current cold-core eddy,* and

4. *To test the Fennel et al. (2006) biological model for its suitability to perform studies on entrainment and upwelling into East Australian Current cold-core eddies.*

These goals are achieved through multiple numerical modelling studies from a model configured for the southeast Australian continental shelf and open ocean region. As well as the typical model outputs of the ocean state, several modelling tools are utilised to aid in interpretation of model output. These include Lagrangian particle tracking and the use of passive tracers.

1.4 Outline

This thesis is organised as follows: Chapter 2 describes the model and configuration setup for the EAC region. Chapter 3 examines a realistic model simulation of a WCE that formed and was overwashed by the EAC in 2008. Chapter 4 and 5 discuss the formation of, entrainment into and upwelling within a CCE in October 2009. A biological model is introduced in Chapter 6 and a summary and future work is presented in Chapter 7. A brief summary of each chapter is included here. Additionally, a more detailed abstract is included at the beginning of Chapters 3, 4, 5 and 6.

1.4.1 Chapter 2

In this chapter the model used to reproduce the ocean state coinciding with the two eddies is described. Details of the development of the configuration is given. The specific options utilised (i.e. boundary and atmospheric forcing, nudging layers and turbulent closure scheme) are listed along with the sources of external forcings.

1.4.2 Chapter 3

A simulation of the 2008 WCE is presented. The dynamics of two stages in the eddy's life cycle, eddy formation and overwashing by the EAC, are described. This study focuses on the overwashing and submergence of the original WCE by the EAC.

1.4.3 Chapter 4

This chapter investigates model simulations of a CCE that formed in October 2009. A sensitivity analysis is performed to investigate the effect of different wind fields, bathymetric features and initial conditions on eddy formation. The transfer of energy from the mean fields to the eddy fields is studied.

1.4.4 Chapter 5

This study utilises a model simulation of the October 2009 CCE to investigate source waters for a CCE. A sensitivity analysis on the effect of the wind field on these source waters is presented. Upwelling into the eddy is investigated as well as the effect of the tilt of the eddy into the continental shelf on patterns of upwelling and downwelling within the eddy. A new paradigm is proposed for the complex upwelling and entrainment processes in a coastal cold-core eddy.

1.4.5 Chapter 6

This study is an extension on the findings of Chapter 5. The feasibility of the Fennel et al. (2006) biological model to investigate biological processes in an East Australian Current cold-core eddy is examined. To do this, a short study into the effect of entrainment of continental shelf waters into the CCE of Chapters 4 and 5 is performed.

1.4.6 Chapter 7

This chapter summarises the main aims and subsequent results of this thesis. The implications of these results are presented along with avenues for future research.

Chapter 2

Methods

2.1 The Regional Ocean Modelling System

The ocean state of the eddies studied in this thesis are simulated using the Regional Ocean Modelling system (ROMS) (Shchepetkin and McWilliams, 2003, 2005). ROMS is a community ocean model that has been developed over a number of years. It is regarded as a state of the art ocean model and has been used in a large number and variety of scientific projects (Budgell, 2005; Colas et al., 2008; Di Lorenzo et al., 2008; Dinniman et al., 2003; Fennel et al., 2006, 2008; Marchesiello et al., 2003; Moore et al., 2009; Peliz et al., 2003). As well as modelling the physical state of the ocean (Colas et al., 2008; Dinniman et al., 2003; Marchesiello et al., 2003; Peliz et al., 2003), ROMS can be implemented with a variety of biological models (Di Lorenzo et al., 2008; Fennel et al., 2006; Moore et al., 2009), chemical models (Fennel et al., 2008) and sea-ice models (Budgell, 2005) as well as the implementation of data assimilation methods (Moore et al., 2009).

ROMS solves the primitive nonlinear, Boussinesq and hydrostatic equations allowing for a time-dependent free surface on a curvilinear, terrain-following grid (Shchepetkin and McWilliams, 2003, 2005). The ROMS kernel is designed to reduce the pressure gradient truncation errors associated with this terrain following scheme (Shchepetkin and McWilliams, 2003). For computational efficiency, ROMS uses a split-explicit scheme with a smaller timestep for computing the (2-dimensional; barotropic) depth integrated continuity and momentum equations than that used for the (3-dimensional; baroclinic) momentum and tracer equations.

2.2 Grid resolution

ROMS is a sigma-coordinate model meaning that, in the vertical, the coordinates are stretched so that they follow the terrain (rather than density contours or z-planes). In this configuration the second vertical transformation function (Vtransform =2) is used in calculating the vertical stretching. This is:

$$z(x, y, \sigma, t) = \zeta(x, y, t) + [\zeta(x, y, t) + h(x, y)]S(x, y, \sigma),$$

where

$$S(x, y, \sigma) = \frac{h_c\sigma + h(x, y)C(\sigma)}{h_c + h(x, y)}$$

Here z=-h(x,y) is the ocean bottom, $z = \zeta(x, y, t)$ is the ocean's free surface, σ is a fractional vertical stretching coordinate ($0 < \sigma < 1$). C(x,y) is a vertical stretching function which, for this configuration, is given by:

$$C(\sigma) = (1 - \theta_B)\frac{\sinh(\theta_S\,\sigma)}{\sinh\theta_S} + \theta_B\left[\frac{\tanh[\theta_S(\sigma + \frac{1}{2})}{\tanh(\frac{1}{2}\theta_S)}\right] - \frac{1}{2}$$

Here θ_s controls how much the resolution is increased in the surface and bottom layers. A larger θ_s increases the resolution in these areas but to maintain numerical stability it should be less than 8. θ_b controls whether this extra resolution should be in the surface and/or the bottom layers. $\theta_b = 0$ means this increased resolution is in the surface and $\theta_b = 1$ means it is spread evenly between the surface and bottom layers.

This coordinate system is implemented using 50 layers with the stretching scheme configured so that most of the resolution is stretched to the top of the water column for depths greater than 250 m (n=50) and $\theta_s = 7$, $\theta_b = 0$. This means that most of the resolution is stretched to the top of the water column at depths above h_c, which is set at 250 m.

2.3 Model configuration

In the configurations used in this thesis, the baroclinic timestep is 60 seconds and there are 60 barotropic timesteps to each baroclinic step. The Mellor and Yamada (1982) 2.5 turbulent closure scheme is used in parameterising vertical mixing. Mixing of momentum is performed on s-surfaces and a 3rd-order upstream biased advection scheme is used (Shchepetkin and McWilliams, 2003, 2005).The full CPP (C Preprocessor) options used in this thesis are shown in tables 2.1 and 2.2.

As the model's initial conditions are already in geostrophic balance, there is

CPP option defined	Description	Chapters
UV_ADV	turn ON advection terms	1-6
UV_COR	turn ON Coriolis term	1-6
UV_VIS2	turn ON harmonic horizontal mixing	1-6
MIX_S_UV	mixing along constant S-surfaces	1-6
TS_DIF2	turn ON harmonic horizontal mixing	1-6
SOLVE3D	solving 3D primitive equations	1-6
SALINITY	having salinity	1-6
NONLIN_EOS	using nonlinear equation of state	1-6
TS_U3HADVECTION	3rd-order upstream biased advection	1-6
DJ_GRADPS	splines density Jacobian	1-6
SPLINES	activate parabolic splines reconstruction	1-6
CURVGRID	curvilinear coordinates grid	1-6
MASKING	land/sea masking	1-6
AVERAGES	writing out NLM time-averaged data	1-6
UV_QDRAG	turn ON quadratic bottom friction	1-6
BULK_FLUXES	bulk fluxes computation	1-6
ANA_SSFLUX	analytical surface salinity flux	1-6
ANA_BSFLUX	analytical bottom passive tracers fluxes	1-6
ANA_BTFLUX	analytical bottom temperature flux	1-6
MY25_MIXING	Mellor/Yamada Level-2.5 closure	1-6
N2S2_HORAVG	horizontal smoothing of buoyancy/shear	1-6
KANTHA_CLAYSON	Kantha and Clayson stability function	1-6
SPONGE	enhanced viscosity/diffusion areas	1-6
TCLIMATOLOGY	processing tracers climatology	1-6
TCLM_NUDGING	nudging tracers climatology	1-6
M3CLIMATOLOGY	processing 3D momentum climatology	1-6
M3CLM_NUDGING	nudging 3D momentum climatology	1-6
BIOCLM_NUDGING	nudging biology climatology	6
NORTH_M2FLATHER	2D momentum Flather condition	1-6
NORTH_KRADIATION	TKE fields radiation condition	1-6
NORTH_TNUDGING	tracers passive/active nudging	1-6
SOUTH_M3RADIATION	3D momentum radiation condition	1-6
SOUTH_FSRADIATION	free-surface radiation condition	1-6
SOUTH_M2RADIATION	2D momentum radiation condition	1-6
SOUTH_TRADIATION	tracers radiation condition	1-6
SOUTH_KRADIATION	TKE fields radiation condition	1-6

Table 2.1: The CPP options utilised, a short description and the chapters in which they were activated.

CPP option defined	Description	Chapters
EAST_M3RADIATION	3D momentum radiation condition	1-6
EAST_FSRADIATION	free-surface radiation condition	1-6
EAST_M2RADIATION	2D momentum radiation condition	1-6
EAST_TRADIATION	tracers radiation condition	1-6
EAST_KRADIATION	TKE fields radiation condition	1-6
WEST_M3RADIATION	3D momentum radiation condition	1-6
WEST_FSRADIATION	free-surface radiation condition	1-6
WEST_M2RADIATION	2D momentum radiation condition	1-6
WEST_TRADIATION	tracers radiation condition	1-6
WEST_KRADIATION	TKE fields radiation condition	1-6
BIO_FENNEL	Fennel et al. (2006) nitrogen-based model	6
ANA_SPFLUX	analytical surface passive tracers fluxes	1-6
ANA_BPFLUX	analytical bottom passive tracers fluxes	1-6
ANA_CLOUD	analytical cloud fraction	1-6
FLOATS	activate simulated Lagrangian drifters	1, 5
T_PASSIVE	inert passive tracers (dyes, etc)	3

Table 2.2: Continuation of the CPP options utilised, a short description and the chapters in which they were activated.

a short spin-up period of 5 days.

There are two grid used. The first is a lower resolution grid used in Chapter 3 and the second is a higher resolution grid used to capture smaller features in Chapters 4-6. Each grid is described below.

2.3.1 The low resolution grid

The model grid is modified from Wilkin and Zhang (2007). The resolution has been increased to approximately 3.5 km by 4.3 km. The resultant grid has 414 grid cells in the East/West direction and 342 grid cells in the North/South direction. This grid covers an area between 26.03°S to 37.33°S and 141.1°E to 161.97°E (Fig. 3.2). A high resolution (2×2min) bathymetry from the Naval Research Lab (DBDB2 V3) has been interpolated onto this new grid. The depth of the model has been limited to 2000 m and the bathymetry has been smoothed using a smooth positive method (Sikiric et al., 2009) with rx0max (the target rx0 roughness factor) equal to 0.2 to minimise the pressure gradient error associated with terrain following models (Mellor et al., 1994).

The vertical resolution has been increased from Wilkin and Zhang (2007) to more accurately depict the mixed layer. The coordinate system is implemented using 50 layers with the stretching scheme configured so that most of the resolution is stretched to the top of the water column for depths greater than 250 m.

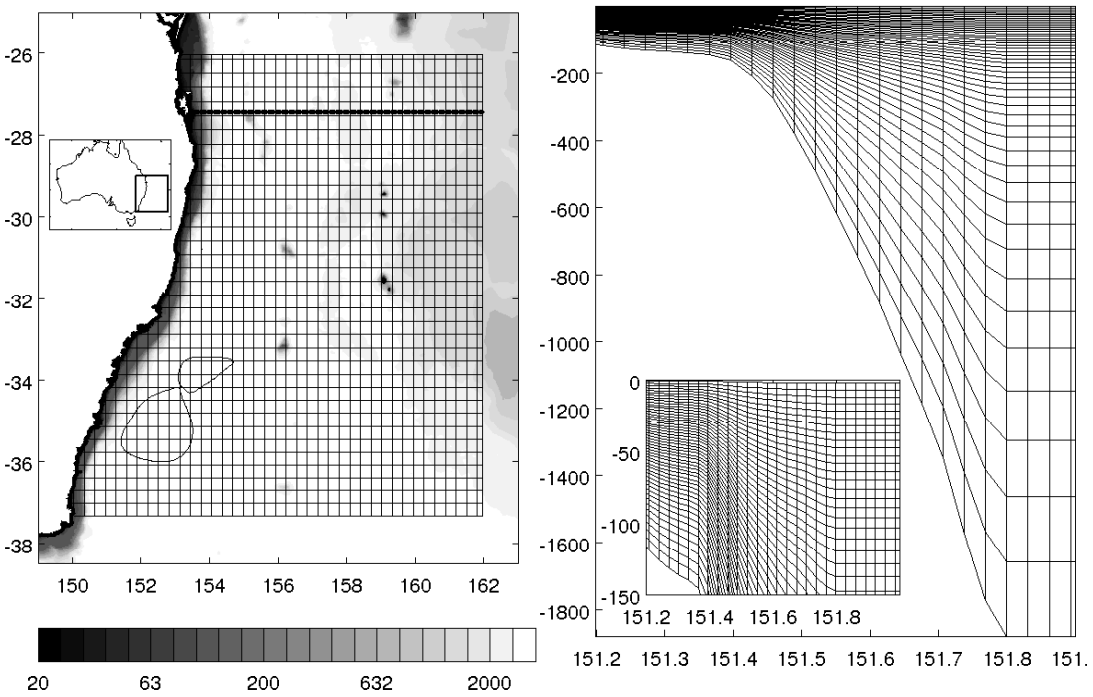

Figure 2.1: The low resolution model grid used in chapter 3. Left shows horizontal resolution. Every 10th grid line is shown and the shading show bathymetry on a log scale. The thick black line in the northern section of the grid indicates the extent of the boundary nudging and the thin curves indicate the boundary of the eddy at the start and the end of the simulation. The location of the model grid is indicated by the rectangle in the insert of Australia. Right shows the vertical resolution for different model depths. The insert shows the vertical resolution for the top 150 m. The coast is indicated as a thick black line.

2.3.2 The high resolution grid

The resolution has been increased to approximately 1.75 km by 2.15 km and no limit has been set on the maximum depth. The resultant grid has 828 grid squares in the zonal direction and 684 grid squares in the meridional direction. The grid covers a region between 29.9°S to 37.33°S and 149.1°E to 159.2°E (Fig. 4.1A). A high resolution (2 × 2min) bathymetry from the Naval Research Lab (DBDB2 V3) has been interpolated onto this new grid. The bathymetry has been smoothed using a smooth positive method (Sikiric et al., 2009) to minimise the pressure gradient error associated with terrain following models (Mellor et al., 1994).

The vertical coordinate system is implemented using 50 layers with the stretching scheme configured so that most of the resolution is stretched to the top of the water column for depths greater than 250 m (Fig. 4.1B).

2.3.3 Initial, boundary and climatology data

SynTS (Ridgway et al., 2008) is a daily, 3D temperature and salinity estimate produced by CSIRO (The Commonwealth Scientific and Industrial Research Organisation) which is based on available satellite sea surface temperature and vertical profiles (Argo floats). Geostrophic currents are calculated from this temperature and salinity field using a reference depth of 2000 m. SynTS products (temperature, salinity and geostrophic currents) are used for model initialisation and the time-varying boundary forcing. For areas of the model below 2000 m, the initial temperature and salinity conditions come from the CSIRO Atlas of Regional Seas (CARS) climatology (Ridgway et al., 2002) and velocity is set to

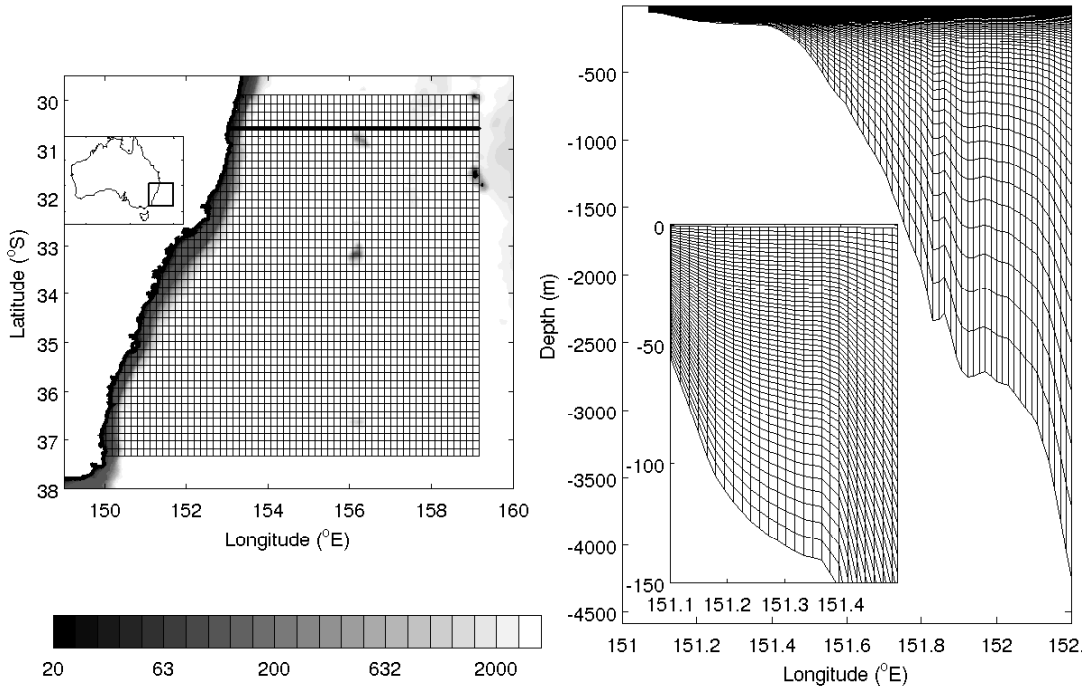

Figure 2.2: The high resolution model grid used in chapters 4-6. Left shows horizontal resolution. Every 10th grid line is shown and the shading show bathymetry on a log scale. The thick black line at 30.58^{o}S indicates the southern extent of the northern boundary nudging. The location of the model grid is indicated by the rectangle in the insert of Australia. Right shows the vertical resolution for different model depths through 34.19^{o}S. The insert shows the vertical resolution for the top 150 m. The coast is indicated as a thick black line.

zero.

2.3.4 Boundary conditions

Boundary conditions are specified for the barotropic and baroclinic velocity fields and the free surface and tracers. The Flather (1976) condition is used for the barotropic velocity components at the northern boundary. The baroclinic velocity field and the tracers on the northern boundary are nudged to external estimates at a timescale of 4 days. This northern boundary forcing comes from SynTS products (described above) and is updated during the simulation to capture the evolution over time. The Chapman (1985) condition is also applied to the northern free surface boundary. At the southern, eastern and western boundaries radiative conditions for each of the variables are applied. Coastal boundaries are specified via a land/sea mask.

For the configurations used in this thesis there is an additional boundary nudging layer in the first 40 grid squares inwards from the northern boundary. The nudging timescale is 1 day on the outer grid squares but tapers linearly to zero in the inner grid squares. This enables the model to be free running in the middle of the domain.

2.3.5 Atmospheric forcing

The Bulk flux method of Fairall et al. (1996) is used at the atmospheric boundary to specify air-sea fluxes of heat and momentum. The surface wind field is obtained from the NOAA/NCDC Blended 6-hourly 0.25-degree Sea Surface Winds data set (Zhang et al., 2006). Longwave radiation, shortwave radiation,

air pressure, relative humidity and surface air temperature are obtained from NCEP 2.5-degree 6 hourly reanalysis data sets (Kalnay et al., 1996).

Chapter 3

The overwashing of a warm-core eddy by the East Australian Current

Abstract

Warm-core eddies (WCEs) often form in the meanders of Western Boundary Currents (WBCs). WCEs are frequently overwashed with less dense waters sourced from the WBC. We use the Regional Ocean Modelling System (ROMS) to investigate the ocean state during the overwashing of one such WCE in October 2008 in the East Australian Current (EAC). Comparisons to satellite SST and vertical profiles show that the model provides a realistic simulation of the eddy during the period when the EAC encircled, and then overwashed, the eddy. During the encircling stage an eddy with closed circulation persisted

at depth. At the surface EAC water entered from the north, encircled the eddy and exited to the east. The overwashing stage was initiated by the expulsion of cyclonic vorticity from the eddy. For the 8 days following the expulsion, waters from the EAC washed over the top of the eddy, transferring heat and anticyclonic vorticity radially inwards. After approximately 1 rotation period of overwashing, the eddy separated from the EAC. The overwashing creates a two-layer system where the maximum velocity in the subsurface occurs at the interface of the two layers. Analysis of water mass properties, Eulerian tracer dynamics and Lagrangian particle tracks show that the original eddy sinks 10-50 m during the overwashing period. Overwashing is observed in many WBCs and occurs in most WCEs in the western Tasman Sea.

3.1 Introduction

Mesoscale eddies are an ubiquitous feature of vigorous western boundary currents (Parker, 1971; Yang et al., 1999; Everett et al., 2012). These can have azimuthal velocities reaching speeds greater than 1 m s^{-1}, diameters in the order 200 km and have been investigated in each of the major western boundary currents (The East Australian Current (Hamon, 1965), The Gulf Stream (Rossby, T., 1987; Oort, 1964), The Agulhas Current (Duncan, 1968), The Kuroshio (Yaochu and Jilan, 1988) and The Brazil Current (Didden and Schott, 1993)). Typically they form in the unstable flow near the western boundary current's retroflection area.

Warm-core (anticyclonic) eddies within these western boundary systems can sink or get pushed under a layer of even warmer water sourced from the Western Boundary Current (WBC), another warm-core eddy (WCE) or surrounding waters after cooling (Nof and Dewar, 1994; Baird et al., 2010; Tranter et al., 1982). The resultant eddy has two distinct layers: a thin surface layer and a lower submerged layer (Fig. 3.1. This process has also been referred to as flooding (in the EAC (Tranter et al., 1982)), submergence (in the EAC (Jeffrey and Hallegraeff, 1987)) and overwashing (in the North Atlantic (Chapman and Nof, 1988)) and has been observed in many different boundary currents (The Gulf Stream (Hitchcock et al., 1985); The East Australian Current (Jeffrey and Hallegraeff, 1987), and the Leeuwin Current (Dietze et al., 2009)). In this paper we refer to the process as overwashing resulting in submergence (after Chapman and Nof (1988)).

3.1.1 Warm-core eddies in the East Australian Current

The East Australian Current (EAC) is a western boundary current that forms large WCEs, located on the east coast of Australia. The EAC bifurcates between 30-34°S (Godfrey et al., 1980b) at which point one branch travels east to form the East Auckland current, while the other branch continues south along the Australian Continental shelf in diminishing strength until Tasmania (42°S). The area of bifurcation is known as the EAC separation zone and is an energetic area with a large eddy variability (Ridgway and Godfrey, 1997). This variability is created by eddies which are shed off from the EAC at an interval of 90-180 days (Bowen et al., 2005; Mata et al., 2006). In this region it has been

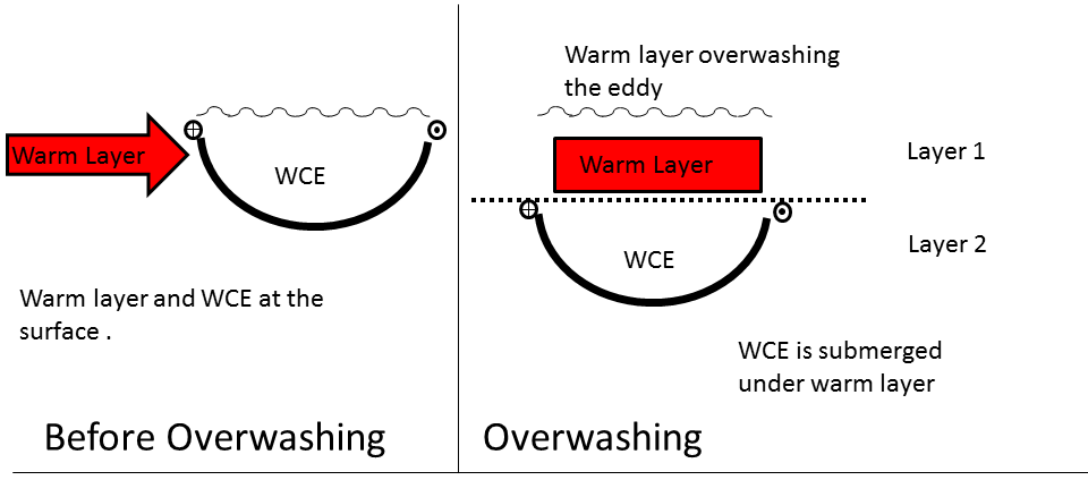

Figure 3.1: Schematic of the overwashing of a warm-core eddy (WCE). Left shows vertical and horizontal position of the less dense overwashing current (warm layer) and the eddy (WCE) before overwashing and right shows the position after overwashing. Black lines show isotherms and are an indication of the boundary of the water masses. The black dotted line on right indicates the barrier between layer 1 and 2 as discussed in Section 3.4.3.

shown that anticyclonic eddies which favor downwelling and low productivity can, after overwashing, produce a subsurface chlorophyll maximum (Baird et al., 2010). One such example of this is a WCE which started to form from an EAC meander in January of 2008 (Baird et al., 2010). In October 2008 the EAC overwashed (referred to as flooded in Baird et al. (2010)) over the surface of the eddy, submerging the original surface layer, creating a two-layer system.

3.1.2 Warm-core eddies, vertical mixing and productivity

In these 2-layered eddy systems the fate of the water in the subsurface layer depends on the process leading up to this layering. In the numerical modelling study of Chapman and Nof (1988) the surface of the eddy is cooled, allowing it to sink below the surrounding water. In Tranter et al. (1980), surface heating creates a surface cap to the eddy and the lower layer does not change its position vertically. In Baird et al. (2010) the process is different again as the surface layer comes from a lateral movement of EAC waters whereby the original eddy sank and water was then expelled from the eddy at depth and moved up the sides.

An unanswered question pertains to the timing of overwashing i.e. "what determines when an eddy will be overwashed?". In the experiments of Chapman and Nof (1988) the eddy completely sinks in a matter of weeks after a buoyancy difference between the eddy and surrounding waters is established. In the observations of a WCE in the EAC, Baird et al. (2010) found that the overwashing process did not even start until a couple of months after the eddy formed. Why this overwashing was delayed has not been examined.

WCEs are also interesting from a biological productivity perspective. WCEs

are conceptually considered to be nutrient deplete with significantly lower productivity than cold-core eddies (Bakun, 2006). Therefore, the vertical mixing processes which have the potential to drive nutrients and seed populations are of critical significance for the production of algal blooms in WCEs (Kahru et al., 2007; McGillicuddy et al., 2007). In addition to the above physical questions, quantifying the vertical structure and resultant mixing processes combined with determining the source of waters entrained into WCEs will lead to a better understanding of algal blooms, production rates and species composition within the eddy.

Other uplift processes have been identified in WCEs. These include the velocity shear between the swiftly moving eddy and the relatively still surrounding ocean (Capet et al., 2008), the frictional decay of the eddy (Nelson et al., 1989; Flierl and Mied, 1985), the coalescence of WCEs (Cresswell, 1983), a deepening of the mixed layer (Tranter et al., 1980) and the separation of a WCE from the continental shelf (Nilsson and Cresswell, 1980).

WCE's are also known to entrain water. Csanady (1979) has developed 2-layered models of WCE's to describe their shape and flow field (see also Csanady (1979, 1977, 1971)). The model (which was in first order agreement with observation) showed velocities on the outer rim reaching 1 m s^{-1}. This current enhanced entrainment of water surrounding the eddy.

Aside from nutrient availability, a further limitation on biological growth in a WCE is light availability. Depth-integrated light can be low in the deep surface mixed layer of a WCE, which results in light-limited phytoplankton growth. Light-limitation can be overcome by overwashing which causes stratification,

thus decreasing the depth of the surface mixed layer. This allows for growth in the new, more shallow, light filled surface mixed layer. This process was identified by Baird et al. (2010) and Tranter et al. (1980), where a nutrient poor, but optically clear, layer of water flooded over the top of a WCE, resulting in an algal bloom in the pycnocline.

To date, investigations of the vertical structure within eddies have been limited to sporadic and coarse resolution observations (e.g. from shipboard CTD casts or Argo float profiles and more recently autonomous glider observations). As such, there are compelling reasons to create a realistic model of surface overwashing in a WCE to better understand vertical movement and the timing of the overwashing mechanism. This will lead to a better understanding of entrainment and possible increased productivity. The model provides much greater spatial and temporal resolution to the observation of Baird et al. (2010) and allows for tracer and particle tracking. In particular we investigate conservation of vorticity, heat and energy in the eddy and how these properties are transferred from the EAC to the eddy.

Here, for the first time, we use the Regional Ocean Modelling System (described in Section 3.2) to investigate the spatial and temporal evolution (formation and shedding) of an overwashing WBC eddy that formed in October 2008 in the EAC. The model reveals significant insights into the vertical structure and mixing processes within the eddy as well as the transfer of vorticity from the EAC to the eddy (Section 3.3). We describe in detail the subsurface properties (temperature, salinity and velocity) and, most importantly, we identify the source waters and the vertical and horizontal movement within and across the

boundary of the eddy. The results are then discussed (Section 3.4) in the context of vorticity and buoyancy issues, providing new insights into the overwashing process.

3.2 Methods

The ocean state of the October 2009 WCE is simulated using the Regional Ocean Modelling system (ROMS). A detailed description of the model's configuration for the EAC region can be found in Chapter 2 and a brief summary is included here. SynTS (Ridgway et al., 2008) is used to prescribe initial, boundary and climatology data. The Flather (1976) condition is used for the barotropic velocity components at the northern boundary. The baroclinic velocity field and the tracers on the northern boundary are nudged to external estimates at a timescale of 4 days. All other boundaries are radiative. NCEP 2.5-degree 6 hourly reanalysis data sets (Kalnay et al., 1996) and the NOAA/NCDC Blended 6-hourly 0.25-degree Sea Surface Winds data set (Zhang et al., 2006) is used to implement the Bulk flux method of Fairall et al. (1996) at the atmospheric boundary. The model is initialised on 3 October 2008 (using SynTS products from the 3 October) and, as it is already in geostrophic balance, has a short spin-up period of 5 days. Model day 1 is 8 October. More details on the forcings and initial conditions can be found in Chapter 2.

The model grid

The model grid is modified from Wilkin and Zhang (2007). The resolution has been increased to approximately 3.5 km by 4.3 km. The resultant grid has

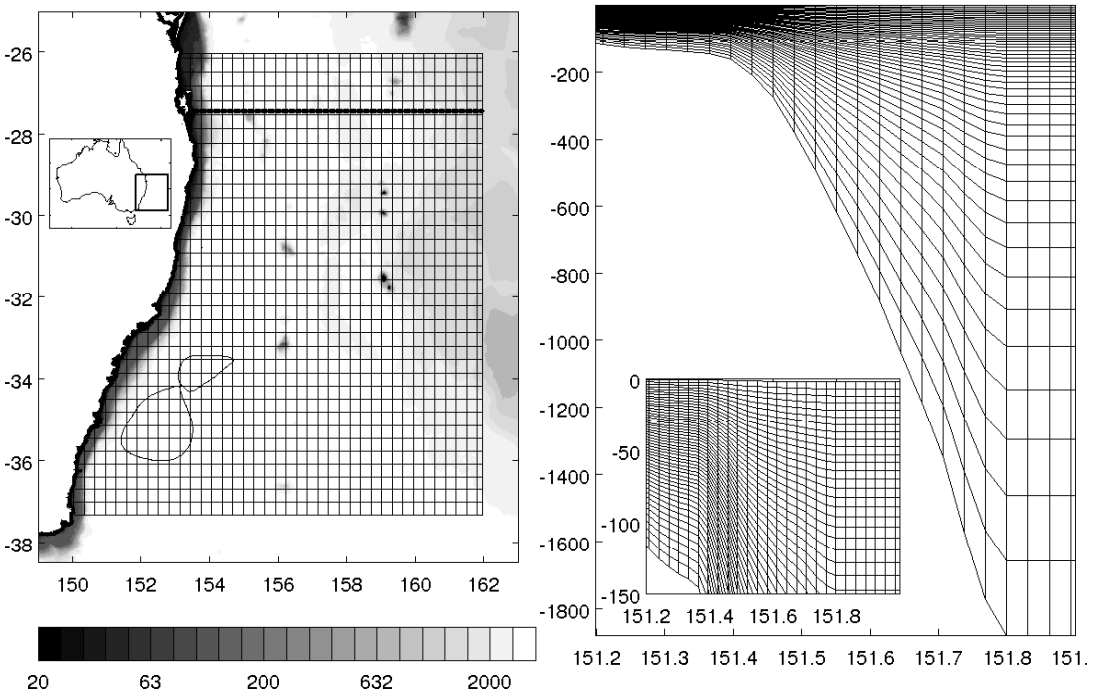

Figure 3.2: The model grid. Left shows horizontal resolution. Every 10th grid line is shown and the shading show bathymetry on a log scale. The thick black line in the northern section of the grid indicates the extent of the boundary nudging and the thin curves indicate the boundary of the eddy at the start and the end of the simulation. The location of the model grid is indicated by the rectangle in the insert of Australia. Right shows the vertical resolution for different model depths. The insert shows the vertical resolution for the top 150 m.

414 grid cells in the East/West direction and 342 grid cells in the North/South direction. This grid covers an area between 26.03°S to 37.33°S and 141.1°E to 161.97°E (Fig. 3.2). A high resolution (2×2min) bathymetry from the Naval Research Lab (DBDB2 V3) has been interpolated onto this new grid. The depth of the model has been limited to 2000 m and the bathymetry has been smoothed using a smooth positive method (Sikiric et al., 2009) with rx0max (the target rx0 roughness factor) equal to 0.2 to minimise the pressure gradient error associated with terrain following models (Mellor et al., 1994).

The vertical resolution has been increased from Wilkin and Zhang (2007) to more accurately depict the mixed layer. The coordinate system is implemented using 50 layers with the stretching scheme configured so that most of the resolution is stretched to the top of the water column for depths greater than 250 m.

3.2.1 Diagnostic tools

A range of measures of circulation are presented as they show different aspects of the circulation. In this section we describe the latitudinal/depth tracer which shows the origin of water within the eddy and Lagrangian particle paths which can show to where a particular body of water (i.e EAC water) travels. Streamlines are used to provide a snapshot of the velocity field. This shows how the velocities on a particular day will be affecting the results of the tracers and particle paths.

Passive tracers

Two diagnostic passive tracers are used in this simulation to visualise transport. The first, a depth tracer, is initialised throughout the model domain and given the value of the depth of the grid cell in which it is initialised. It is advanced in time following the formula for advection and mixing of a conservative passive tracer which has no sources or sinks. It is reset at the start of each day so that the value of the depth tracer within a particular grid cell is representative of the average initial (at the start of the day) depth of the water contained within the grid cell at that particular time. To estimate the vertical movement of the water over a day the depth of the grid cell is subtracted from the value of the

depth tracer (at the end of the day). The boundaries for the passive tracer are treated in a similar fashion to temperature and salinity with the external boundary nudging data given a value equal to the initial conditions for each day. In a similar manner, the average vertical movement of water since day 1 is calculated by only setting the tracer to its depth on day 1 of the simulation.

The second passive tracer is a latitudinal tracer which is initialised on day 1 with the value of the latitude of each water parcel on day 1. In a similar manner to the depth tracer, the value of the latitudinal tracer at a given moment in time indicates the average initial latitude of the water contained within a grid cell.

These passive tracers differ from a daily/simulation long-term average of zonal/vertical velocities as the tracers show an average while following parcels of water rather than the average of all parcels of water which pass a point. These passive tracers are a good approximation of the integration of zonal and vertical movement while following the parcels of water.

Lagrangian paths

Lagrangian particle trajectories are a useful tool for investigating transport pathways (Roughan et al. (2003, 2011)). In this paper 3D Lagrangian particle tracks are calculated without random walks. Particles are released into the EAC on day 5 (13 October) along a transect at 31.2°S at approximately 1 km intervals between 153.2°E and 153.5°E at depths of 1 m, 50 m and 100 m. These particles are advected inside the model at each timestep using the modelled velocities. The particles are released upstream of the eddy to show where the EAC waters enter and circulate in the eddy.

3.3 Results

3.3.1 Comparison of model and observations of the eddy

Model output is compared to various observations of the ocean state to assess the ability of the model to capture a Warm-Core Eddy (WCE) that formed during October 2008 (Fig. 3.3), hereafter referred to as "the eddy". On model day 7 (14 October) the model's sea surface temperature (SST) shows a WCE in a similar position and orientation to the eddy depicted in the AVHRR (Advanced Very High Resolution Radiometer) satellite estimates of SST (Fig. 3.3 A and B).

Following Chapman and Nof (1988), we will use the term "overwashing" to describe the process whereby a surface layer of fresher and/or warmer water moves onto the eddy surface. By model day 23 (30 October) the modelled overwashing (the tongue of warmer surface water) has reached the eddy centre.

Vertical profiles of T and S in the model are compared with observations obtained from a CTD cast and an Argo float at various stages of the evolution of the eddy. The CTD cast was taken during an RV Southern Surveyor Cruise (SS200810, CTD12) on the 14 October (model day 7). The Argo profile was taken by the Argo float 5900562, profile 147 on the 30 October (model day 23). The vertical T/S profile on model day 7 was taken on the boundary of the EAC and the eddy at the beginning of the overwashing process. The Argo profile measured on day 23 was taken in the middle of the overwashing, located near the centre of the eddy. The horizontal position of the vertical profiles in the model have been positioned to align with the same features in the observations as seen in the SST (Fig. 3.3 A, B, D and E).

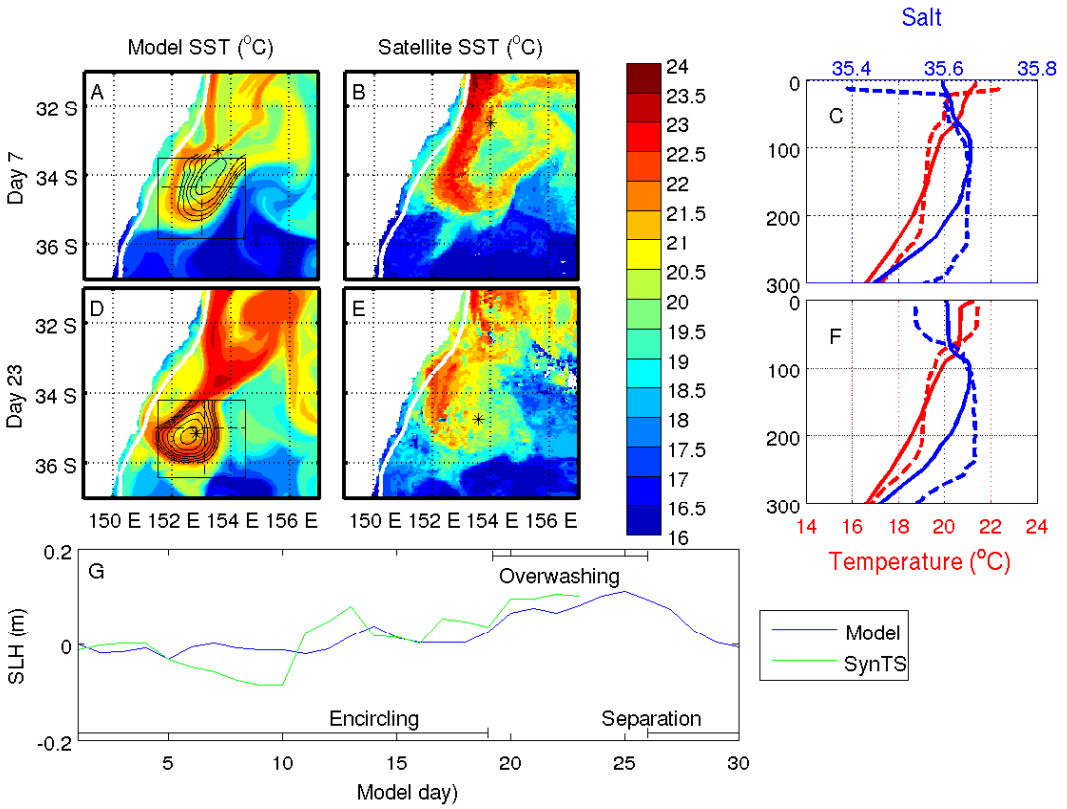

Figure 3.3: Left: model sea surface temperature (A and D; SST), middle: satellite (AVHRR) SST (B and E) and, right (C and F): vertical profiles of temperature (red) and salinity (blue). Dashed profiles are from observational data (CTD and Argo floats) and solid profiles are from the model output. The 200 m isobath is indicated in white on left and middle. The positions of the profiles are indicated by a * on left for profiles from the model and middle for the Argo/CTD profiles. Each row is for a different day: top is day 7 and bottom day 23. The boxes indicate the positions of the 3D profiles in Figs. 3.9, 3.11 and 3.12. Bottom: Evolution of the eddy's maximum sea-level height versus day for model (blue) and SynTS minus 0.3 m (Green).

To assess the overwashing process in subsurface layers, vertical profiles from the model are compared to observations (Fig. 3.3, right hand side). The impact of overwashing is evident in the observations as a subsurface, homogeneous (original eddy) mixed-layer of salinity 35.65 and temperature 19.2°C which is capped on the surface by a warmer/less saline (EAC) layer. On model day 7 (14 October) the model has a subsurface isothermal layer (80 m to 180 m; Fig. 3.3 C) whose upper limit is in a similar position in the water column. However, due to a shallower mixed layer depth in the initial (SynTS) conditions within the WCE, the isothermal layer does not extend as deep as that of the observations (80 m to 220 m). By model day 23 (30 October; Fig. 3.3 I) the sub-surface, homogeneous T and S mixed-layer is at a depth of 100 m, which is similar to the observed submerged homogeneous layer.

On day 7, the EAC entering the eddy is approximately 1^{o}C cooler in the model compared to the satellite data (Fig. 2 A and B) so the resultant overwashing signature (the surface homogeneous layer in Fig. 2 C and F) has a different temperature and salinity in the model as compared to the observations. As discussed later there is also some mixing between the surface EAC and submerged eddy layer which could compound this effect. In both the model and observations, however, the result is a surface mixed layer on top of a sub-surface, homogeneous layer.

The biggest difference in the model and observational profiles is at depth. The observed TS profiles on days 7 and 23 show an isothermal layer extending from 100 m to 250 m, a result of the deep convective mixing over winter. The model is initialised on the 3-October using SynTS, which smooths the bottom

of the isothermal layer with the water below. Isolated from the surface and with low vertical mixing, this deep water maintains its TS signature over the 30 day simulation. The model mismatch at the base of the eddy is an initialisation problem but this mismatch is not critical to the results as the area of interest is the eddy above the bottom of the original eddy's mixed layer.

From this comparison of vertical profiles it appears that the submergence of the original homogeneous-mixed layer in the model occurs to the same extent, albeit 10 days later than the observations. While this could be an artifact of the positioning of the T and S profiles in the comparison of the observed T and S profiles, the apparent delayed overwashing (and hence sinking of the mixed layer) in the model is also evident in the SST comparisons made. So, while the sinking occurs up to 10 days later in the model, these model comparisons with observed data show that the model does capture the evolution of a WCE in a similar manner to that of the eddy observed in October 2008.

Model sea-surface height is compared to contours of altimeter derived tidal-residual, isostatically-adjusted sea-level data (Deng et al., 2010). Changes in maximum sea-level height is in fairly good agreement between the model and observations (Fig. 3.3G). Both capture the increase in sea-level height between days 10 and 23.

3.3.2 Analysis of the model eddy

In the model, the EAC encircled the original WCE from the beginning of the simulation until overwashing began on day 19. During this encircling stage the EAC extends southward around the eddy then retroflects northward, forming an

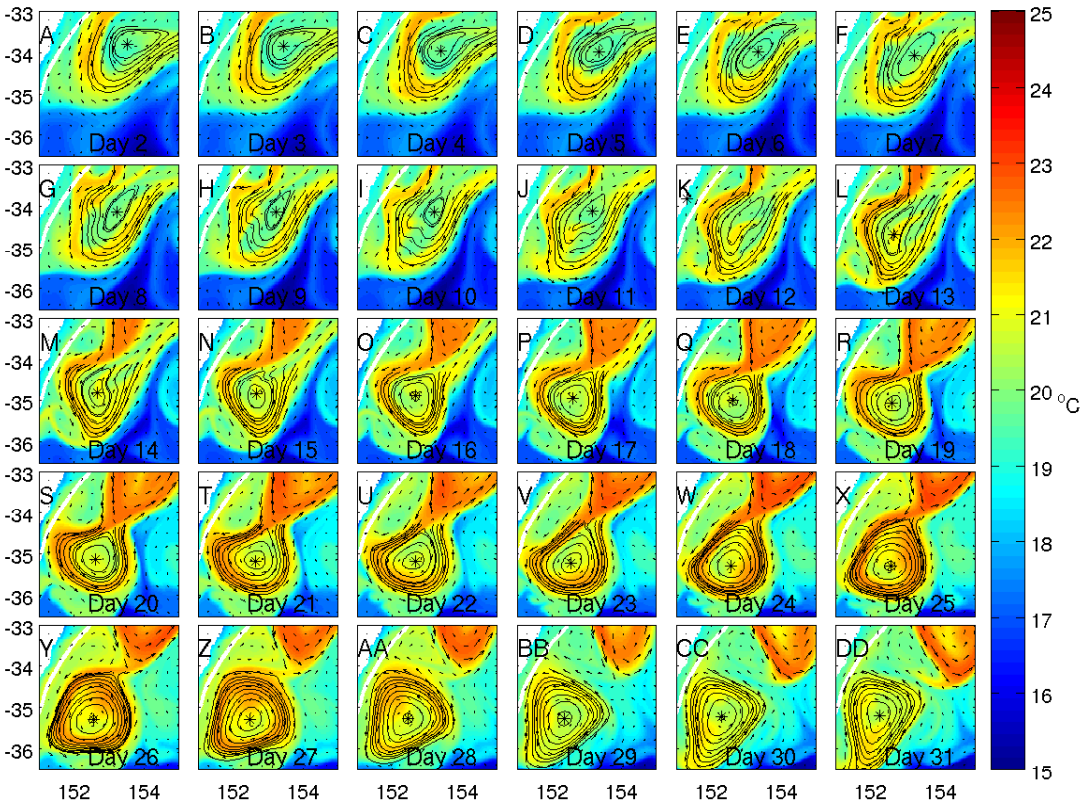

Figure 3.4: Model sea surface temperature (°C) for model days 2 to 31. The centre is marked with a * and sea-level contours around the eddy are shown in black. The 200 m isobath is shown in white.

anticlockwise u-shape around the eddy (Fig. 3.4A-P). The eddy becomes more elliptical as it is squeezed by the retroflection (Fig. 3.4A-P). Water is pushed out of the eddy to the north (Fig. 3.4G-N). The WCE has a temperature of 20°C and a salinity of 35.65-35.7 (Fig. 3.5, left column).

The overwashing occurs between days 19 and 27 when the EAC (characterised by a temperature of 21-24°C and a salinity of 35.5-35.6) encloses around the eddy, adding a ring of EAC waters to the eddy. Throughout the overwashing stage a thin layer of warm water from the EAC overwashes across the top of the eddy as it rotates with the eddy (Fig. 3.5, middle column). This EAC layer is

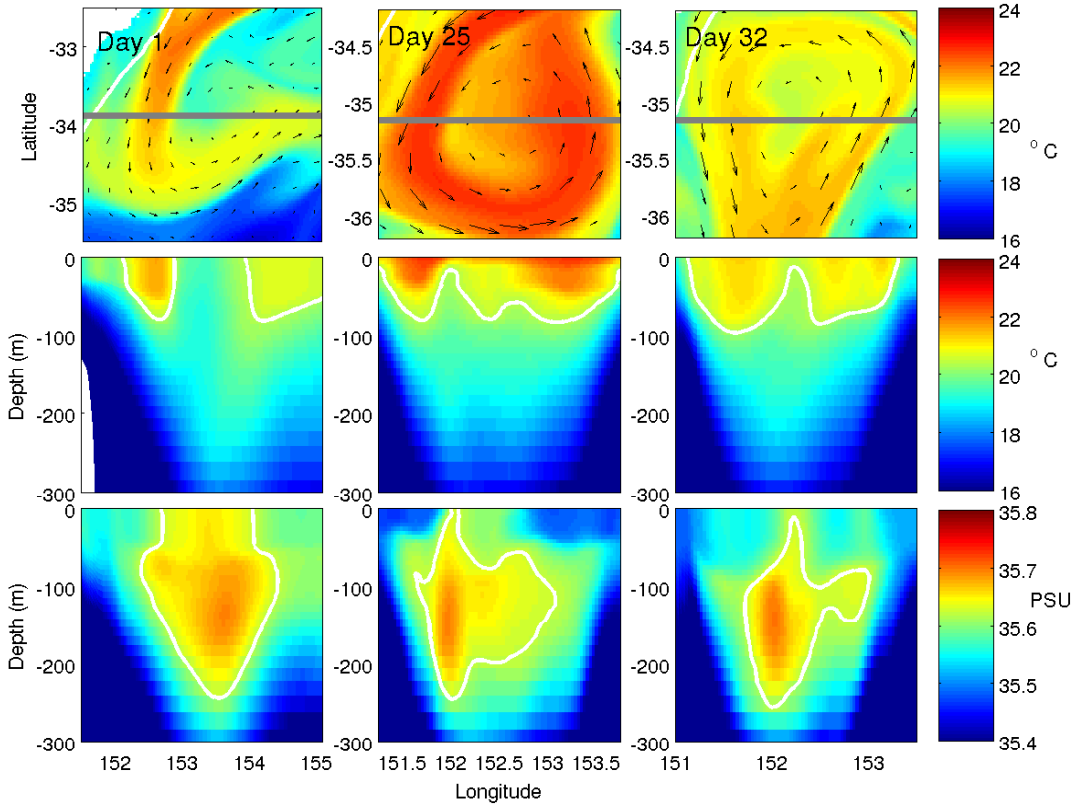

Figure 3.5: SST (top row), vertical profiles of temperature (middle row) and salinity (bottom row) for days 1 (left column), 25 (middle column) and 32 (right column). The grey lines on the panels in the top row indicate the position of the vertical profiles in the bottom two rows while the white lines indicate the 200 m isobath. The 20.5°C isotherm in indicated in white on the panels in the middle row and the 35.61 isohaline is indicated on the panels in the bottom row. the latitude of the transects change each day to ensure that they are in the eddy.

identified as a warming of about 3°C along the edges of the eddy which progresses radially inwards as it moves around the eddy. The EAC which encircled the eddy (located on the outer perimeter) has a signature down to a depth of 50 m and the overwashed EAC (in the centre of the eddy) is evident down to a depth of 10-30 m (Fig. 3.5).

At day 27, approximately one rotation period after overwashing began, the eddy separates from the EAC completely and evolves separately from the EAC as an overwashed WCE.

The overwashed EAC waters then actively mix down with the rest of the eddy (Fig. 3.5, right column). This is evident in the deepening of the surface mixed layer (Fig. 3.5, right column) combined with a cooling of the eddy surface between model days 27 to 31 (Fig. 3.4Z-DD). Thus the surface layer becomes a mixture of eddy and EAC waters with an intact submerged layer below 100 m.

3.3.3 Vorticity

A typical eddy has a vorticity maximum at the centre with the vorticity decreasing radially outwards. This holds true in this simulation for the eddy at depths below the eddy/EAC interaction (Fig. 3.6) but not at the surface (Fig. 3.7). In a similar manner to temperature the EAC which encircles the eddy initially (Day 7-19) has a greater vorticity than the eddy. This leads to a reversed vorticity gradient with the vorticity increasing radially outwards at the surface.

In addition to this reversed vorticity gradient, the eddy forms with cyclonic vorticity at the interface of the eddy and the EAC (thin blue filament in Fig. 3.7).

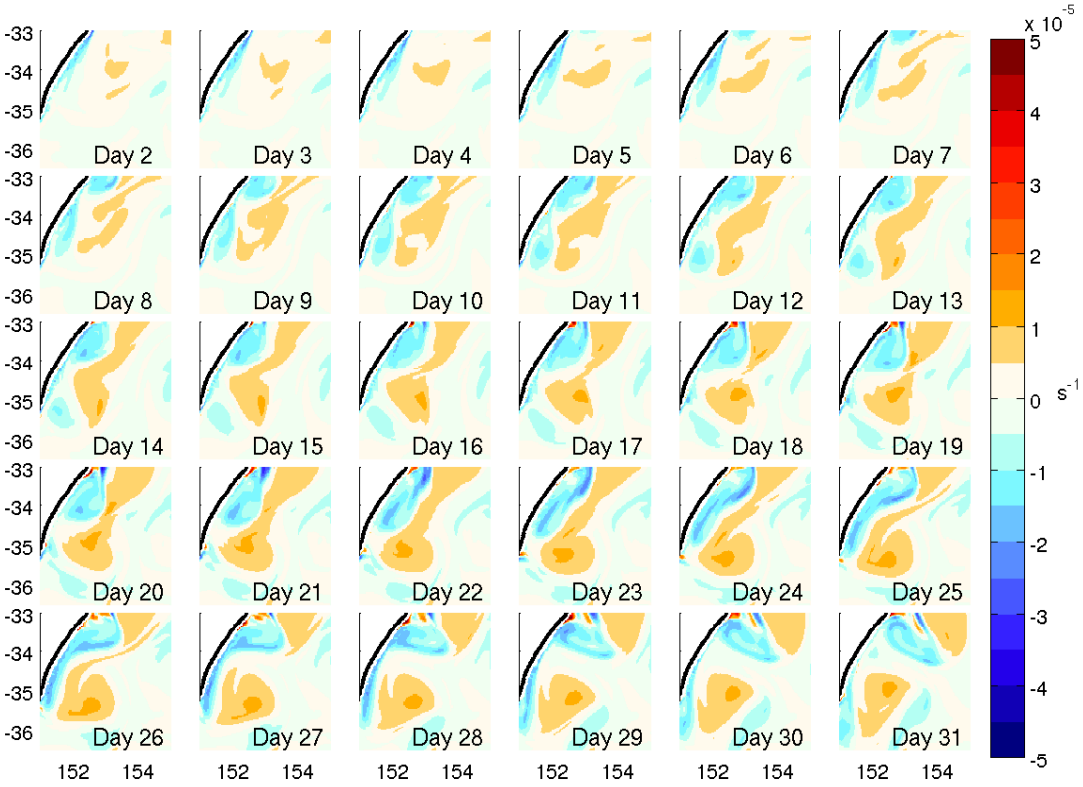

Figure 3.6: Vorticity (s^{-1}) at 500 m depth for model days 2 to 31. Negative (blue) indicates cyclonic vorticity and positive (red) indicates anticyclonic vorticity.

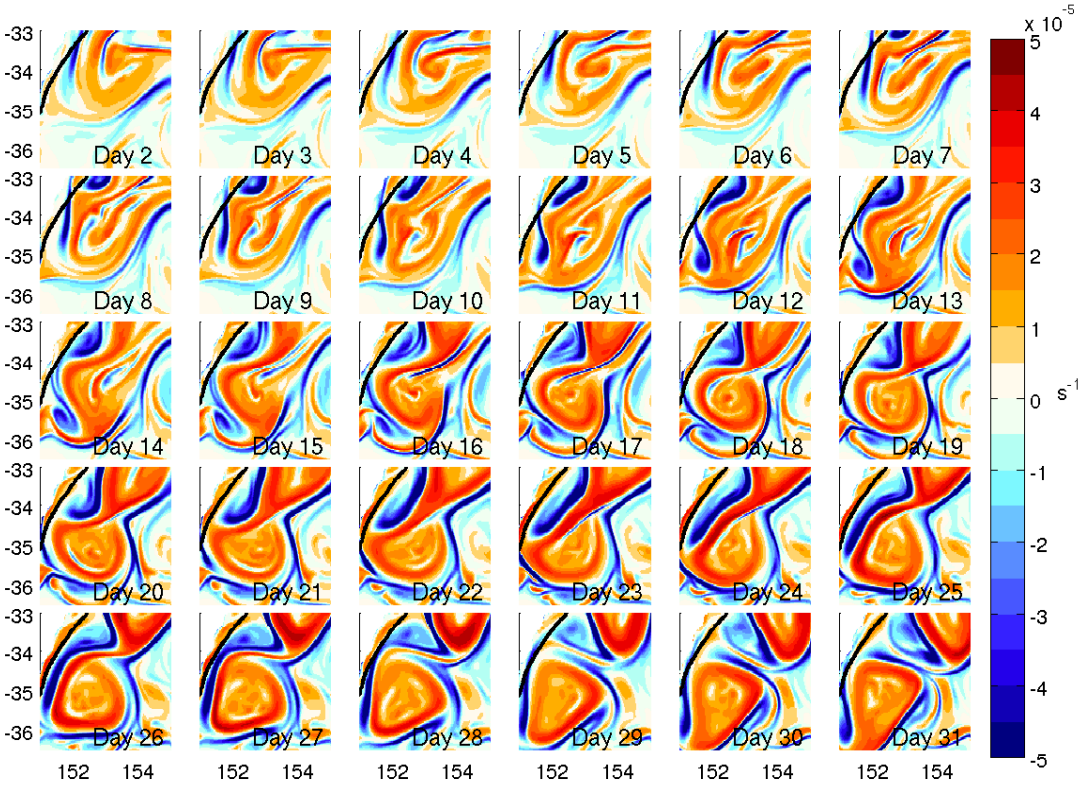

Figure 3.7: Surface vorticity (s^{-1}) for model days 2 to 31. Negative (blue) indicates cyclonic vorticity and positive (red) indicates anticyclonic vorticity. The 200 m isobath is indicated in black.

This cyclonic vorticity moves into the centre of the eddy between days 2 and 9 and is then expelled from the eddy between day 13 and 18.

The expulsion of cyclonic waters allows the overwashing of a filament of high vorticity waters which leads to an increase of vorticity at the centre of the eddy. At the start of the simulation, the centre of the eddy had a vorticity from approx -2×10^{-5} which increased to around 2.5×10^{-5} s^{-1} by the end of the simulation. The vorticity of the outside ring of the eddy decreases during this vorticity transfer from 3.4×10^{-5} to 2.5×10^{-5} s^{-1}.

3.3.4 Water movement within the eddy

Streamlines can define the subsurface boundary of an eddy while giving a snapshot of the velocity field at a particular time. In particular they show regions of upwelling and downwelling. The passive tracers and the Lagrangian paths of the next section show the movement of water parcels. Streamlines differ from this as they capture the structure of the current field of the eddy at a given time. As it can take up to 8 days to complete a rotation around the eddy, the streamlines may have changed during that time, so it should be noted that these are not an indication of the path that a particular particle within the eddy will take.

Streamlines are calculated using the Matlab function *stream3* with a step-size of 1/10th of cell and maximum verticies of 10000. The streamlines were calculated using daily averaged 3D velocity field with an initial position located through an east/west transect from the outside to the centre of the eddy (by 0.05° intervals from 152.6°E to 153.1°E at 34°S, 152.1°E to 153°E at 34.6°S and

151.5°E to 154.9°E at 35.4°S on model days 7, 13 and 23 respectively). This is conducted with streamlines originating at 1 m and repeated at 200 m depth giving a 3D picture of the flow within the eddy.

On model day 7 (14 October; Fig. 3.8A-F) the streamlines indicate that there is a large eddy which extends vertically through the water column as evidenced by the closed streamlines at 0 and 200 m (Fig. 3.8 A and D). There is a flow of EAC water encircling the eddy which exits in a northeast direction. Most of the streamlines at both depths are spiraling down (Fig. 3.8B and E; indicating downward spiral of water in this section of the eddy). The exception to this is a small area in the centre at 200 m depth where the streamlines spiral up to the surface due to a small but intense upwelling (shown by red lines; Fig. 3.8E).

On model day 13 (20 October; Fig. 3.8G-L) the surface streamlines are not closed (Fig. 3.8G). This means that they leave the eddy rather than completing a 360^o rotation around the eddy. This is due to flow into and out of the eddy, flushing out most of the surface waters of the eddy. At 200 m depth the streamlines are closed, indicating that the flushing only occurs in the surface and that an eddy still exists underneath (Fig. 3.8G). There is a small amount of downwelling in the centre of the eddy but an upward spiral of water on the edge of the eddy (Fig. 3.8K). This shows a tendency for the water to downwell at the centre but upwell near the edges (opposite to day 7).

By model day 23 (30 October; Fig. 3.8 M-R), during the overwashing, the surface streamlines have closed again (Fig. 3.8M). This leaves a large eddy enclosed by the streamlines. In the middle of the eddy the water is trapped at the surface, with no downward spiral. At depth there is downwelling so that

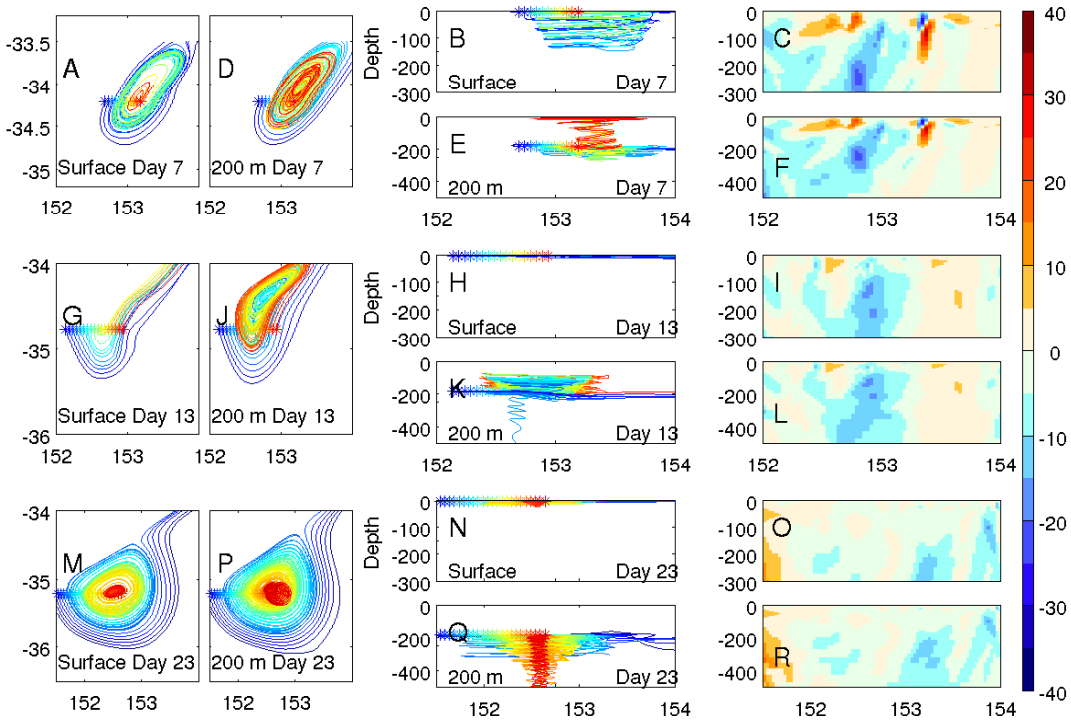

Figure 3.8: Streamlines calculated with 10000 steps of 1/10 of cell (of size $0.1^o \times 0.1^o \times 10$ m) and vertical velocities within the eddy. A view of the streamlines is shown from on top (left) and one side (middle). Panels on the left and middle show streamlines from 2 different depths (surface and 200 m). Colours show radial distance at the beginning of the streamline. This is on model day 7 (top two rows; A, B, D and E), model day 13 (middle two rows; G, H, J, K) and model day 23 (bottom two rows; M, N, P, Q). Right shows a vertical transect of the vertical components of velocity (m d^{-1}) through the eddy on model days 7, 13 and 23 (corresponding to the streamlines on the left). A red velocity is an upward velocity and a blue velocity is a downward velocity. The velocity fields used in this figure are daily averages. Note a * indicates the starting points. Day 7 is A-F, Day 13 G-L and Day 23 M-R.

the lateral transport into the eddy at the surface is balanced by the downward movement of water (Fig. 3.8Q).

The subsurface temperature of the eddy

The 3D structure of the eddy's temperature is visualised by removing the southwest quadrant to show vertical sections along 35°S and 153°E. The EAC can be seen by the warmer water around the edge of the eddy (Fig. 3.9B). Ten days later (model day 23; 30 October) the EAC has overwashed the eddy and has formed a layer (20-90 m thick) of 24°C water on top of the eddy.

3.3.5 Movement of water

During the simulation, EAC waters enter and exit the eddy in the north. On day 24 the net flow for areas above 285 m through a transect north of the eddy is 5 Sv into the eddy (not shown). This extra water entering the eddy will either result in water leaving the eddy, the eddy growing, or the surface waters sinking. On day 24, 1.2 Sv of the incoming water is balanced by sinking water. The remainder is ejected from the eddy or contributes to the growth of the eddy. This section looks at the sinking waters.

Between days 19 to 27 the vertical velocity in the eddy becomes a strong, downward flow, averaging 1.4 m d^{-1} (Fig. 3.10 Top). Over this period the average sinking in the eddy is 11.4 m. After day 27 the eddy separates from the EAC, eliminating the source of EAC waters to the eddy and sinking stops.

This sinking is also evident in profiles of temperature and salinity (Fig. 3.10 bottom right and left). Temperature and salinity profiles through the centre of

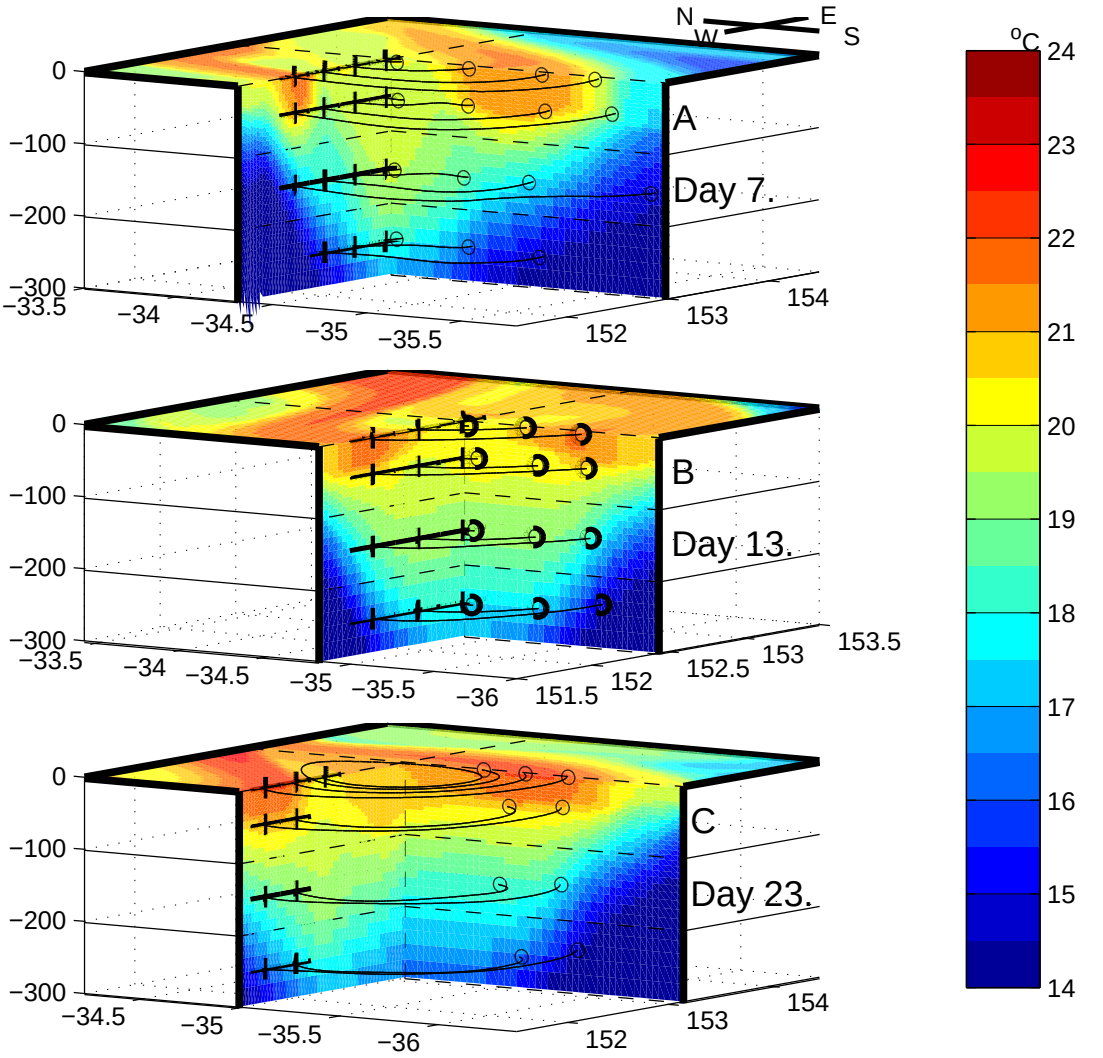

Figure 3.9: 3D profiles of temperature (°C) from model day 7 (top), 13 (middle) and 23 (bottom). Streamlines within the eddy are shown as an indication of the eddy boundary. These streamlines are initialised along the west/east line (34.3°S in A and B and 35°S in C) at surface, 50 m, 150 m and 250 m depth at 0.3° longitude intervals. Only those streamlines which stay within the eddy are shown.

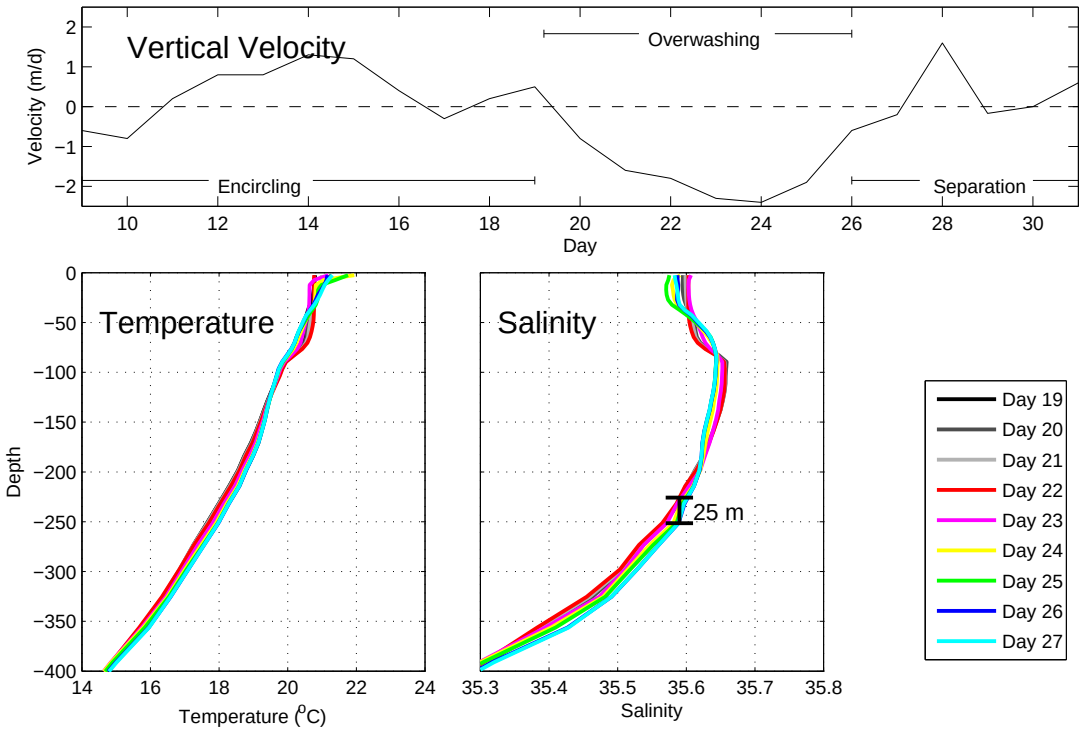

Figure 3.10: Average vertical velocity at 285 m in the eddy (top). Negative indicates downward movement and positive indicates upward movement. Profiles of temperature (bottom left) and salinity (bottom right) through the centre point (as defined by the highest sea-level elevation) of the eddy. These profiles are for days 19 to 27, coloured as indicated by the legend. The vertical movement of the isohalines in indicated on right.

the eddy show that, at depths below 100 m, T and S properties sink by 10-25 m over days 19-27. The spatial extent of this downward vertical movement is also evident in the depth tracer.

The depth tracer quantifies the vertical movement of water over the course of a day (Fig. 3.11 A-C) or from the time since model day 1 (Fig. 3.11 D). The 3D structure of the tracer properties within the eddy are visualised by removing the southwest quadrant to show vertical sections along 35°S and 153°E (in a similar manner to Fig. 3.9). A layer of water that has risen, sitting above a layer of water that has sunk (i.e. red on blue), can be a result of vertical mixing. This is evident in the surface layer of the eddy from model day 7 (14 October; Fig. 3.11 A). During the overwashing (day 23; 30 October; Fig. 3.11 C) the submergence is occurring in the eddy centre and water from the edge of the eddy is being uplifted.

Over the course of the simulation, up to model day 23 (30 October; Fig. 3.11 D), there is a subducted area in the south of the eddy (35° S-35.7°S, along the 153°E line). This core of the eddy (originally sitting at 0-200 m depth) has sunk 20-90 m since the beginning of the simulation.

The results of the depth tracer could be affected by vertical mixing. The surface mixed layer of the eddy is 50-100 m thick (Fig. 3.10) so it is not expected that the results of the depth tracer below this depth will be changed by mixing. The Peclet ($Pe = \frac{wL}{A_v}$ where w is the vertical velocity, L is a length scale and A_v is the vertical diffusivity) number can be used to determine if the vertical movement regime is dominated by diffusion or advection. Small Peclet numbers indicate that the vertical movement is dominated by diffusion. If the eddy is

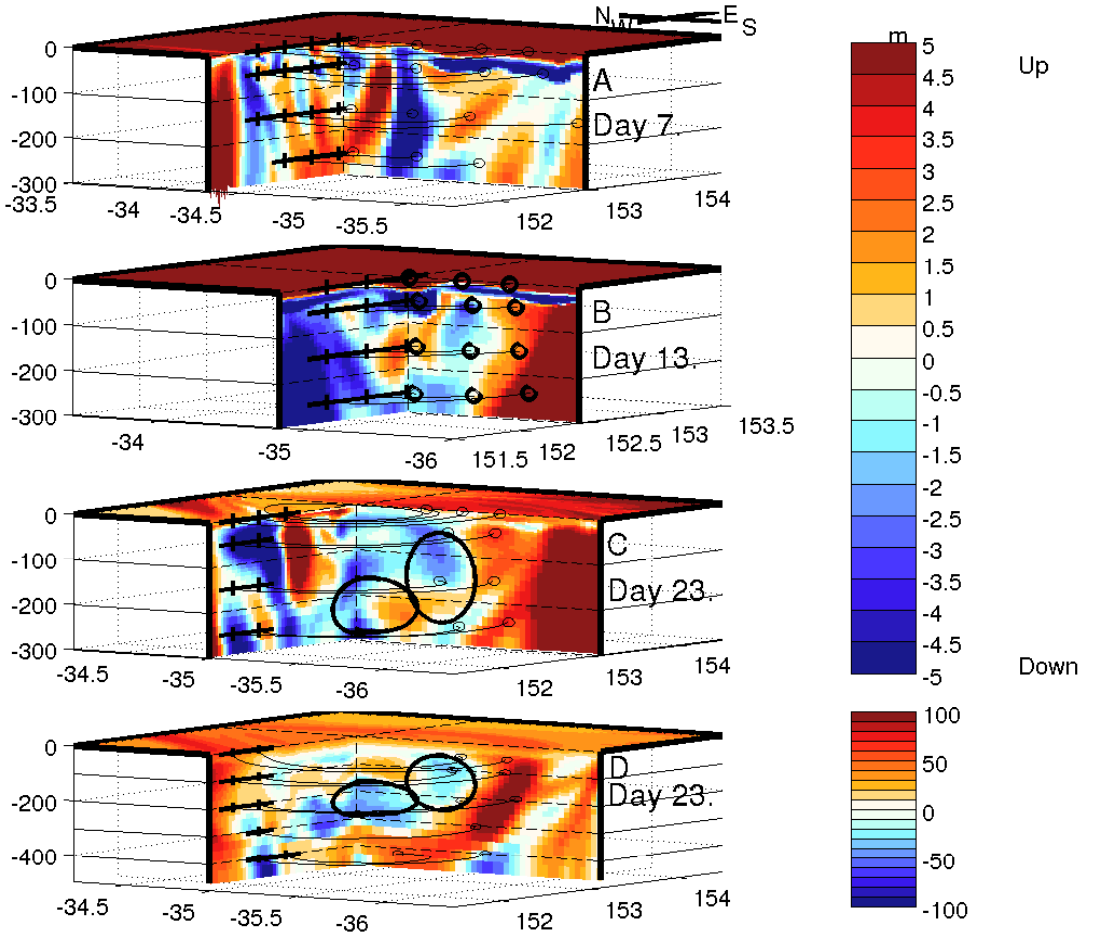

Figure 3.11: 3D profiles of depth tracer. This is the change in tracer concentration over the period of a day for model day 7 (A; top), 13 (B; middle-top) and 23 (C; bottom-top). Red indicates that the water has been uplifted and blue indicates that it has been downwelled over the period of a day. Bottom (D) shows the vertical movement of water between the beginning of the simulation and day 23. Note the depth limits on D go down to 500 m. Streamlines within the eddy are shown as an indication of the eddy boundary. These streamlines are initialised along the west/east line (34.3°S in A and B and 35°S in C and D) at surface, 50 m 150 m and 250 m depth at 0.3° longitude intervals. Only those streamlines which stay within the eddy are shown. The black ovals indicate the areas referenced in Sec. 3.3.5 which are submerged original eddy waters.

dominated by diffusion a length scale for this diffusion can be estimated from A_v/f where f is the Coriolis parameter. Here we use a daily average of A_v and w for each day during the simulation and the mixed layer depth as a length scale.

In the model, areas above 100 m depth have a Peclet number less than 1000 and the diffusive mixing scale is 0.1-1 m depth. Below 100 m the Peclet number is greater than 1×10^5 and the mixing scale is 0.1 m. Therefore, while the depth tracer for areas above 120 m could be affected by mixing, the vertical movement below 120 m seen in Fig. 3.11 is due to vertical advection, not mixing.

The latitudinal tracer (Fig. 3.12) indicates the latitude at which a parcel of water was either located on model day 1, or entered into the model domain. The eddy's initial latitudinal range was 33-35°S and the EAC entering the model domain from the northern boundary is given a value of 26.03°S. During the overwashing (model day 23) water from the original eddy (33°S) can easily be differentiated from the EAC water that encircled the eddy (Fig. 3.12 C). On model day 7 (14 October; before the overwashing begins) the EAC can be seen encircling the eddy. By model day 13 the EAC is still rotating around the eddy and a small amount of EAC waters can be seen near the centre of the eddy.

By model day 23 (30 October) the eddy has grown and the EAC has flushed the eddy. Using T and S properties to calculate how much water was originally in the eddy and the latitudinal tracer as a marker to calculate how much was left shows that, for areas above 300 m, only about 30 % of the water remaining in the eddy was present originally. A small core of original eddy waters exist at 35-35.7°S along the 153°E line, corresponding to regions of sinking (circled in Fig. 3.12E and 3.11D). This shows that there is a small part of the eddy which

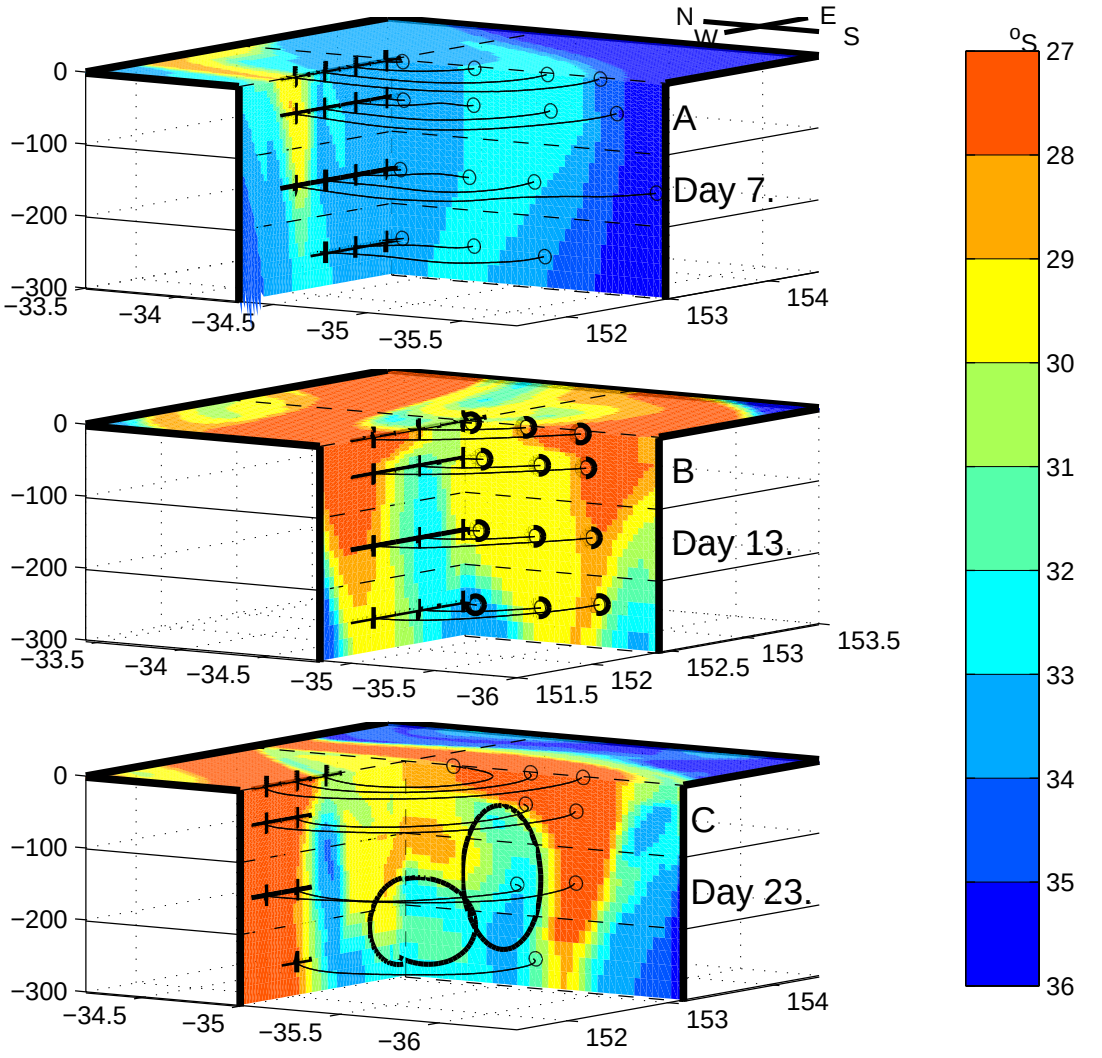

Figure 3.12: 3D profiles of latitude tracer from model day 7 (top), 13 (middle) and 23 (bottom). Red indicates water that has originated from the north and blue indicates water that has originated from the south. Streamlines within the eddy are shown as an indication of the eddy boundary. These streamlines are initialised along the west/east line (34.3°S in A and B and 35°S in C) at surface, 50 m 150 m and 250 m depth at 0.3° longitude intervals. Only those streamlines which stay within the eddy are shown. The black ovals indicate the areas referenced in Sec. 3.3.5 which are submerged original eddy waters.

has been submerged due to the surface overwashing, leaving an EAC layer above the original eddy.

The rest of the eddy has a small portion of EAC waters (27°S) in the surface 50 m, and water from 31°S to 28°S in the lower waters. This signal could be due to water that originated in the EAC at approximately 30°S, or a mixture of EAC and eddy waters.

3.3.6 Lagrangian pathways within the EAC

To investigate the Lagrangian pathways of the EAC around and over the eddy particles are released on day 5 in the EAC upstream of the eddy (north at 31.2°S) at the surface, 50 m and 100 m depth (Fig. 3.13). Upstream of the eddy there is little vertical movement within the EAC so when the particles reach the eddy they are at a similar depth as their starting position (Fig. 3.13, bottom row). Between days 13 and 25 the EAC (and Lagrangian particles) enters the eddy. How these particles enter the eddy differs for particles released at different depths.

The surface release particles flow onto the top and into the middle of the eddy with the surface overwashing current. These particles then sink with the eddy. Most of the particles released at 50 m and 100 m depth rotate around the eddy and leave with the EAC through the northeast corner. Approximately a third join the eddy as the EAC closes around the eddy, forming a complete loop. Unlike the surface release particles (which move into the centre of the eddy with the overwashing EAC), these particles stay on the periphery of the eddy.

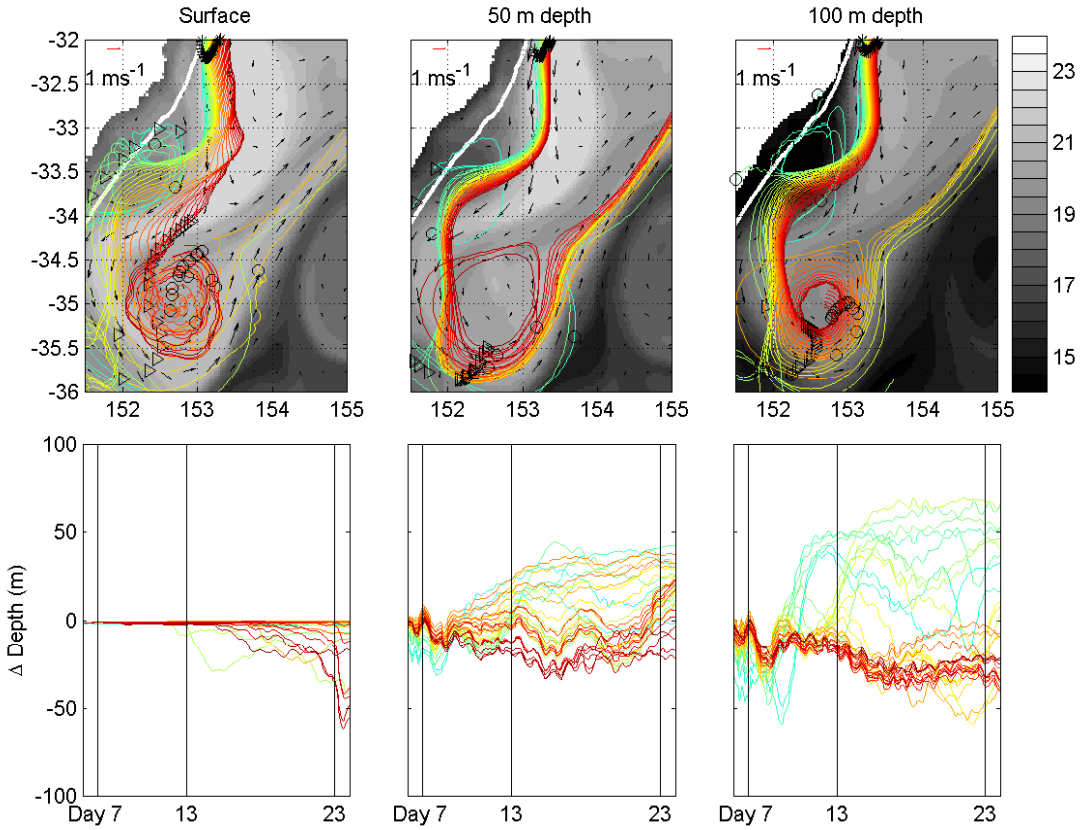

Figure 3.13: Lagrangian paths of particles released on day 5 within the EAC. Left is at the surface, middle is 50-60 m and right is 100-120 m. The top row shows the horizontal view of the particle tracks and the bottom shows the vertical displacement of the particles versus time. The colours of each particle in the top row corresponds to the colours of the particles in the bottom row. A white * in the top row indicates the particle position on day 7, a triangle indicates the particle position on day 13 and an o indicates the particles position on day 23. The shading indicates temperature and the arrows indicate velocity (direction and relative speed) on model day 5 for each of the three depths (surface, 50 m and 100 m from left to right).

3.4 Discussion

3.4.1 Buoyancy

The eddy grows in the EAC retroflection zone by the transfer of vorticity and mass from the EAC into the eddy. In this case overwashing provides a process for this energy transfer to occur. The density gradient between a WCE and surrounding waters is such that, typically, the eddy is more buoyant than the surrounding waters, making movement over the eddy (or overwashing) impossible without another forcing. However, in the case presented here the surface density gradient between the WCE and the EAC is reversed to that of a typical WCE in that the surrounding (EAC) waters are more buoyant than the eddy waters. As such, a process such as overwashing is expected. Despite this buoyancy difference the overwashing did not occur from the beginning of the simulation. Why this is the case can be answered by looking at the evolution of vorticity within the eddy.

3.4.2 Causes of the overwashing

During the simulation the eddy transforms from an unstable eddy where the vorticity gradients increase outwards and the density distribution is not at its lowest state of available (gravitational) potential energy to a stable (typical) eddy where the vorticity gradients decrease outwards. The eddy begins in a state of disequilibrium with a higher vorticity ring on the outside. Cyclonic vorticity (Fig. 3.7; at the density front between the EAC and the eddy) acts as a barrier to prevent this high vorticity EAC water from entering the eddy. During

days 7 to 18 the waters of cyclonic vorticity are expelled from the eddy and a filament of high vorticity water is pulled from the EAC into the centre of the eddy. The vorticity intensification at the eddy centre results in convergence and downwelling. This in turn pulls in more high-vorticity filaments of water from the EAC ring around the edge of the eddy. This feeds the vorticity intensification and, from day 19, there is high vorticity water spiraling into the eddy centre. The question which remains is what caused the eddy to expel the cyclonic vorticity waters?

A warm-core eddy will have surface convergence and downwelling at the eddy base when it is forming, but upwelling and surface divergence when it is decaying (Bakun, 2006). The cyclonic vorticity made the eddy unstable so that it expelled water to the north. Once the cyclonic vorticity had been expelled the areas of divergence associated with the cyclonic waters disappeared and the eddy transformed to a more balanced state (convergent in the centre, pulling in water from the warm-ring on the edge). This then drove the overwashing of water from the EAC (and even perhaps separation of the eddy).

3.4.3 Conceptual description of the overwashing process

The overwashing process results in a two layered system (for this conceptual model divided at a depth of around 70 m; Fig. 3.14 A and B). The bottom layer (layer 2) is a classical WCE with a warm, less dense centre and density *increasing* radially outwards. The top layer (layer 1) extends from 70 m to the surface and is where the EAC is interacting with the eddy. As the EAC which wraps around the eddy is deeper than the shallow flooding current the density in

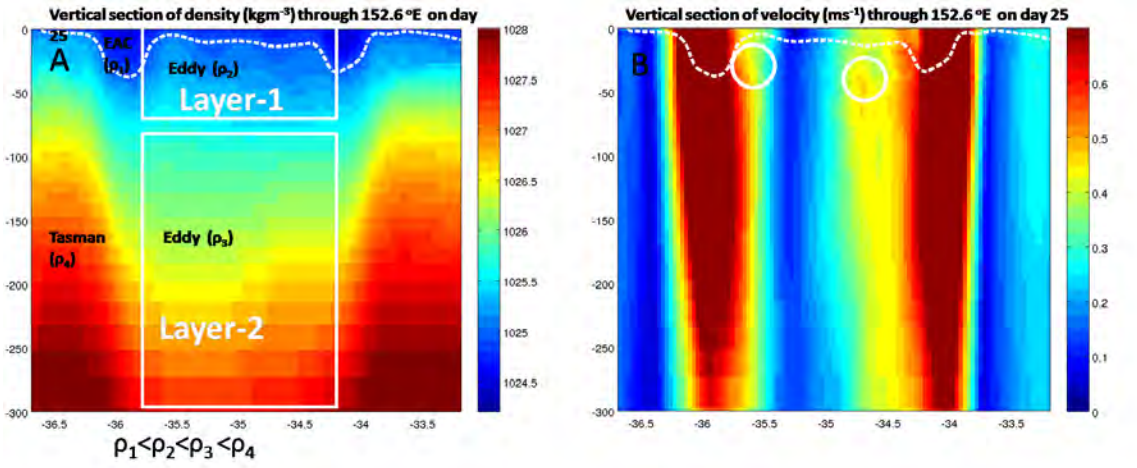

Figure 3.14: A density cross-section through the eddy at 152.6 °E on day 25 (left). The layer in which the EAC is overwashing (Layer 1) and the traditional eddy layer (Layer 2) are indicated. Right: a vertical cross-section of horizontal velocity magnitude through the eddy at 152.6 °E on day 25. The white circles indicate positioning of subsurface velocity maximums. The dashed white density contour on both left and right (1024.9 kg m^{-3}) indicates the overwashing EAC.

this layer *decreases* radially outwards as the EAC (overwashing from the outer edge initially and then moving towards the centre of the eddy) is also less dense than the eddy.

To show the contributions of each layer to the overall velocity field we investigate the geostrophic currents using the dynamic height anomaly in each layer. As the dynamic height anomaly of the bottom layer will contribute to the overall geostrophic currents of the upper layer (i.e from 100 m to the surface) the currents in the top layer are calculated assuming no height anomaly at 100 m depth.

Although the WCE is rotating anti-cyclonically, there is a cyclonic component of the velocity field along the front between the EAC and the WCE (Fig. 3.15 B and Fig 3.7, Day 25). This cyclonic component of velocity, although small relative

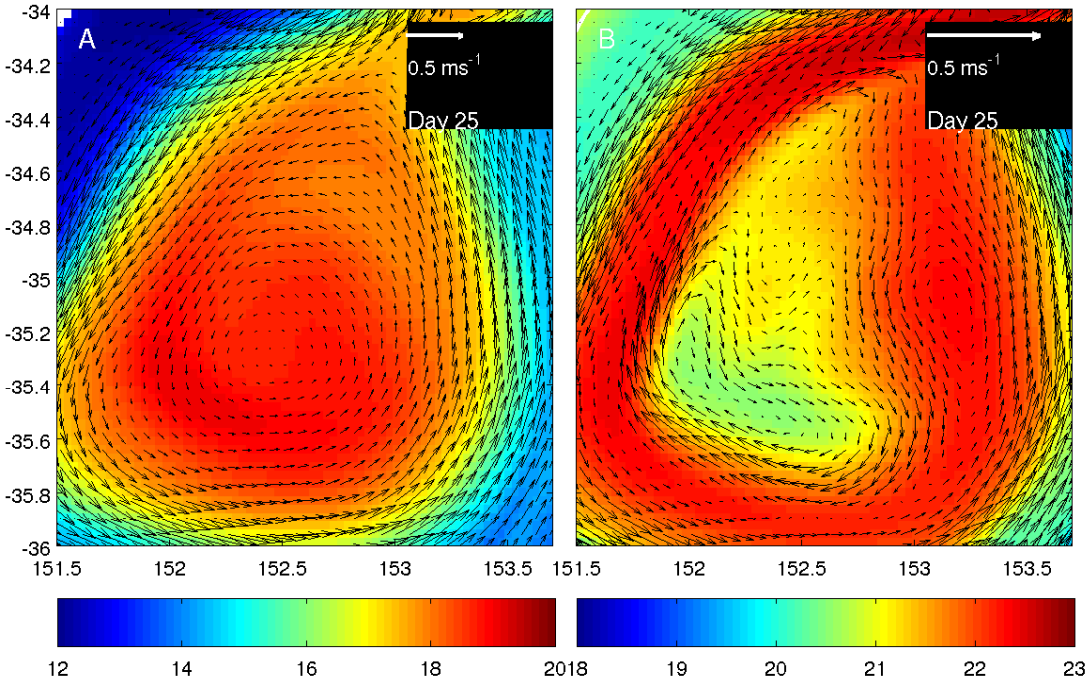

Figure 3.15: Temperature at a depth of 100 m (A) and at the surface (B) on day 25. Arrows represent the geostrophic velocity through the water column (A) and in the top layer (B), i.e. assuming a level of no motion at a depth of 100m. Note the velocity scale is different between the two panels.

to the surface velocity, is opposite to that of the anti-cyclonic flow of the eddy (Fig. 3.15). The resultant velocity is an anti-cyclonic flow in the top layer which is slower than the flow of the eddy directly underneath it resulting in a subsurface velocity maximum (Fig. 3.14 B).

3.4.4 Could the causes of overwashing be different between the model and observations?

The modelled eddy is similar to the eddy as observed in Baird et al. (2010). There are some differences between the model and observations which will be

explored as they could be an indication of (or lead to) different processes within the eddy.

In the model the eddy separates from the EAC on model day 27 (around the 2 November) whereas the observed eddy does not separate for another 31 days (3 December). In addition, the submergence in the observations started earlier and was more extensive (approximately 50 m). This could also be an indication of different processes driving the submergence and will directly affect the volume of EAC waters entering the eddy. Less water entering the eddy is the most likely cause of the shallower submerged depth in the model as compared to the observations. While a direct measure of other effects that these differences could have on the results presented here cannot be obtained, there are some indirect measures which can show how robust the conclusions of this paper are.

One of the main results of this paper is that vorticity intensification drives some of the overwashing. An eddy in geostrophic balance rotate due to the sea-level gradient. Hence, sea-level height changes are a good indication of changes in vorticity and both the observed and modelled sea-level height changes evolve similarly. In particular, the sea level height changes in the observations and model from days 17 to 26 are generally in good agreement (Fig. 3.3G). This is when the vorticity intensification occurs in the model so it is likely that it is also occurring in the observed eddy.

The cyclonic vorticity which appeared as a barrier between the EAC and the eddy could not be resolved in the geostrophic currents derived from altimetry. As the overwashing in the observed WCE preceded that of the modelled WCE it is possible that this barrier might not exist in the observed eddy. The observed

eddy, however, did not immediately start sinking below the EAC (despite the EAC having a greater buoyancy from the start) so a barrier to the submergence does exist.

3.5 Summary

For the first time, we have successfully modelled a WCE observed off south-east Australia that was encircled and then overwashed by the EAC before separation. This simulation provided the ideal opportunity to investigate the spatial and temporal evolution of an overwashing WCE in a western boundary current. We have identified 2 distinct stages in the process, the encircling of the eddy (days 1-18) and the overwashing of the eddy (days 19-27).

During the encircling phase the eddy was a small, typical downwelling eddy. While both the EAC and the eddy had an anticyclonic vorticity, a cyclonic barrier formed between them. The EAC encircled the eddy and this cyclonic water was ejected from the eddy to the north. This pulled in high-vorticity waters from the EAC which then spun up the eddy.

During the overwashing phase the EAC retroflection formed a closed loop around the eddy, becoming part of the eddy. A shallow surface current moved across the original eddy, mixing with the original eddy waters. The mixed overwashing current submerged the original eddy which resulted in a two-layered system where the bottom comprised of the original Tasman Sea eddy water and the top comprised of EAC waters. This two-layered system had a subsurface maximum velocity at the interface of the two layers. The vertical circulation structure changes during the overwashing process whereby the eddy was sub-

merged at the core and then pushed up the edges.

Chapter 4

The formation of a cold-core eddy in a Western Boundary Current.

Abstract

Cold-Core Eddies (CCEs) are a common feature in Western Boundary Currents such as the East Australian Current (EAC). We use the Regional Ocean Modelling System to investigate the ocean state during the formation of one such CCE in the EAC during October 2009. The eddy initially appears as a small billow (approx. 50 km in length) which cuts into the edge of the EAC. The billow grows into a mesoscale CCE (approx. 100 km in diameter), diverting the EAC around it. We investigate potential drivers of eddy formation such as lateral gradients in temperature and velocity. The impact of

3 wind forcing scenarios: upwelling, downwelling and realistic winds are investigated. In all three cases a cold-core eddy formed, although the location, size and magnitude of isotherm uplift changed. The eddy in the upwelling wind scenario formed further south and moved further south than the other 2 scenarios. The maximum uplift of the 16^{o}C isotherm was produced in the downwelling wind scenario due to a stronger northward flow on the continental shelf which drove greater velocity shear. The curvature of the coastline and gradients in density from shelf to slope water were necessary for eddy formation. Analysis of energy transformation shows the prevailing source of CCE eddy kinetic energy was the EAC.

4.1 Cold-core eddies

4.1.1 Review of cold-core eddies

CCEs generally form from instabilities in the flow in the vicinity of major western boundary currents (e.g. the Kuroshio (Kasai et al., 2002; Kimura et al., 1997), The Gulf Stream (Lee et al., 1991) The Agulhas Current (Lutjeharms et al., 2003), and the East Australian Current (Everett et al., 2011)). These CCEs within western boundary current systems have sizes ranging from submesoscale (diameter $\sim$10 km) to mesoscale (diameter $\sim$ 100 km) and last for timescales of days to weeks.

One type of CCE that forms in and around western boundary currents (WBCs) are called frontal (Lee et al., 1991; Kimura et al., 1997) or shear-edge

(Lutjeharms et al., 2003) eddies. This group of eddies is small, of the submesoscale to mesoscale size. They form on the inshore edge of the WBC on the front between the warmer WBC and the typically cooler coastal waters. Their formation is attributed to baroclinic instabilities (Ikeda et al., 1989; Lutjeharms et al., 2003; Jia et al., 2011), or a combination of baroclinic and barotropic instabilities (Lutjeharms et al., 2003; Oke and Griffin, 2010).

Studies on frontal CCEs can be difficult, resulting in sparse research being performed on them. These small, submesoscale frontal cold-core eddies are hard to capture in satellite altimetry. This means that they can be under represented in automated eddy census methods such as that of Chelton et al. (2011). Additionally, their short lived life spans mean that they are often missed by autonomous observation systems such as ARGO or surface drifters and can be difficult to target with glider or research cruises.

Theoretical models of the coastal zone Csanady (1979, 1977, 1971) can reproduce features of eddies and upwelling in the coastal region while only looking at simple interactions. This indicates that often seemingly complex coastal features can be explained by simple processes. A realistic estimation of these eddies is, however, hard to capture in numerical modelling studies. Their small scale (10-100 km) necessitates a high resolution model. However, the larger scale features (like the WBC) are required to form the barotropic or baroclinic instabilities that contribute to eddy formation. This means that the model needs a high resolution (<5 km) over a large area or a nested grid to capture the formation of these eddies. Even with a sufficient resolution, frontal eddies form in a highly variable and energetic area, making them difficult to capture in a modelling study. It is

no surprise then, that these eddies are under-studied.

4.1.2 Cold-core eddies in the East Australian Current

Physical and biological processes on the continental shelf off southeast Australia are dominated by the presence of the East Australian Current (EAC), a poleward flowing western boundary current (Godfrey et al., 1980b). The evolution of the EAC has been described by Ridgway and Dunn (2003). The EAC forms between 15^0S and 25^0S, and extends along the East Australian coast, intensifying as the shelf narrows. The EAC has been observed to travel at speeds greater than 1 m s^{-1} (Godfrey et al., 1980a; Nilsson and Cresswell, 1980) and can extend to depths of 2000 m. The EAC bifurcates between 30^0S and 31.5^0S. The eddy variability associated with this bifurcation can be larger than the current itself so the EAC is not always distinguishable as a coherent current (Godfrey et al., 1980b).

Previous modelling studies of the EAC have focused on large scale features like the EAC separation and shedding of eddies (Marchesiello and Middleton, 2000; Tilburg et al., 2001; Wilkin and Zhang, 2007), long timescales (Wilkin and Zhang, 2007; Roughan et al., 2011), or biogeochemical processes (Baird et al., 2006a,b; Macdonald et al., 2009; Roughan et al., 2003). The smaller scale eddies ($\sim$100 km) occurring on short timescales (days to weeks) have not been adequately resolved in previous modelling studies and, as such, have not been fully investigated in this region.

One of the few modelling studies on CCE's in the EAC region (Oke and Griffin, 2010) found that an eddy formed via a combination of baroclinic and

barotropic instabilities. Oke and Griffin (2010) propose that the eddy formation was connected to the strong upwelling events that occurred at the same time. A direct link could not be found as the model representation of the eddy formation was assisted by a data assimilation process.

Oke and Griffin (2010) also found that CCEs could tilt onto the continental shelf (i.e. the centre point of the eddy in the surface is closer to the coast than the centre point of the eddy at depth) and Brassington et al. (2011) have confirmed that tilting eddies are a common feature for the Tasman sea. In a Southern Hemisphere WBC the coastward tilt of the CCE results in uplift of the water in the southern part of the eddy, as the flow is onshore, and downwelling in the northern segment.

In October of 2009 a CCE formed between the EAC and the Australian coastline. It was observed using different platforms including satellite sea-surface temperature (SST), gliders and shipboard CTD and ADCP instruments. The numerous observations of the eddy make it an ideal case study to assess the ability of a numerical model to reproduce the eddy while also adding spatial and temporal resolution to the observational data on the eddy.

The aims of this study are to ascertain how well the model can reproduce a small scale CCE in the EAC and then to understand the forcing mechanisms driving eddy formation. In particular, we can look at how this eddy changes over time and how vorticity contributes to the eddy formation (Sec. 4.3.2). To investigate the importance of barotropic, baroclinic and bathymetric factors a sensitivity analysis is performed with different wind fields (Sec. 4.3.3), bathymetric and initial conditions (Sec. 4.4.5). The transfer of kinetic and potential

energy between the mean field and the eddy field is investigated in terms of barotropic and baroclinic instabilities (Sec 4.4.4).

4.2 Methods

4.2.1 The model configuration

The ocean state of the October 2009 CCE is simulated using the Regional Ocean Modelling system (ROMS). A detailed description of the model's configuration for the EAC region can be found in Chapter 2 and a brief summary is included here. SynTS (Ridgway et al., 2008) is used to prescribe initial, boundary and climatology data. The Flather (1976) condition is used for the barotropic velocity components at the northern boundary. The baroclinic velocity field and the tracers on the northern boundary are nudged to external estimates at a timescale of 4 days. All other boundaries are radiative. NCEP 2.5-degree 6 hourly reanalysis data sets (Kalnay et al., 1996) and the NOAA/NCDC Blended 6-hourly 0.25-degree Sea Surface Winds data set (Zhang et al., 2006) is used to implement the Bulk flux method of Fairall et al. (1996) at the atmospheric boundary. The model is initialised on 18 September 2009 and has a 5-day spin-up. More details on the grid, forcings and initial conditions can be found in Chapter 2.

4.2.2 The model grid

The model grid is modified from that used in Chapter 3. The resolution has been increased to approximately 1.75 km by 2.15 km and no limit has been set

on the maximum depth. The resultant grid has 828 grid squares in the zonal direction and 684 grid squares in the meridional direction. The grid covers a region between 29.9°S to 37.33°S and 149.1°E to 159.2°E (Fig. 4.1A). A high resolution (2 × 2min) bathymetry from the Naval Research Lab (DBDB2 V3) has been interpolated onto this new grid. The bathymetry has been smoothed using a smooth positive method (Sikiric et al., 2009) to minimise the pressure gradient error associated with terrain following models (Mellor et al., 1994).

The vertical coordinate system is implemented using 50 layers with the stretching scheme configured so that most of the resolution is stretched to the top of the water column for depths greater than 250 m (Fig. 4.1B).

Bass Strait is situated just south of the model's southern boundary and is a geographical origin for coastally trapped waves (CTW) (Middleton, 1988). The southern boundary of the model is radiative so that these CTWs do not enter the domain and, hence, do not influence the model's solution. This limits errors originating from CTW formed from initialisation shock at the start of the simulation. The exclusion of CTWs does, however, place some limitations on the constant upwelling wind forcing described in the next section. The constant wind field should initiate the northward propagation of CTWs originating in Bass Strait. These waves will travel at speeds of c=fL (where f is the Coriolis parameter, 8×10^{-5}, and L is the shelf width, 50 km for this estimate). This yields a speed for the CTW of about 345 km d^{-1} and the CTW will reach the eddy formation area after 2-days. These CTWs act to shut down upwelling (Middleton and Leth, 2004) so that the uplift reported in the upwelling wind scenario will be larger than that which will would occur if CTW were included. The aim of these

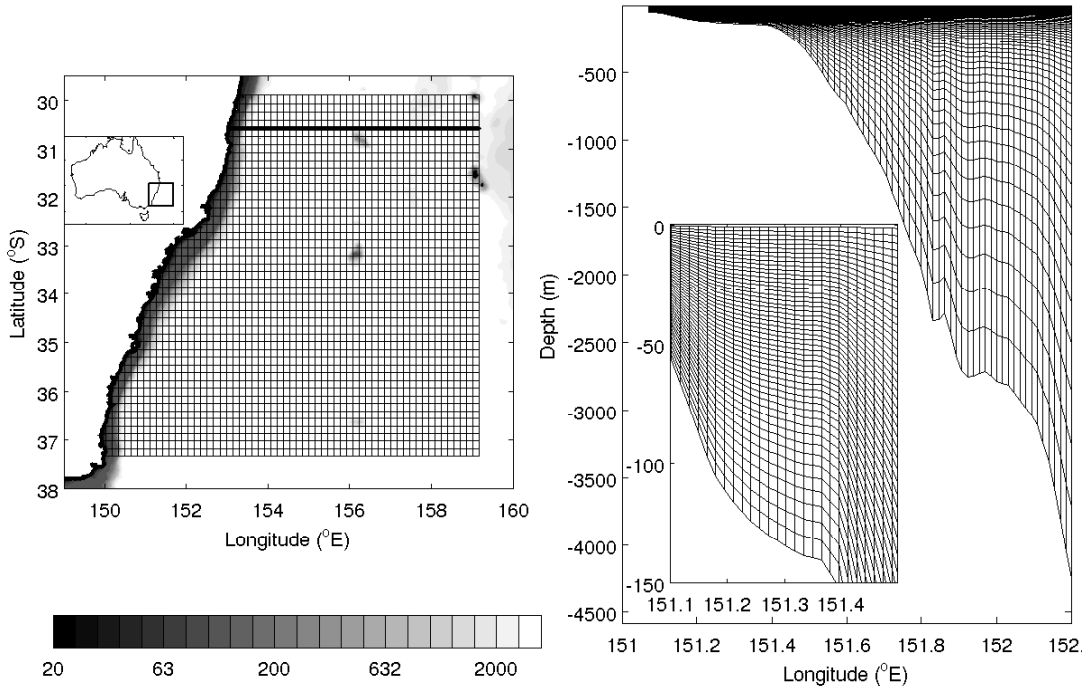

Figure 4.1: The model grid. Left shows horizontal resolution. Every 10th grid line is shown and the shading show bathymetry on a log scale. The thick black line at 30.58^{o}S indicates the southern extent of the northern boundary nudging. The location of the model grid is indicated by the rectangle in the insert of Australia. Right shows the vertical resolution for different model depths through 34.19^{o}S. The insert shows the vertical resolution for the top 150 m.

idealistic scenarios is not to represent a realistic situation for this study area. Rather the simulations aim to create a reaction to a known change in forcing (i.e. upwelling and downwelling on the continental shelf due to the windfield) so it is thought that the lack of CTW will not significantly affect the conclusions.

4.2.3 Model simulations

We explore the effect of the wind field, bathymetry and initial conditions on the eddy generation through a suite of numerical simulations (summarised

in Table 4.1). To explore to effect of the wind field, three different scenarios are presented. Each scenario has the same forcing with the exception of the wind field. In the 1st simulation the model is forced with realistic winds (RWS) from the NOAA/NCDC Blended Winds data set (Fig.4.2; $\sim$ 30 days). A further two scenarios are given a constant 10 m s^{-1} idealised wind field of (1) upwelling favorable wind (UWS) and, (2) downwelling favorable wind (DWS). The realistic wind field tends to be more downwelling favourable than upwelling favourable during the period of the simulation (Fig. 4.2).

Five other experiments were performed to further investigate changes in density gradients, wind and bathymetry on the eddy formation (Table 4.1). In the no cross-shelf density gradient (NCSD) experiment the initial conditions were altered so that the continental shelf density field was given the same vertical profile as the density field immediately offshelf. This eliminated the cross-shelf density gradient. In addition to this, downwelling winds were applied throughout the simulation so that there was no uplift onto the continental shelf. In a contrasting experiment (the Slow EAC experiment; SEAC) the EAC was slowed down in the northern nudging zone by nudging the southward component of velocity to zero at a timescale of 1 d^{-1}. A further experiment (the BOTH experiment) was a combination of both the above experiments. In the north/south coastline (NSC) and the north/south coastline and initial (NSCAI) experiments the continental shelf and bathymetry were altered so that the coastline and the 200 m isobath were parallel to meridional lines. In the NSC experiment the initial conditions are the same as the initial conditions in previous experiments (i.e. the EAC is initialised at the same longitude) but some coastal waters are not present in

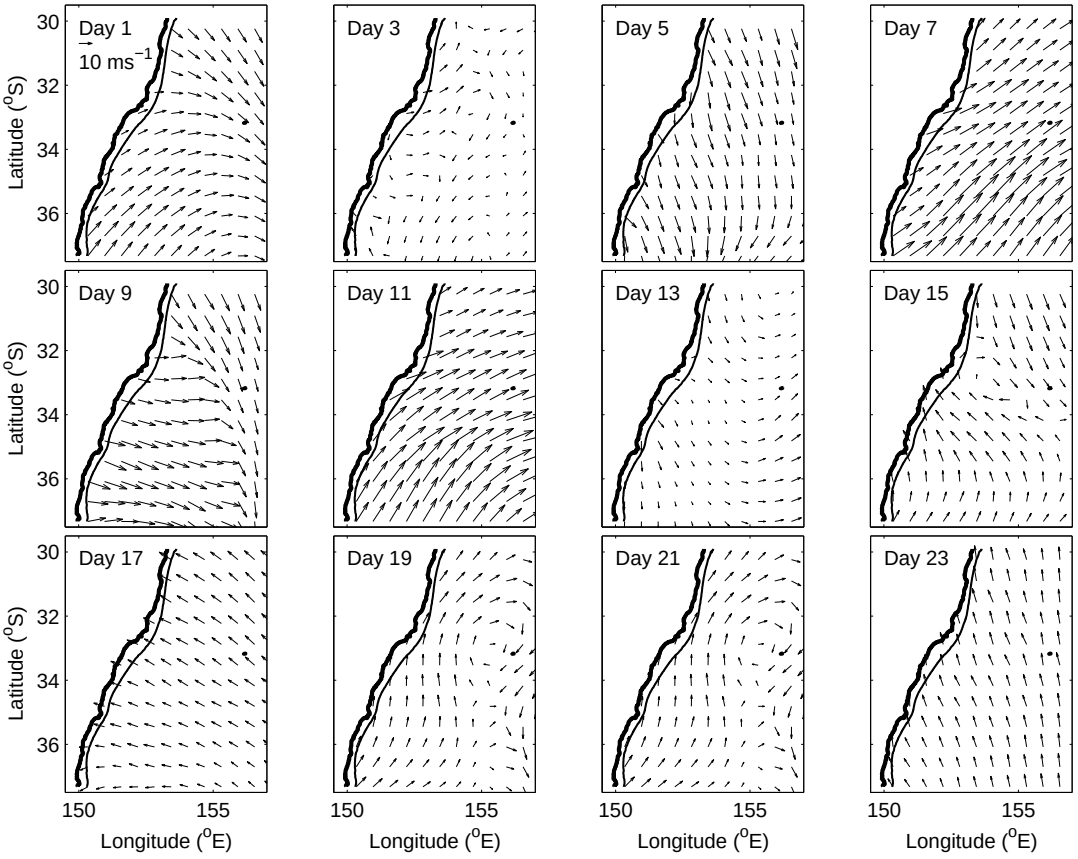

Figure 4.2: The NOAA/NCDC Blended 6-hourly 0.25-degree Sea Surface Winds used in the RWS. The arrows show magnitude (as indicated in the key) and direction. The 200 m isobath is shown.

this simulation as the coast is moved east. In the NSCAI experiment the initial conditions are moved east with the coastline so that the coastal waters are still present in the initial conditions.

Simulation name	Acronym	Description
Realistic Wind Scenario	RWS	Realistic wind forcing.
Upwelling Wind Scenario	UWS	An idealised upwelling northerly wind of 10 m s^{-1}
Downwelling Wind Scenario	DWS	An idealised downwelling southerly wind of 10 m s^{-1}
No cross-shelf density	NCSD	Initial continental shelf density is the same as the offshelf density.
Slow EAC	SEAC	The EAC is slowed via nudging of velocities in the northern nudging layer.
Both NCSD and SEAC	BOTH	The EAC is slowed and the initial continental shelf density is the same as the offshelf density.
North/south coastline	NSC	The coastline is moved to the east so that it is parallel to meridional lines.
NSC and initial	NSCAI	As above, except the initial density field is also moved east by the same distance as the coast.

Table 4.1: The simulations performed, their acronym and a description.

4.3 Results

4.3.1 Model and data comparison

Sea surface temperature output from the realistic wind scenario (RWS) is compared to satellite AVHRR estimates of sea-surface temperature (Fig. 4.3). Initially neither the modelled or observed SST field shows evidence of the eddy, although the observed SST field suggests an eddy may form (Fig. 4.3 A1 and A2).

In the observed and modelled SST fields there is a sharp temperature gradient between the warm EAC water and the cooler coastal waters. Evidence of a complete eddy forming on this front can be seen in the observations from day 3 (Fig 4.3 B2). The model also produces this eddy at the front between the EAC and coastal waters, although it first appears on model day 9 (Fig. 4.3 E1). In both the observations and the model the eddy emerges as a small billow which cuts into the edge of the EAC. The model's eddy then evolves in a similar manner to the observed eddy, albeit 6 days behind. By day 23, the model has produced an eddy which is of a similar size and orientation to the eddy that appears in the satellite observations (remembering that the model simulation is independent of the AVHRR SST; Fig. 4.3 L1 and L2).

4.3.2 Formation of the eddy

Movement of the 16^{o}C isotherm

The CCE forms at 33^{o}S and a transect of temperature through the centre of the eddy shows uplift of the 16^{o}C isotherm over the course of the simulation (Fig. 4.4). Initially the 16^{o}C isotherm is slanted upwards towards the continental

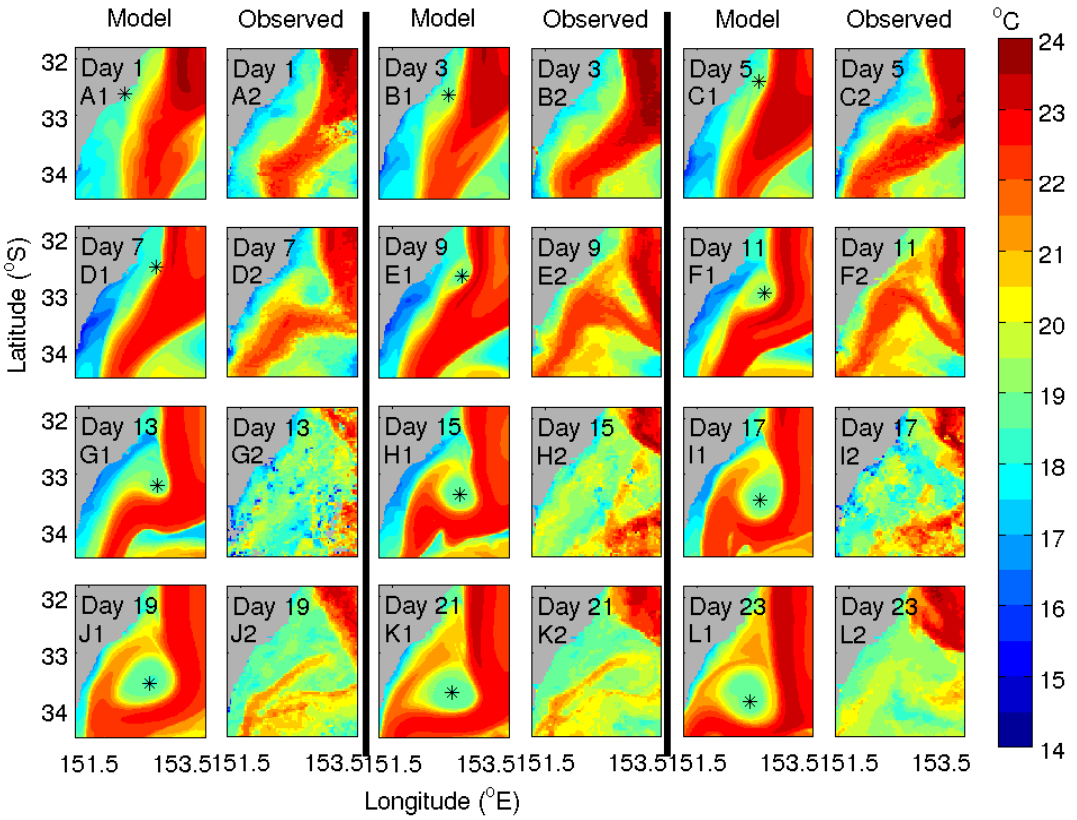

Figure 4.3: Model sea surface temperature (for the RWS) and AVHRR satellite sea surface temperature (as indicated by the title on each column). Different model days are shown as indicated in each panel. The * indicates the centre of the modelled eddy as determined by the position of lowest sea-level.

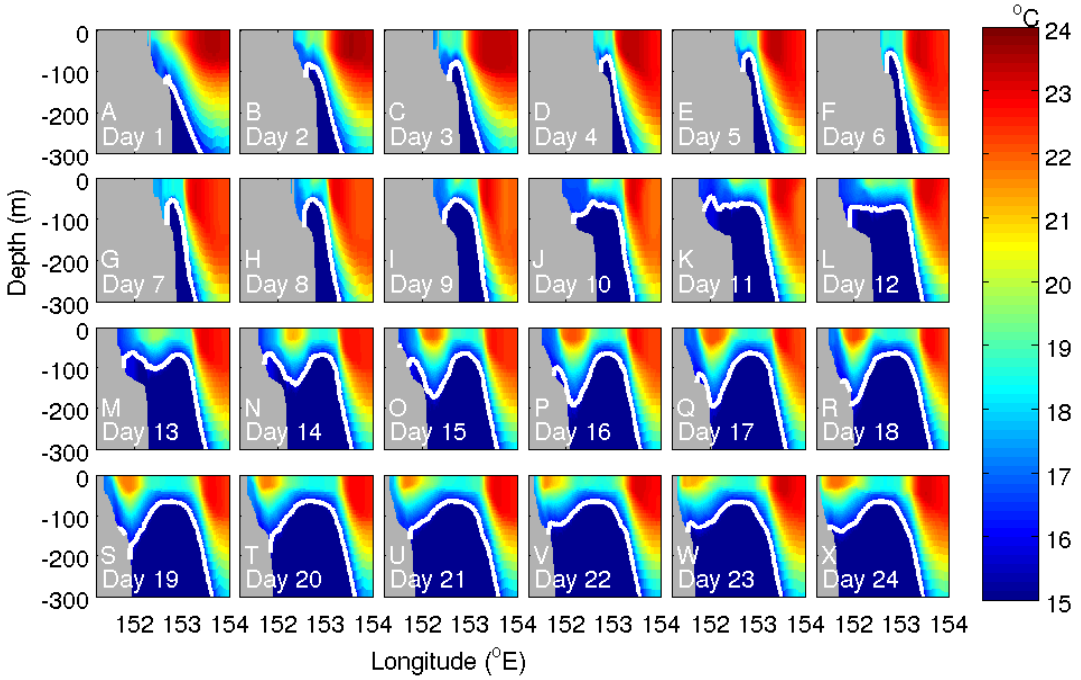

Figure 4.4: A vertical cross-section of temperature through the middle of the eddy (as indicated by the * in Fig. 4.3) for days 1-24 for the realistic wind scenario. The 16^{o}C isotherm is shown in white.

shelf, indicating upwelling on the continental shelf and slope (Fig. 4.4A). This is common as the EAC drives upwelling on the continental shelf (Baird et al., 2006a; Roughan and Middleton, 2002). Over the course of the simulation, uplift due to the formation of the CCE becomes greater than just EAC preconditioning on the continental shelf, centred at $\sim$ 152.5^{o}E. This manifests as an upwards bump which forms on the tilting isotherm (at 152.5^{o}S on day 6; Fig. 4.4F).

From days 8-19 this upwelling bump moves offshore and the 16^{o}C isotherm on the shore side of the bump is suppressed (Fig. 4.4 H-S). This suppression is due to advection of warm EAC waters around the outside rim of the eddy (Fig. 4.3 E1-J1).

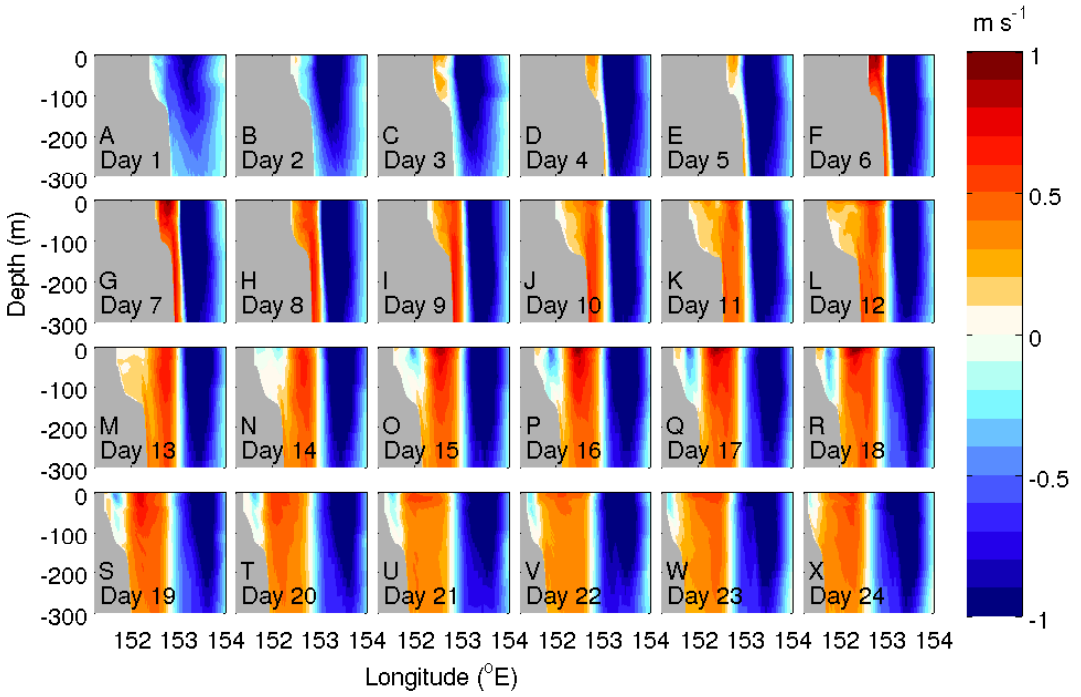

Figure 4.5: A vertical cross-section of velocity through the middle of the eddy (as indicated by the * in Fig. 4.3) for days 1-24 for the realistic wind scenario. A positive (red) value indicates a northward flow and a negative (blue) value indicates a southward flow.

Velocity field

A CCE in the Southern Hemisphere will rotate clockwise and have a southward flow on the east side and a northward flow on the west side. Initially, the area where the eddy forms (the coastal areas at 33^o S) is dominated by a southward flow (due to the EAC; Fig. 4.5A). From day 2 a northward flow on the continental shelf and slope develops (Fig. 4.5B-F). This flow forms the western side of the eddy and becomes stronger throughout the simulation. The eddy then moves offshore (days 13-24) and a weak southward flow develops on the continental shelf again (Fig. 4.5M-X).

Vorticity field

In the Southern Hemisphere, planetary vorticity is negative (f<0) and the relative vorticity of a cyclonic, CCE is negative. Uplift in a CCE (as evidenced in Sec. 4.3.1 and 4.3.2) occurs with a decreasing (more negative) vorticity. Initially there are negative vorticity waters on the continental shelf and slope and waters of positive vorticity (due to the EAC) off the shelf (Fig. 4.6A).

Between days 7 and 10 a filament of positive vorticity water forms on the continental shelf inshore of the negative vorticity waters (Fig. 4.6 G-J). This pushes the negative vorticity waters off the shelf and forms the CCE (Fig. 4.6I). The CCE grows and entrains water of negative vorticity from the continental shelf just north of the eddy. The negative vorticity spirals into the centre of the eddy, increasing the eddy growth and intensification (Fig. 4.6J-X).

By day 15 (Fig. 4.6O) waters of negative vorticity inside the eddy appear to be completely encircled by the EAC (which has positive vorticity). Negative vorticity at the core of the eddy is at a maximum on day 2, after which the intensity decreases again, signaling the decay of the eddy.

4.3.3 Sensitivity to wind forcing

That the model can reproduce the CCE without data assimilation methods indicates that the eddy formation is due to processes captured in the model, driven by either initial conditions or external forcings, such as the initial density field, atmospheric forcing or boundary forcing. Here we investigate the effect of the wind field. While it is not expected that the wind field will have a large direct effect on the eddy formation, it will affect upwelling and water masses on

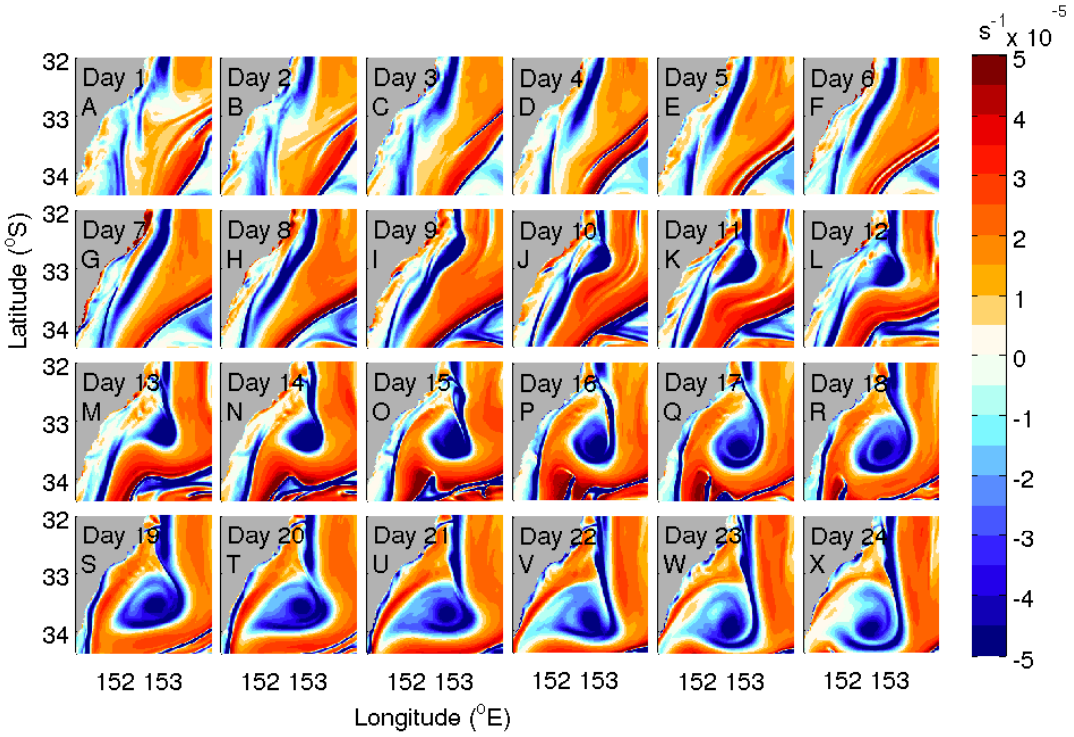

Figure 4.6: Surface vorticity (s^{-1}) in the realistic wind scenario for days 1-24.

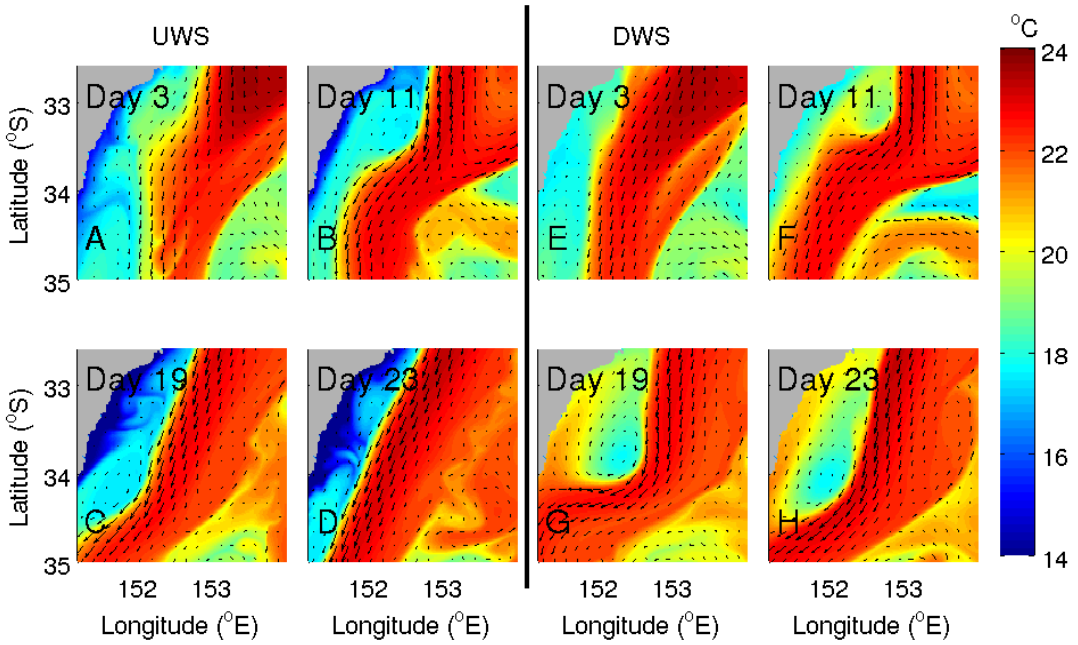

Figure 4.7: SST on model days 3, 11, 19 and 23 for the upwelling wind scenario (cols. 1-2) and the downwelling wind scenario (cols. 3-4).

the shelf. This, in turn, affects the temperature gradient between the continental shelf and the EAC. Thus, while the change is to the wind field, the effect that is being studied is that of a changing cross-shelf density gradient.

A sensitivity analysis is performed whereby the wind field is changed to produce an idealised upwelling wind scenario (southward wind of 10 m s^{-1}, hereafter called UWS); and an idealised downwelling wind scenario (northward winds of 10 m s^{-1}, hereafter called DWS). The most significant change this makes is in the temperature field on the continental shelf (Fig 4.7). Upwelling winds lift water from the continental slope and therefore increase the density of shelf waters. Both the UWS and DWS form a CCE (Fig. 4.7) although it is different in each case.

	RWS	UWS	DWS
Area (km^2 $\times 10^{-3}$)	26.0	22.6	42.4
Min elevation (m)	-0.95	-0.87	-0.93
Southward movement (km)	39.24	78.05	58.71

Table 4.2: The area (on day 11), minimum elevation (on day 11) and southward movement of the eddy (between days 11 and 19) in the 3 different wind scenarios.

In the UWS (Fig. 4.7 A-D), cold, upwelled waters dominate the continental shelf region. This enhances the temperature gradient between the EAC and the continental shelf water (ΔT=7^{o}C). An eddy (as evidenced by a circulating velocity field) forms around model day 11 (Fig. 4.7 B). When compared to the realistic winds scenario (RWS), the UWS eddy forms further south (Figs. 4.3 E1 and 4.7 B). In a similar manner to the RWS the eddy is formed as a small billow which cuts into the edge of the EAC. In the UWS this billow does not cut into the EAC as far as in the RWS. The UWS eddy is more elongated and forms closer to the shelf. By day 23 this eddy is in a different position and location to the RWS eddy (Figs. 4.3 L1 and 4.7 D) and is smaller (Table 4.2). The enhanced temperature gradient between the continental shelf and the EAC (as caused by the upwelling wind stress) did not enhance the size of the eddy.

In the DWS the water on the continental shelf is warmer than that of the realistic (and upwelling) wind scenario (Fig 4.7 E-H), resulting in a smaller temperature gradient between the continental shelf and the EAC (ΔT = 5). The CCE forms on the front between the EAC and continental shelf waters as a billow which cuts into the EAC. This formation is similar to the RWS and the UWS.

By day 23 this eddy is of a similar shape to the RWS, albeit slightly closer to the continental shelf (Fig. 4.7H and Table 4.2).

The largest eddy forms in the DWS and both the DWS and RWS have a greater sea-level depression than the UWS (Table 4.2). In the scenarios presented here, the upwelling wind scenario produces the smallest eddy. This eddy also moves further southward during the simulation.

The three wind scenarios also differ in the magnitude of uplift in the centre the eddy. Here uplift is measured by the change in depth of the 16^oC isotherm. Out of the 3 scenarios (RWS, UWS and DWS) the largest uplift occurs in the DWS where the 16^oC isotherm is lifted up to 40 m below the surface (Fig. 4.8C). In the RWS the 16^oC isotherm is lifted up to 70 m below the surface (Fig. 4.8A). A point of maximum uplift is difficult to determine in the upwelling wind scenario as the isotherms are not suppressed on the continental shelf side of the eddy, indicating a less defined eddy. Using temperature contours as an indication of the edge of the eddy, in the UWS the 16^oC isotherm was lifted up to 50 m below the surface (Fig. 4.8B). Counter intuitively, rather than halting or inhibiting eddy formation, the downwelling winds enhance the uplift within the eddy. Possible causes for this are discussed in Section 4.4.

4.4 Discussion

4.4.1 Seasonal wind fields

We have investigated the effect of different wind fields on the eddy formation. In this section we look at how often these wind regimes occur and, hence, how

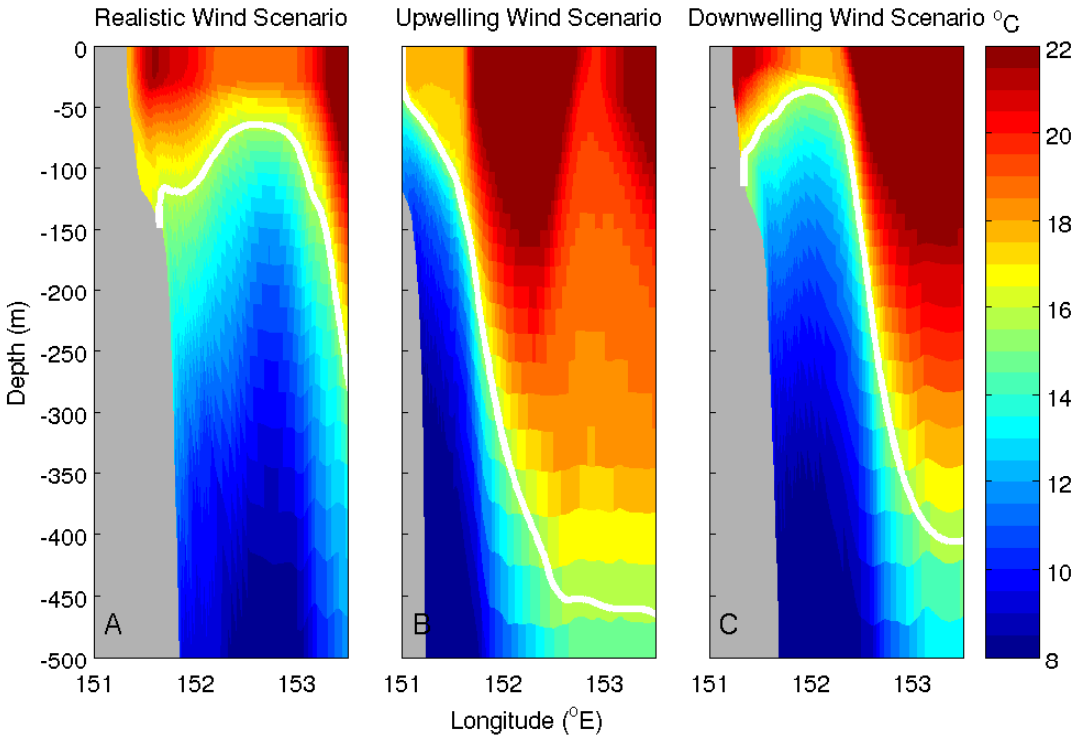

Figure 4.8: A vertical cross-section of temperature on day 21 for each scenario (as labelled in the title for each panel). The cross-section is through the middle of the eddy for each scenario (33.15^{o}S for the realistic wind scenario, 33.76^{o}S for the upwelling wind scenario and 32.26^{o}S for the downwelling wind scenario). The 16^{o}C isotherm is indicated in white.

our results apply in general to frontal eddies on the southeast coast of Australia (Fig. 4.9). In autumn the winds tend to be northerly and in winter they tend to be northeasterly. These upwelling favourable winds will lead to eddies similar to the upwelling wind scenario (elongated with less uplift). In summer the winds tend to be southwesterlies and northwesterlies which are upwelling and downwelling favourable respectively, leading to the possibility of both types of eddies forming.

The intensity of the summer winds differs between southward and northward. The northward wind intensity is less than 12 m s^{-1} and rarely becomes as large as 12 m s^{-1}. As a consequence, the effects of the northward winds seen in the model (a northward flow on the continental shelf leading to a larger eddy) will not often occur to the same extent as that seen in the model.

4.4.2 The eddy formation

The eddy formed in both the UWS and the DWS, meaning that the strong uplift of water on the continental slope in the upwelling case was not necessary for eddy formation. However, the model is initialised with an upwelling signal and, in addition, the current (the EAC) drives upwelling. As such temperature gradients between the continental shelf and the open ocean did exist in both simulations, albeit to a different strength (a 4^oC temperature difference in the UWS and a 3^oC in the DWS; Fig. 4.7A and F). Despite these differences an eddy formed in both simulations. Unexpectedly, the maximum uplift of the 16^oC isotherm was greatest in the DWS (Fig. 4.8 C). Therefore, while coastal upwelling cannot be ruled out as a factor contributing to the eddy's formation, other factors also need to contribute to the eddy formation. Such factors include velocity gradients

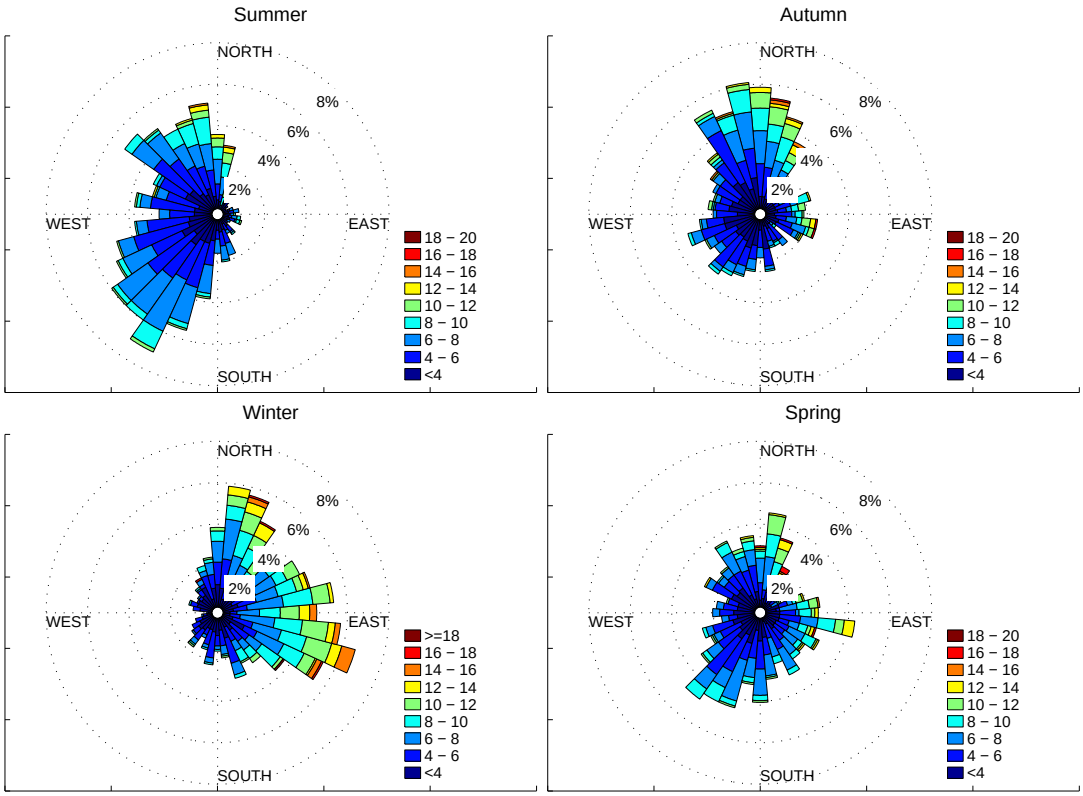

Figure 4.9: Wind roses in the vicinity of the cold-core eddy (32.5^{o}S and 152.5^{o}E) for each season (as indicated by the titles) using NCEP winds from 1992-2004 (Kalnay et al., 1996). Colour shows magnitude in m s^{-1}.

between the continental shelf and deep ocean and the conservation and advection of vorticity.

All scenarios are initialised with a negative vorticity on the continental shelf which builds throughout the simulation (Figs. 4.6A-G). The EAC forms a perturbation as, locally, the current moves away from the continental shelf, advecting the negative-vorticity waters off the continental shelf (Figs. 4.6J-R). As this negative-vorticity water moves into the deeper ocean, it becomes more cyclonic to conserve potential vorticity, creating a localised area of strong negative vorticity which forms the eddy.

In the UWS the eddy tends to be more elongated and moves south, staying in close proximity to the continental shelf. In the DWS the eddy became more circular and moved away from the shelf. The UWS eddy also spun-down towards the end of the simulation, leaving no evidence of the eddy by day 29 (Fig. 4.7D). The most noticeable difference was the vertical movement of the 16^{o}C isotherm which was greatest in the downwelling wind scenario. This can be explained by looking at vertical cross-sections of velocity within the eddy.

4.4.3 Upwelling in the downwelling wind scenario

To understand why more uplift occurred in the DWS we examine the velocity field. In the lead up to the RWS and DWS eddy a northward current appeared on the continental shelf (Fig 4.10 A-E and K-O). In the UWS, this continental shelf northward current wasn't apparent at the surface (Fig. 4.10 F-J). There was, however, a subsurface current (Fig. 4.11 F-J). As a consequence, when the eddy grew, the northward flow on the coastal side of the eddy was weaker at

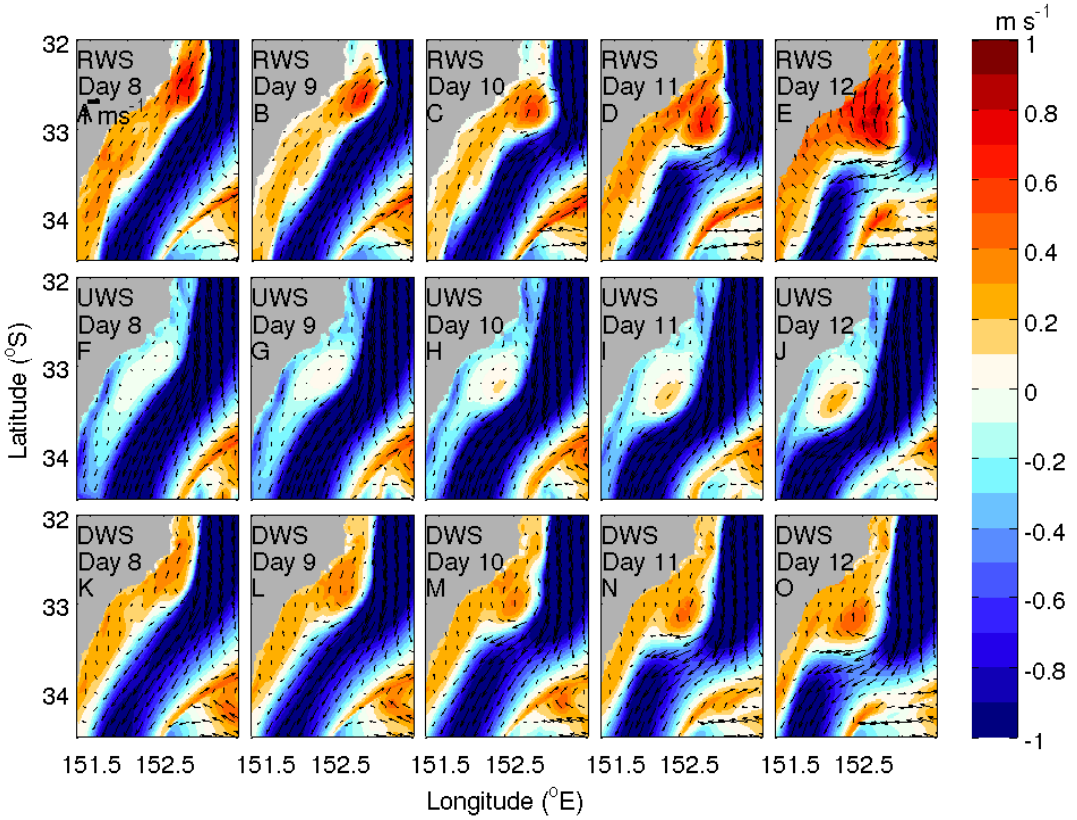

Figure 4.10: The meridional component of velocity (colourscale) in the realistic wind scenario (top), the upwelling wind scenario (middle) and the downwelling wind scenario (bottom). Red indicates a northward flow and blue indicates a southward flow. The arrows indicate direction and relative speed of the flow.

the surface. Further, it is expected that uplift due to velocity shear should be reduced in the UWS. This may explain why, in the UWS, the 16^{o}C isotherm (which was originally above the subsurface maximum velocity) was not uplifted as much. To study this further, transfers of kinetic and potential energy to the eddy are investigated.

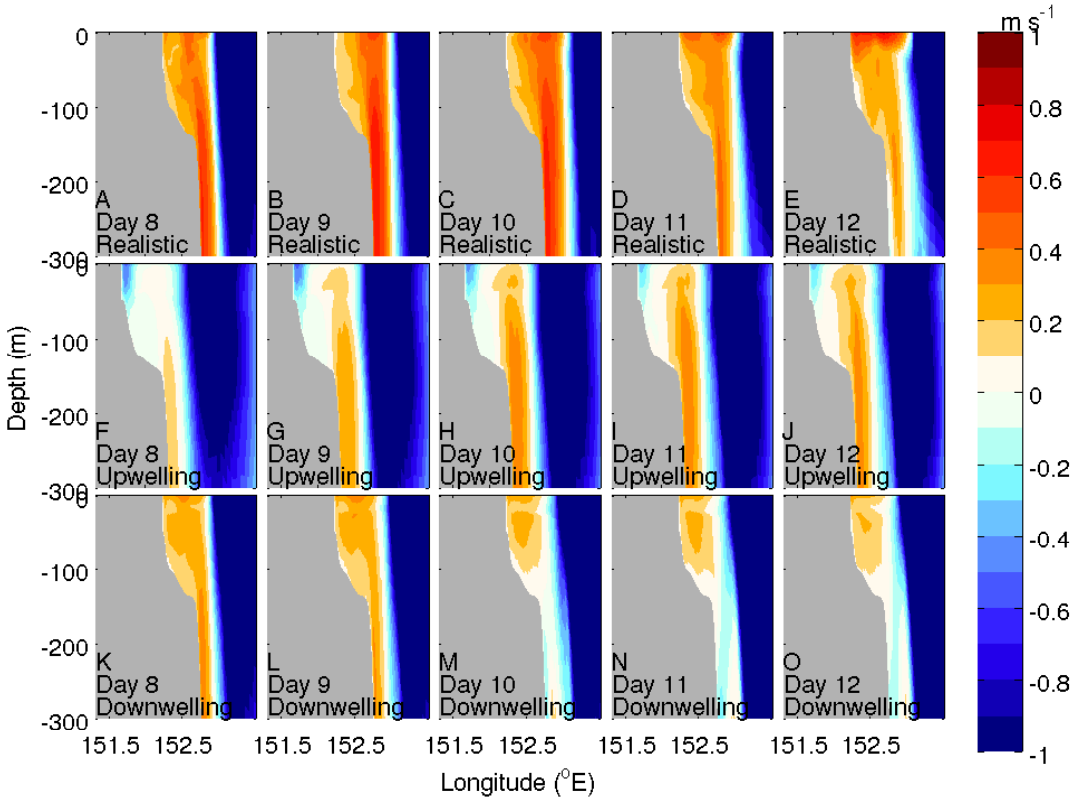

Figure 4.11: Vertical transects of northward flow through 32.75^{o}S in the realistic wind scenario (top), 33.2^{o}S in the upwelling wind scenario (middle) and 32.75^{o}S in the downwelling wind scenario (bottom). Red indicates a northward flow and blue indicates a southward flow.

4.4.4 Transfer of kinetic and available potential energy

The transfer of mean kinetic energy (MKE) and mean available potential energy (MAPE) to eddy kinetic energy (EKE) and eddy available potential energy (EAPE) respectively can be investigated to determine which processes (barotropic or baroclinic) contribute to eddy generation. In a similar manner to Rubio et al. (2009) the following formulas are used:

$$MKE \Rightarrow EKE = -\int \overline{u'u'}\frac{\partial \overline{u}}{\partial x} + \overline{v'v'}\frac{\partial \overline{v}}{\partial y} + \overline{u'v'}(\frac{\partial \overline{v}}{\partial x} + \frac{\partial \overline{u}}{\partial y})dz$$

$$MAPE \Rightarrow EAPE = \frac{g}{\rho_0}\int (\frac{\partial \overline{\sigma}}{\partial z})^{-1}(\overline{u'\rho'}\frac{\partial \overline{\rho}}{\partial x} + \overline{v'\rho'}\frac{\partial \overline{\rho}}{\partial y})dz$$

where overbars represent temporal averages (9 days between model day 2 and 10 in this case), primes indicate turbulent quantities (departures from the time mean; i.e. $u' = \overline{u} - u$), u and v are the zonal (x) and meridional (y) components to the velocity, ρ is the density, ρ_0 is a reference density and σ is the average density at each depth.

In all three scenarios there is a large transfer of MKE to EKE and from MAPE to EAPE energy on the continental slope during eddy formation, indicating both a barotropic and baroclinic contribution to the eddy during this time (Fig 4.12). There are losses and gains in EKE and EAPE so that a spatial average is included to show the net transfers of energy. The net transfers show that in all scenarios there is a transfer of MKE to EKE with 7.5 $\times 10^{-5}$ m^2 s^{-3} in the RWS, 4 $\times 10^{-5}$ m^2 s^{-3} in the UWS and 4 $\times 10^{-5}$ m^2 s^{-3} in the DWS. It is the kinetic energy (KE) of the EAC that provides the energy for CCE formation

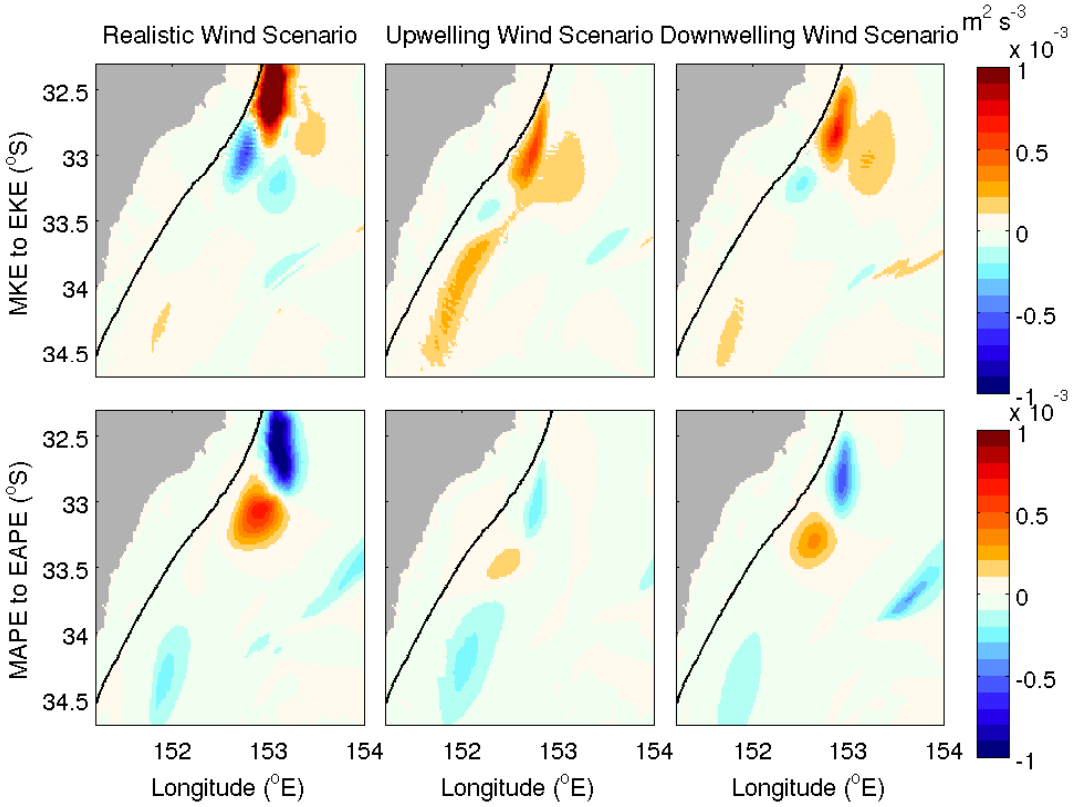

Figure 4.12: Energy transfers from mean kinetic energy (MKE) to eddy kinetic energy (EKE; top row) and mean available potential energy (MAPE) to eddy available potential energy (EAPE; bottom row) for 9-day average between days 2 and 10). For reference, the EKE of the eddy reaches up to 2 m^2 s^{-2}. The 200 m isobath is shown in black.Positive (negative) values indicate that there is a transfer of energy from the mean (eddy) to the eddy (mean).

via the transfer of KE to the eddy. There is also a transfer of MAPE to EAPE. This is greatest in the RWS and smallest in the UWS. In this case, the upwelled water destroys the temperature gradient between the continental shelf and the eddy, resulting in reduced transfer of energy. These results indicate that both barotropic and baroclinic processes are important.

4.4.5 Other factors influencing eddy formation

Other factors such as changing the initial density field and the bathymetry and coastline are investigated. In the NCSD scenario the initial continental shelf density field is the same as the offshelf density field. In the SEAC scenario the EAC is slowed down via nudging of velocities in the northern nudging layer. The BOTH scenario is a combination of the two. In the NSC the coastline is moved to the east so that it is parallel to meridional lines and the NSCAI also has the initial density field moved east by the same distance as the coast. For more details on the simulations see Sec.4.2.3 and Table 4.1.

All three of the NCSD, SEAC and BOTH experiments produce an eddy (Fig. 4.13). The eddy that is produced is smaller than that of the realistic wind scenario, indicating that these factors have some effect on the formation of the eddy. This is as expected as both barotropic and baroclinic processes are important in eddy formation. The SEAC eddy forms later and further offshore, suggesting that it is the speed of the EAC that keeps the eddy close to shore.

The density and shear gradients cannot be completely removed from the simulation. So, while we cannot say if the complete removal of these factors will halt the formation of the eddy, other factors determining the formation can be investigated. In particular, the effects of a coastline which slopes to the west are removed in the NSC and the NSCAI experiments (Fig. 4.14). If the effects of the temperature gradient between the open ocean and the continental shelf are also removed, the eddy does not form (Fig. 4.14 A-D). Clearly both the effects of the southwest running coastline and the cross-shelf density gradient are important for eddy formation. From Section 4.3.3 we can see that, once formed, the speed

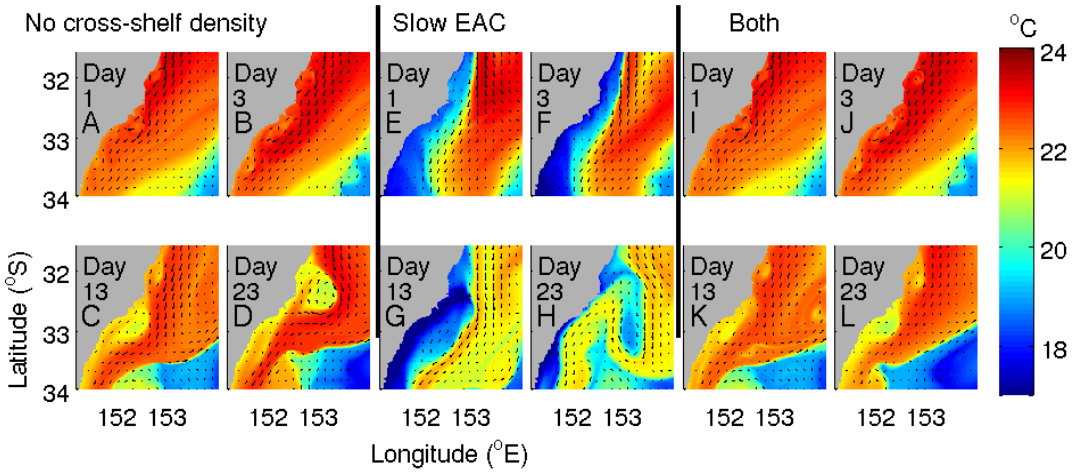

Figure 4.13: SST on days 1, 3, 13 and 23 of the eddy for the No cross-shelf density scenario (NCSD; cols. 1-2), the Slow EAC scenario (SEAC; cols. 3-4) and the No cross-shelf density and Slow EAC scenario (BOTH; cols. 5-6).

of the current (or the amount of upwelling on the shelf) will have an effect on the size of the eddy and the amount of upwelling present within it.

4.5 Summary

A cold-core eddy (CCE) which formed off the south east coast of Australia was investigated using a successful Regional Ocean Modelling System (ROMS) configuration. The eddy formed as a billow of continental shelf waters which cut into the East Australian Current (EAC). Negative relative vorticity waters are pulled off the continental shelf creating a strong relative negative vorticity area which forms into the eddy. The effect of different wind fields (realistic, upwelling and downwelling favourable winds) were investigated. The different wind fields changed the density structure and flow on the continental shelf. The simulation with the greatest temperature gradients between the continental shelf

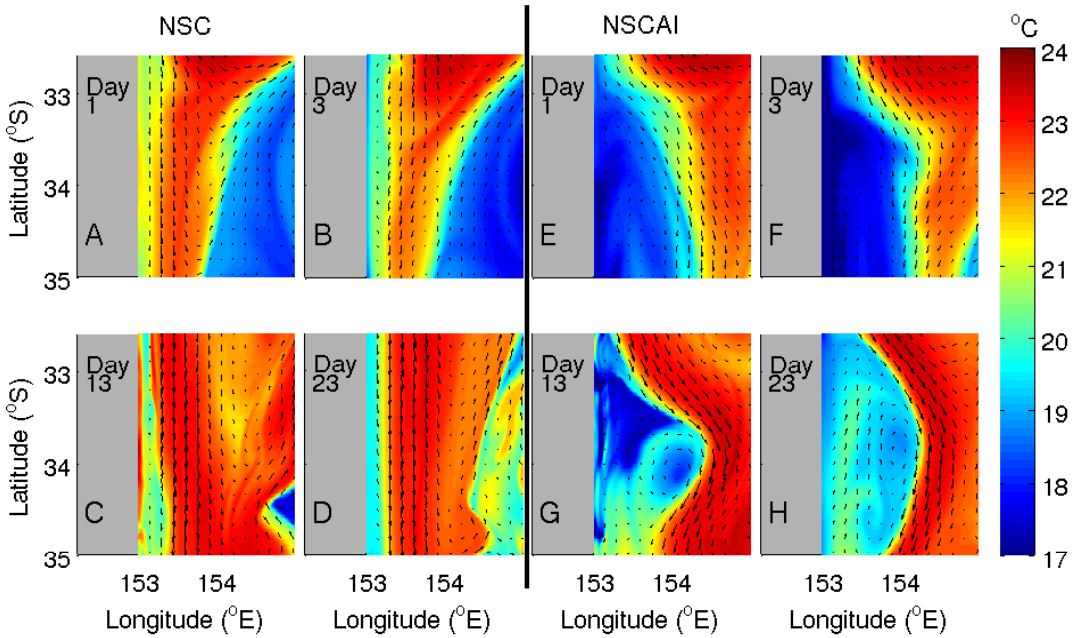

Figure 4.14: SST on days 1, 3, 13 and 23 of the eddy for the north/south coastline scenario (cols. 1-2) and the north/south coastline and initial scenario (cols. 3-4).

and slope did not enhance eddy formation and the eddy with the greatest uplift formed when there was downwelling on the continental shelf. The largest eddy with strongest isotherm uplift occurred in simulations that were not upwelling favorable on the continental shelf due to a strengthening of a northward flow on the continental shelf. Vorticity transport, velocity shear and temperature gradients are all potential drivers of the eddy formation. Manipulations of the bathymetry and density gradients slowed the CCE formation with a NE-SW oriented coastline. Analysis of energy transformation shows the largest source of CCE eddy kinetic energy was the kinetic energy of the EAC. These experiments show that the currents contribute significantly to the formation of this cold-core eddy.

Chapter 5

Entrainment of coastal waters into a cold-core eddy

Abstract

Western boundary current cold-core eddies (CCEs) can be important for coastal ecosystems as they have the potential to entrain continental shelf waters. We use the Regional Ocean Modelling System (ROMS) to investigate the entrainment of water into one such cold-core eddy that formed in coastal waters near the East Australian Current (EAC) in September and October 2009. The CCE comprises water which has been uplifted from depth and water which has been advected off the continental shelf. The waters entrained from the continental shelf come from a wide latitudinal range from north and south of the eddy. This range can be attributed to both the strong southward flowing EAC and a northward flowing current on

the continental shelf and slope. A sensitivity analysis is performed to investigate the impact of upwelling and downwelling winds on the entrainment of coastal waters. The upwelling winds suppressed the northward flow on the continental shelf and slope, reducing the latitudinal range from which water was entrained into the eddy. This affected the temperature and salinity properties of the eddy as distinct water types from the south were not entrained. In all scenarios upwelled deeper water that was entrained into the eddy came from north of the eddy. The eddy and, hence, upwelling of water appeared at depth before becoming evident in the surface fields. The eddy initially tilts onto the continental shelf but becomes more vertical (stands up) as it evolves. This affects patterns of upwelling and downwelling within the eddy, creating upwelling on the southern side and downwelling on the northern side of the eddy.

5.1 Introduction

5.1.1 Entrainment and upwelling in cold-core eddies.

Cold-core eddies (CCEs) frequently form in the energetic areas of western boundary currents (WBC). Both the entrainment and uplift of water is important for biological production in these eddies. CCEs that form near the coastal zone, as they often do in WBCs, entrain coastal larval species more frequently than their warm-core eddy counterparts. Conceptually, these CCEs should be full of nutrients for biological production (Bakun, 2006). Upwelling in the eddy centre

brings nutrient rich waters into the euphotic zone which is required for growth by the (previously nutrient limited) entrained coastal species (Kasai et al., 2002; Henschke et al., 2011; Sponaugle et al., 2005; Kimura et al., 1997).

Entrainment of coastal species into CCEs which leads to an enhancement of biological production has been observed in many different CCEs in WBCs. In the Kuroshio extension CCEs have been observed to have chlorophyll concentrations that increase by 3-5 μg l^{-1} in 3-4 days (Kimura et al., 1997). In a case study Kasai et al. (2002) looked at entrainment of coastal waters into a frontal CCE. Prior to entrainment, the coastal water was situated at the Kuroshio Front and was low in nutrients and productivity. After entrainment upwelling within the eddy introduced nutrients to the surface waters, increasing the productivity of the entrained water. As such, the location of the seeding water into a CCE is important to determine which, if any, species are to benefit from the nutrients provided by a CCE. If the source of the entrained water comes from the continental shelf the coastal communities can thrive, creating a productive eddy, as was the case in Kimura et al. (1997). If the entrained water comes from a biologically poor region the CCE could be less productive for higher trophic species.

The physical conditions within a CCE can also affect the survival of the entrained coastal species. As Sponaugle et al. (2005) found CCEs do not always enhance productivity of the entrained water. In the Florida Current two out of the three mesoscale CCEs they studied produced a multi-taxa larval pulse. A third mesoscale CCE did not yield this multi-taxa larval pulse, due to a mismatch in the biological and physical conditions in the eddy.

A major physical constraint on biological production in CCEs is the depth

from which upwelling occurs. Another physical constraint to algal growth is the depth to which the upwelling reaches (Hayward and Mantyla, 1990). The upwelled water may be high in nutrients but, as it has recently been below the euphotic zone, will be low in phytoplankton. If the upwelling is too strong the algal blooms can be pushed to the edge of the eddies, as was the case in Hayward and Mantyla (1990). As physical conditions can affect the biological growth, physical constraints such as the location and vertical uplift of upwelled water need to be understood to gain an understanding of the biological system.

When coastal species are entrained into an eddy with physical conditions conducive to primary production the location of this production is not always in the centre of the eddy as predicted by simple geostrophic models. Filaments of high phytoplankton biomass can trail behind detached cyclonic eddies as the eddies propagate away from a front. This is due to divergence in the eddy's surface layer, pushing the algal blooms out of the eddy (Lima et al., 2002). This can be complicated further if the eddies become elongated or tilt towards the continental shelf (McGillicuddy and Robinson, 1997; Oke and Griffin, 2010).

Clearly, to gain an understanding of biological processes in the energetic coastal WBC regions, knowledge of physical processes such as the source of entrained and upwelled water into an eddy is needed, as well as the distribution of the upwelling within the eddy. A model can be advantageous for studying upwelling and entrainment as it provides both a high spatial and temporal resolution (McGillicuddy and Robinson, 1997; Lima et al., 2002). When this can be combined with intensive bio-physical field studies the model becomes a robust tool in which to study upwelling and entrainment in CCEs. As physical pro-

cesses vary between regions, a region specific study is required to investigate this entrainment and uplift into CCEs. In this study a numerical model has been configured for an area off southeast Australia which is dominated by the East Australian Current (EAC).

5.1.2 EAC counter currents and entrained water

The source of water entrained into an eddy will be affected by currents on the continental shelf adjacent to the eddy. The continental shelf off southeast Australia is dominated by the EAC, a southward flowing WBC and its eddy field (Suthers et al., 2011). Inshore of the southward flowing EAC, northward flows on the continental shelf have been observed and modelled (Godfrey et al., 1980b; Tranter et al., 1986; Roughan et al., 2003). Theoretical studies by Condie (1995) found the flow on the continental shelf is affected by the proximity of the current to the shelf. When the current is well off the shelf, there is a weak equatorward flow on the continental shelf and the water is weakly downwelling favourable. When the current encroaches upon the continental shelf the interactions with the shelf create upwelling and poleward flow inshore. A counter current similar to this has been modelled on the continental shelf inshore of the EAC, flowing north to the EAC bifurcation point (Godfrey et al., 1980b). In addition to this, a counter current flowing northward has also been observed on the continental shelf and slope (Tranter et al., 1986). Little is known about this flow and it is unclear how often these northward currents occur. These northward flowing currents on the continental shelf and slope, however, have important biological implications as larval species can travel northward (Roughan et al., 2011) and

affect the source of waters entrained into CCEs. As such, study of this flow is essential and a modelling study focusing on entrainment of coastal water will need to be able to reproduce these northward currents as well as the major currents (such as the EAC).

5.1.3 Cold-core eddies in the East Australian Current

In the EAC region there are a limited number of studies on the physical aspects of CCEs (Brassington et al., 2011; Oke and Griffin, 2010; Everett et al., 2011) and on the biology of cold-core eddies (Henschke et al., 2011; Oke and Griffin, 2010; Everett et al., 2011) but few studies look at entrainment and upwelling into/within these eddies. Oke and Griffin (2010) used a coarser resolution model (10 km) to simulate an eddy with significant upwelling and, in a similar manner to Hayward and Mantyla (1990), the chlorophyll bloom formed on the edge of the eddy rather than the centre. The pattern of upwelling and downwelling was complicated by the tilt of the eddy onto the continental shelf. This created upwelling in the south of the eddy and downwelling in the north of the eddy.

In an observational study of a different CCE Everett et al. (2011) found that high salp biomass was located at the vertical boundary between entrained shelf waters and the upwelled nutrient rich waters of the CCE. This lends weight to the viewpoint that both the depth of the upwelled water and the entrained waters are important and a quantification of where the entrained and upwelled waters comes from is needed.

In this work we will look at the entrainment and upwelling for an eddy in the EAC region that formed in October 2009. The biological and physical character-

istics of this eddy were the focus of an intensive field study. Using a model we can add spatial and temporal resolution to this data. We can then answer questions such as: "What are the source waters into the eddy and how does this change under different wind scenarios?", "How do counter-currents on the continental shelf affect entrainment and uplift into the eddy", and "How do these northward flows affect water type properties within the eddy?".

In Section 5.3.1 we look at source water into the eddy and how this changes under different wind scenarios and in Section 5.3.2 we investigate northward flows on the continental shelf in light of this entrainment. In Section 5.3.3 we look at entrainment of deeper waters into the eddy. In Section 5.3.4 we compare the T and S signatures for different wind scenarios. In Section 5.4.1-5.4.2 we look at the tilt of the eddy and interpret this in light of upwelling and downwelling within the eddy. In Section 5.4.3 we then compare the northward flow seen in the model to the northwards flow seen in observations to assess the validity of the results.

5.2 Methods

5.2.1 The model configuration

The ocean state of the October 2009 CCE is simulated using the Regional Ocean Modelling system (ROMS). A detailed description of the model's configuration for the EAC region can be found in Chapter 2 and a brief summary is included here. SynTS (Ridgway et al., 2008) is used to prescribe initial, boundary and climatology data. The Flather (1976) condition is used for the barotropic

velocity components at the northern boundary. The baroclinic velocity field and the tracers on the northern boundary are nudged to external estimates from SynTS (Ridgway et al., 2008) at a timescale of 4 days. All other boundaries are radiative. NCEP 2.5-degree 6 hourly reanalysis data sets (Kalnay et al., 1996) and the NOAA/NCDC Blended 6-hourly 0.25-degree Sea Surface Winds data sets (Zhang et al., 2006) are used to implement the Bulk flux method of Fairall et al. (1996) at the atmospheric boundary. The model is initialised on 18 September 2009 and has a 5-day spin-up. More details on the forcings and initial conditions can be found in in Chapter 2. The grid used is the same as that used in Chapter 4.

5.2.2 The model simulations

In this chapter the effect of the three winds scenarios from Chapter 4, the realistic winds scenario (RWS), the upwelling winds scenario (UWS) and the downwelling winds scenario (DWS), are examined more closely. In the realistic wind scenario the model is forced with winds from the NOAA/NCDC Blended 6-hourly 0.25-degree Sea Surface Winds data set (Zhang et al., 2006). In the UWS (DWS) a constant 10 m s^{-1} upwelling (downwelling) wind is applied. For a more detailed description of the simulations the reader is referred to Chapter 4.

5.2.3 Lagrangan particle paths

In all three of the simulations (RWS, UWS and DWS), Lagrangian particles are released. Particles are released on model day 1 in 0.3 degree increments ($\sim$30 km) between 30-36°S and 0.05 degree ($\sim$50 km) increments between 151-

154^{o}E. In the vertical they are released every 50 m from 0-600 m water depth. This gives a total of 11,130 particles released (Fig. 5.1 and 5.2). These particles are advected (with no random walk) within the model at each timestep. No random walk is implemented as probability distributions are not calculated.

5.3 Results

5.3.1 Entrainment of particles

The eddy forms on day 12. Of the 11,130 particles released, 388 are entrained into the eddy on day 12 in the RWS (Fig. 5.3 and Table. 5.1). These particles come from all depths. Of the surface release particles, close to 100 % of particles that were entrained into the eddy come from the continental shelf. Fewer particles in total were entrained in the UWS. In the RWS, the UWS and the DWS most particles were entrained from releases above 200 m ($\sim$6-11%) and below 500 m ($\sim$ 1.5-3%; Table. 5.1). In all scenarios fewer particles came from the 200-500 m range indicating that the CCE waters are comprised mainly of waters that have been upwelled from the deeper ocean and waters that have been stripped off the continental shelf.

In the horizontal direction water was entrained into the eddy from both the north and the south (Fig. 5.3). Entrainment from the north is due to the predominately southward flow of the EAC. These waters come from the surface down to below 500 m indicating that, for waters below 500 m, upwelling was present. Particles were also entrained from as far south of the eddy as 35.2^{o}S ($\sim$200 km). These particles did not come from as deep as those entrained from the north but

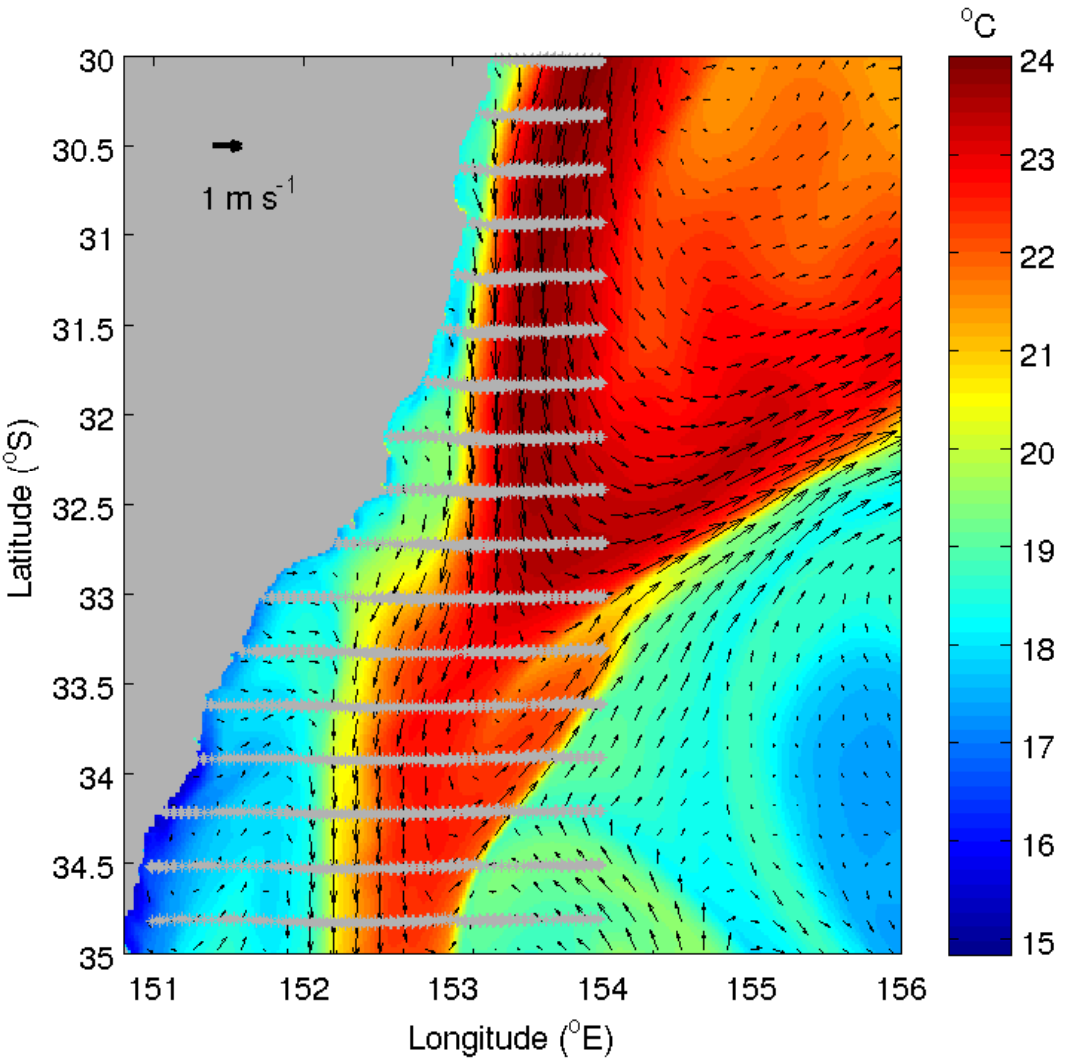

Figure 5.1: The initial position of particles (*) and sea-surface temperature (shading) on model day 1. Arrows indicate velocity.

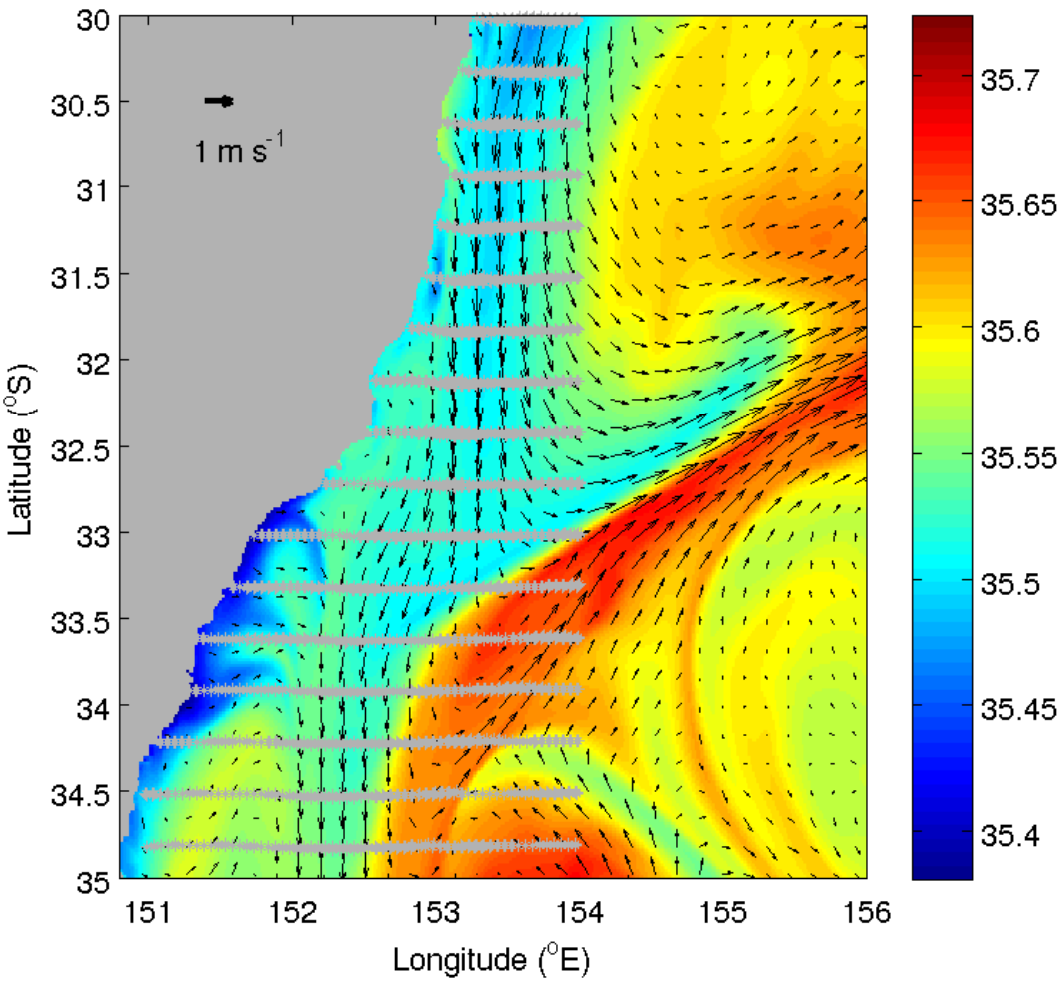

Figure 5.2: The initial position of particles (*) and sea-surface salinity (shading) on model day 1. Arrows indicate velocity.

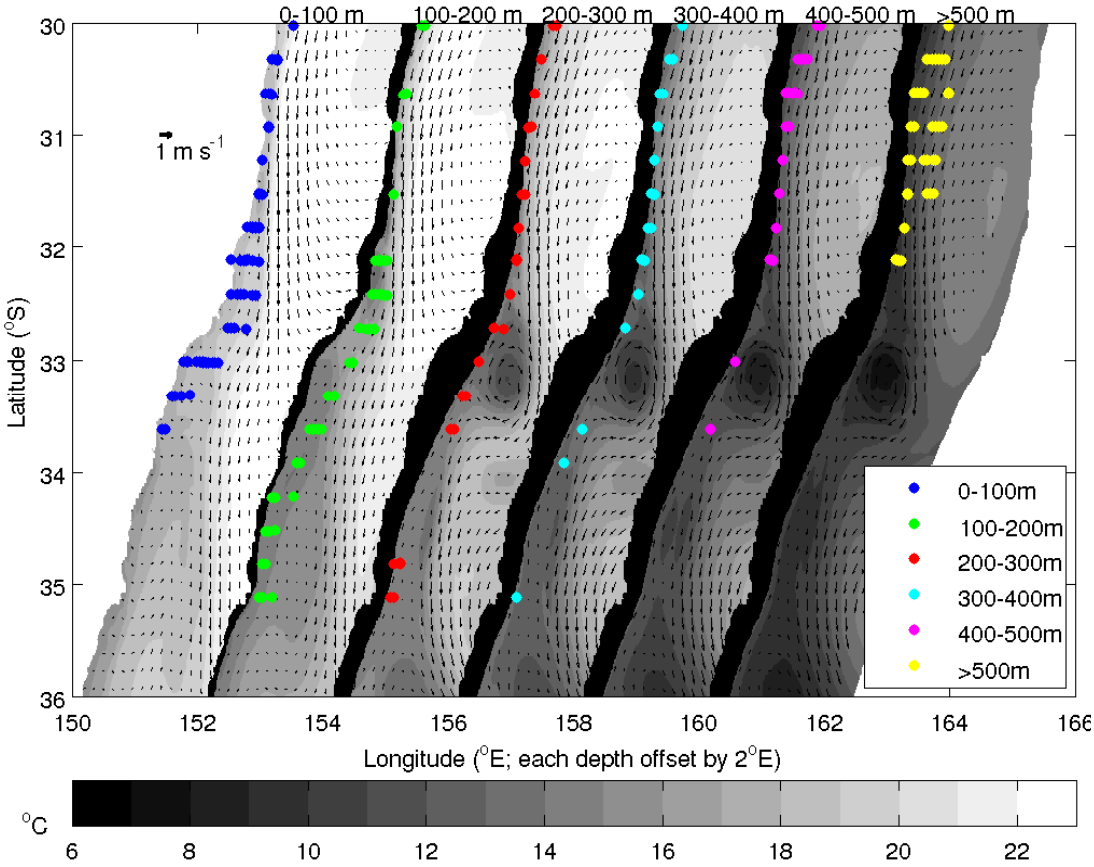

Figure 5.3: The initial (on the 23rd Sep; day 1) position of particles that were entrained into the eddy for the realistic wind scenario. Dots indicate initial position of the seeding particles. Colours of the particles indicate initial depth, shading indicates temperature and arrows indicate velocity on the 23 Sep. The temperature, velocity field and particle positions are shown offset by 2°E for each depth to allow comparison.

	RWS	UWS	DWS
<100 m (%)	8.8 (197)	5.55 (124)	8.32 (183)
100-200 m (%)	2.85 (44)	0.71 (11)	2.97 (46)
200-300 m (%)	1.79 (26)	0.69 (10)	1.58 (23)
300-400 m (%)	1.53 (22)	1.46 (21)	2.37 (34)
400-500 m (%)	1.77 (25)	2.05 (29)	2.41 (34)
>500 m (%)	2.27 (48)	2.41 (51)	3.03 (64)

Table 5.1: The percent of particles released at each depth interval that were entrained into the eddy. Actual number of particles entrained are in brackets.

the particles from 100-200 m traveled from further south than those from 0-100 m (by ∼150 km; Fig. 5.3 0-100 m and 100-200 m panels). Entrainment of these shelf and slope particles from the south indicate that there is a northward flow on the continental shelf and slope in the lead up to eddy formation (as mentioned in Chapter 4, Fig 4.10 and described in more details in the Section 5.3.2).

In the UWS less particles are entrained into the eddy (Fig. 5.4). This is as expected as the eddy is smaller. Fewer particles are entrained from south of the eddy in the UWS. The southward range of entrainment is reduced as particles entrained come from only as far south as 33.8^{o}S. The particles that do become entrained from the south tend to come from deeper releases. This lack of entrainment is due to a lack of northward flow on the continental shelf and slope in the UWS. There are more particles entrained in the DWS than both the RWS and the UWS (Fig. 5.5).

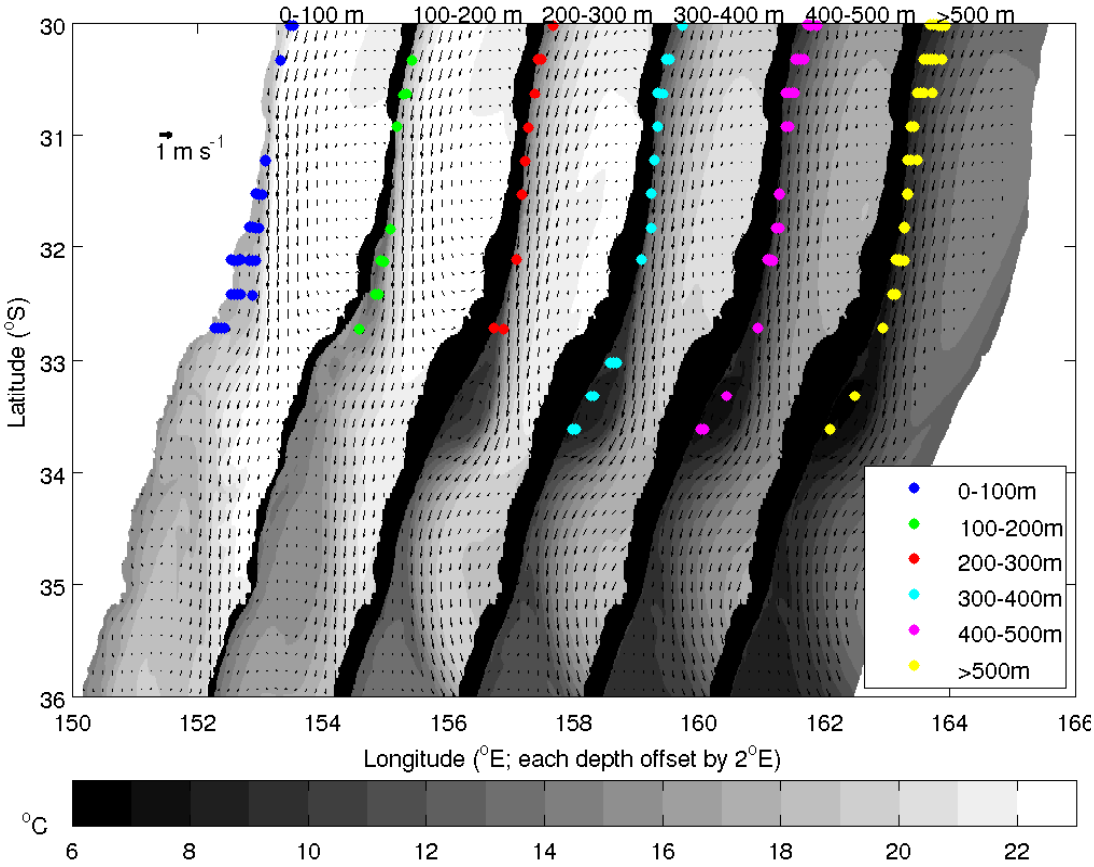

Figure 5.4: The initial (on the 23rd Sep; day 1) position of particles that were entrained into the eddy for the upwelling wind scenario. Dots indicate initial position of the seeding particles. Colours of the particles indicate initial depth, shading indicates temperature and arrows indicate velocity on the 23 Sep. The temperature, velocity field and particle positions are shown offset by 2°E for each depth to allow comparison.

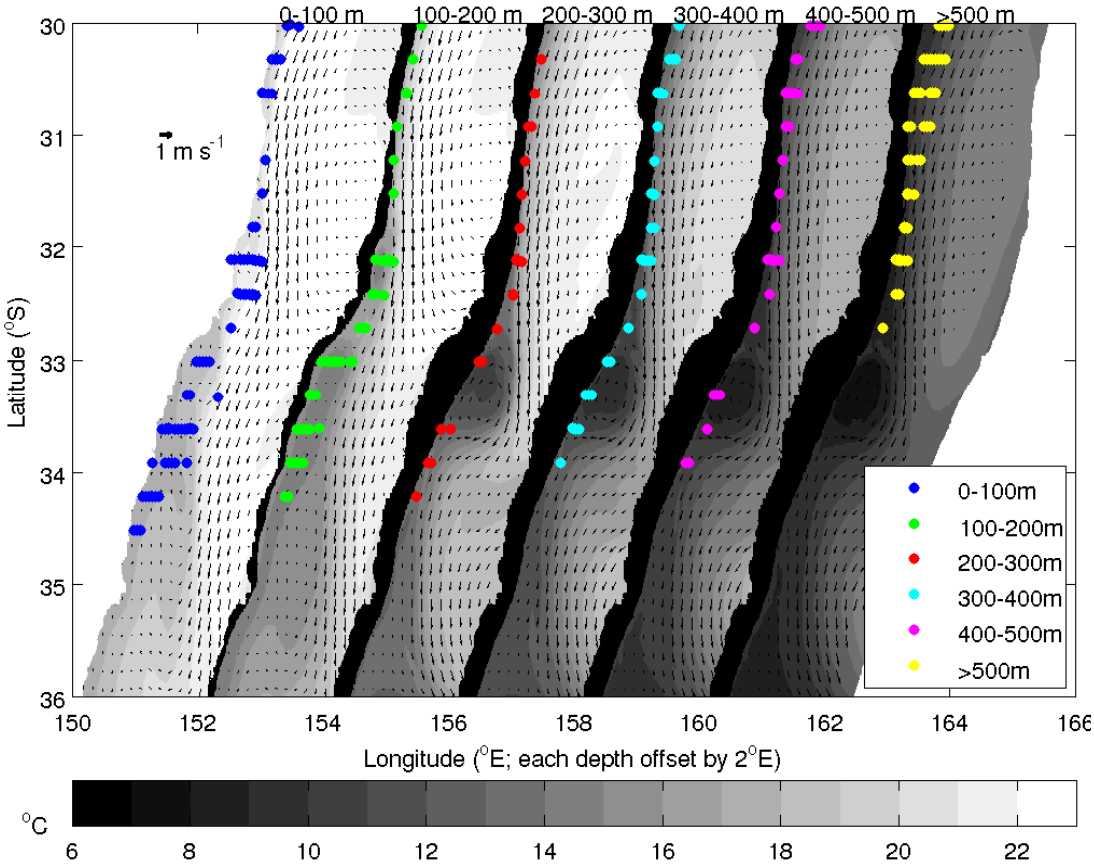

Figure 5.5: The initial (on the 23rd Sep; day 1) position of particles that were entrained into the eddy for the downwelling wind scenario. Dots indicate initial position of the seeding particles. Colours of the particles indicate initial depth, shading indicates temperature and arrows indicate velocity on the 23 Sep. The temperature, velocity field and particle positions are shown offset by 2°E for each depth to allow comparison.

5.3.2 Northward flow

The model domain is dominated by the southward flowing EAC so it is expected that particles are entrained into the eddy from the north. The entrainment of particles south of the eddy, particularly in the RWS and the DWS, is due to a northward flow on the continental shelf and slope (Fig. 5.6). This northward flow exists south of the eddy formation area and has a speed of about 0.2-0.5 m s^{-1} in the RWS and the DWS at 33^{o}S. By 32^{o}S this flow has weakened and is mainly in the surface layers, on the continental shelf. By 31^{o}S there is no evidence of this flow and the southward flow of the EAC dominates the area. In the UWS, while fewer particles are entrained from the south, there is still a small northward flow at depth. The currents on the shelf range from -0.2 to 0.2 m s^{-1}. By 32^{o}S all evidence of this northward flow is gone and the currents tend to be southward between 0-0.2 m s^{-1}.

5.3.3 Entrainment of deep water

The particles that are entrained into the eddy from below 500 m come from as deep as 700 m. There is little net vertical movement as the particles move south towards the eddy formation area (not shown). Once they are in the vicinity of the eddy, at 33^{o}S, they undergo upwelling into the eddy (Fig 5.7). This region of intense upwelling in the vicinity of the eddy formation location appears near the start of the simulation long before evidence of the eddy appeared in the modelled surface fields.

In the RWS and the DWS there are two groups of particles that become entrained into the eddy (Fig 5.7). One is situated on the continental slope (153-

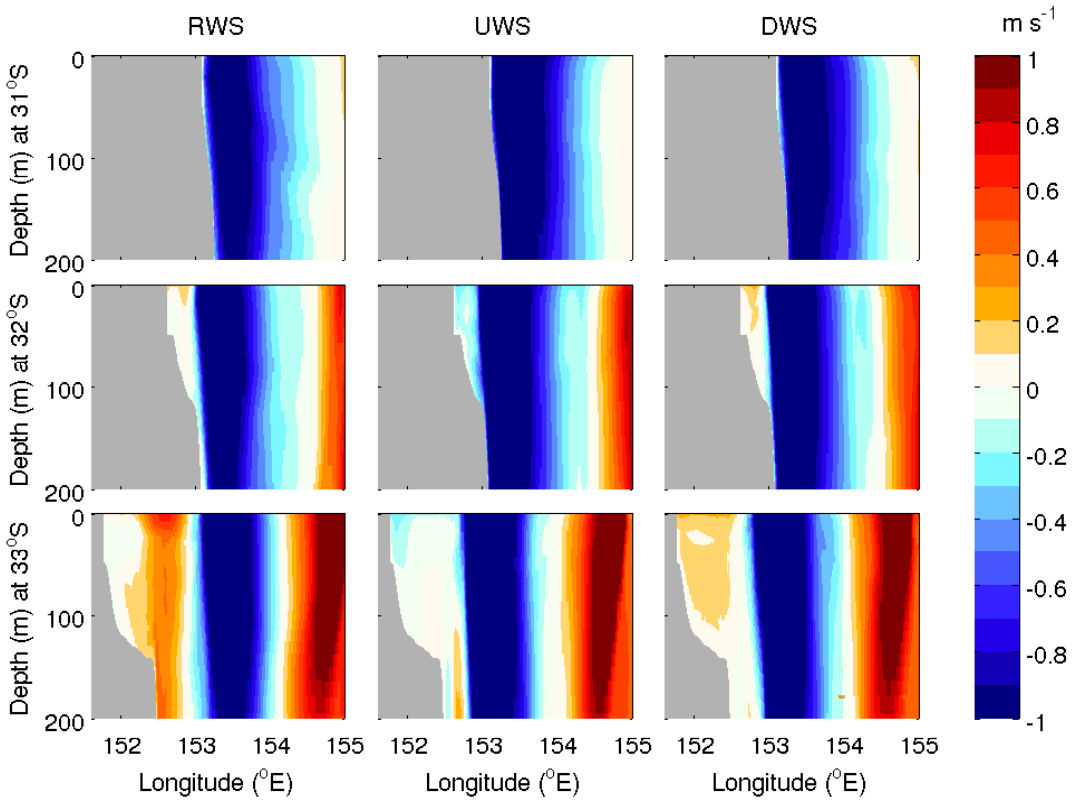

Figure 5.6: Vertical cross-sections of the north/south component of velocity for the RWS (left), the UWS (middle) the DWS (right) on model day 15. These cross-sections are through 31^{o}S (top), 32^{o}S (middle) and 33^{o}S (bottom). Red indicates a northward flow and blue indicates a southward flow.

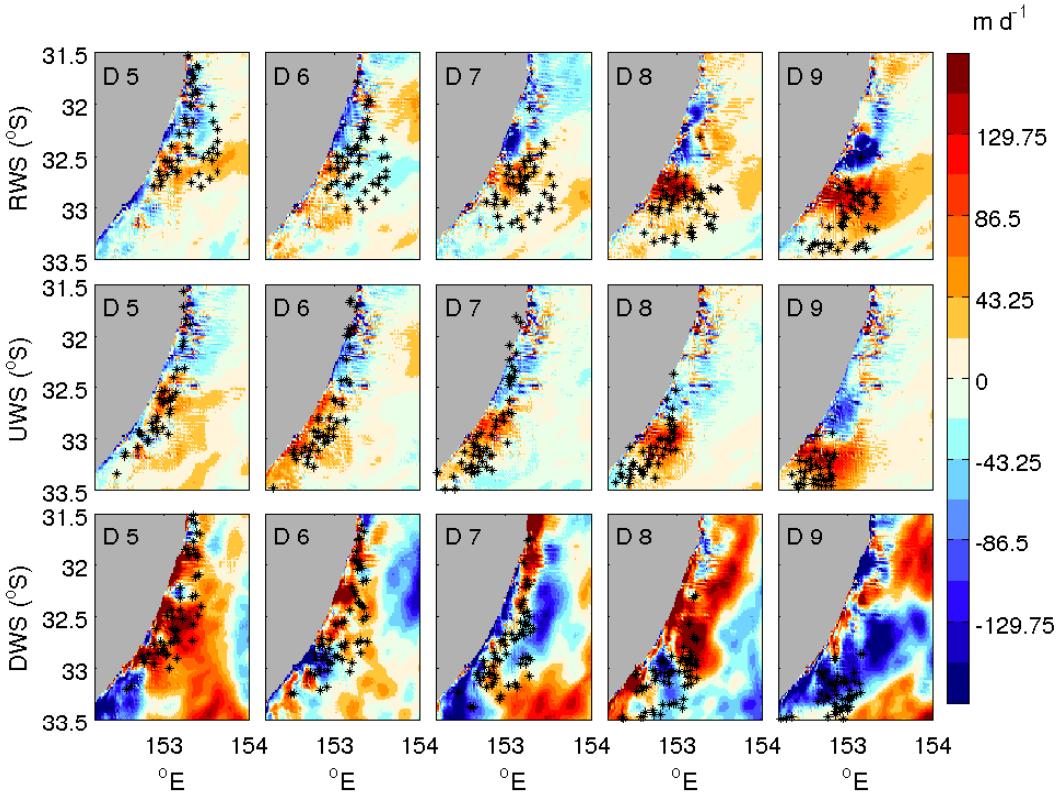

Figure 5.7: Vertical velocities at 500 m in the lead up to eddy formation (days 5-9). Red indicates upwelling and blue indicates downwelling. Daily position of particles that were released below 500 m that end up in the eddy are also shown (*).

153.5^{o}E) and flows south, straight into the middle of the intense upwelling region at 153^{o}E, 33.7^{o}S. The second group of entrained particles are seeded well off-shore (153.5-154^{o}E) and overshoot the upwelling region. These particles then rotate cyclonically around the upwelling region and are entrained into the northward flowing current on the continental slope before being entrained into the eddy.

This upwelling and cyclonic flow are evidence of the cyclonic eddy at depth pre-existing the cyclonic eddy as viewed in the surface. There is also evidence of the eddy first forming in the subsurface temperature and velocity fields (shown in the 300-500 m depth panels in Figs. 5.3 to 5.5). The eddy formed at depth, before extending up to the surface, entraining the continental shelf waters. This could be an explanation as to why the eddy waters are comprised of mainly deep and surface waters, but entrain less waters from 200-300 m range.

5.3.4 T and S properties of the entrained water

T and S signatures can be used to identify water types within the eddy (Fig. 5.8). In the RWS the less dense waters are sourced from the continental shelf (blue particles in Fig. 5.8). These are a distinct water type which have a density ranging from 1024.8-1026 kg m^{-3}. As expected the T-S signature generally has a decreasing density with a decreasing initial depth. The exception to this are the particles which were upwelled from below 500 m, north of the eddy (yellow particles in Fig. 5.8). These particles span the T-S signature of the particles sourced from the continental slope. This is likely to be the case as slope waters are sometimes sourced from the deeper waters due to uplift on the continental slope.

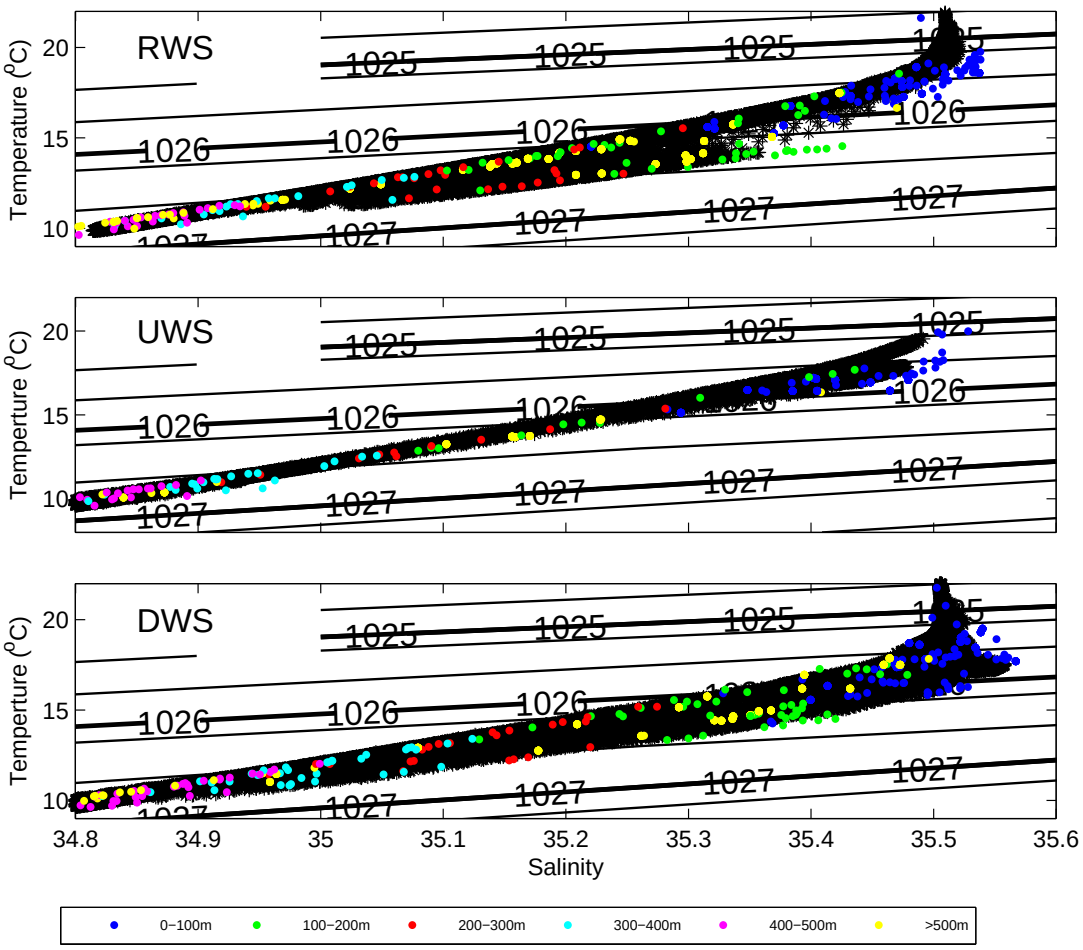

Figure 5.8: A T and S diagram for the RWS (top), the UWS (middle) and the DWS (bottom) eddy on day 12 (black). The initial T and S properties of particles that were entrained into the eddy are also shown in different colours according to their initial depth (as indicated in the legend).

Changing the wind field affects the water that is entrained into the eddy and, as such, results in different T and S properties in the eddy. In the UWS the T and S curve has two noticeable differences to that of the RWS. The first is that the waters of density <1025.2 kg m^{-3}, that were entrained from the continental shelf in the RWS, are missing in the UWS T and S curve. The UWS eddy does entrain continental shelf waters, as evidenced by the (blue) entrained continental shelf particles, but the continental shelf waters are, in general, more dense (due to upwelling). The second difference in the UWS is that the UWS eddy's T and S curve is missing a line of more dense water (situated under the main T and S curve). This more dense water has a salinity between 35-35.4 and temperature 11^oC-13^oC. These waters are also likely to have originated south of the eddy in the RWS and are missing in the UWS as waters south of the eddy were not entrained. The DWS has a similar T and S curve to the RWS. The main difference is in the more dense waters which sit under the main T and S curve. This line is thicker in the DWS as compared to the RWS and reaches the 1026 kg m^{-3} density contour.

5.4 Discussion

5.4.1 The tilting eddy

In a study of a CCE in the EAC region Oke and Griffin (2010) found that a CCE could tilt onto the continental shelf. In this section we see if we can confirm these findings for the RWS eddy in this model configuration. Using the point of minimum velocity in the eddy at different depths as the centre point for the

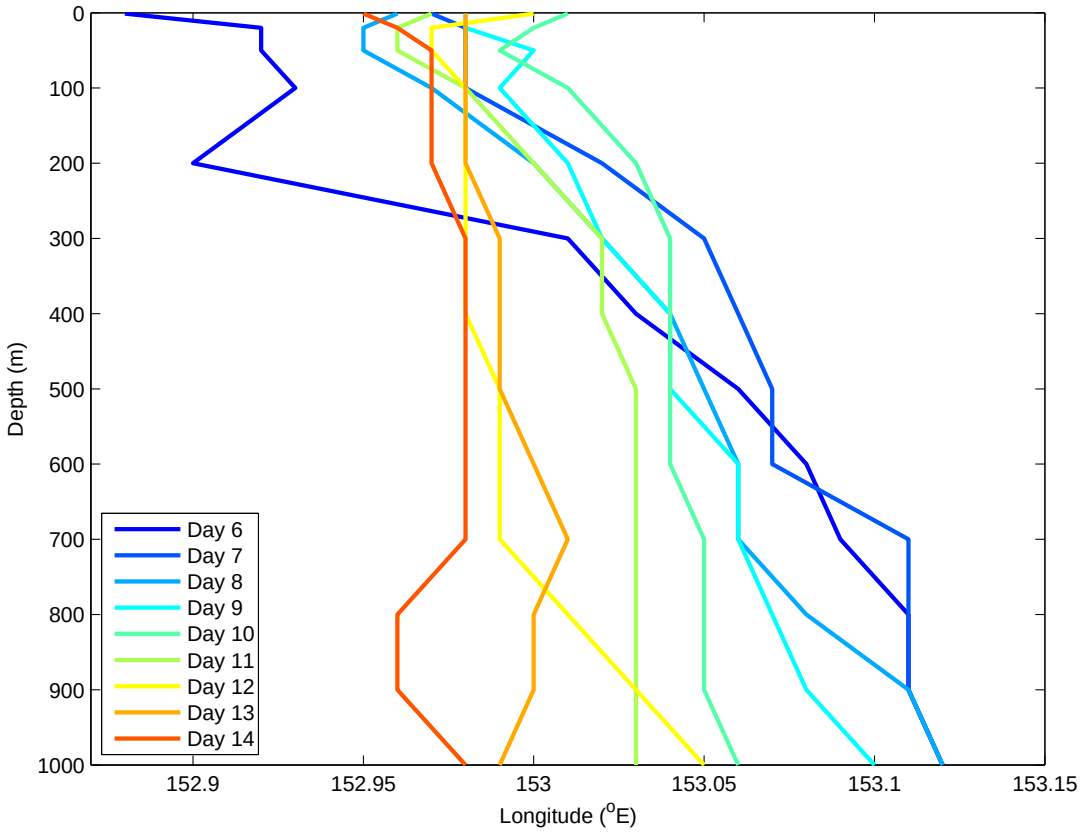

Figure 5.9: Lines of the centre point of the eddy over depth. These lines show how the eddy tilts and how this changes for different days (colour).

eddy, a line determining the tilt of the eddy can be drawn (Fig. 5.9).

On day 10 the eddy tilts across the continental shelf (Fig. 5.9), confirming that this eddy is similar to the Jun 2007 eddy of Oke and Griffin (2010). The eddy in this study initially tilts 37-56 km over the 1000 m depth of the eddy. This is a far greater tilt than the 28 km over 4500 m that was seen in Oke and Griffin (2010). Over the course of the simulation the eddy becomes less elongated and stands up.

Initially the bottom of the eddy is not in contact with the continental shelf. When the eddy stands up the surface layer of the eddy moves offshore and the

foot of the eddy moves towards the continental shelf. From day 14 the foot of the eddy moves away from the continental shelf with the surface of the eddy (not shown).

The time when the eddy is tilting coincides with when the eddy is forming. In this case, the tilting could be part of the forming stage of the eddy as shear is created between a northward current on the slope and the EAC. In addition to this, eddies that are growing through extraction of potential energy from the mean flow can tilt upstream against the mean flow as they grow. The tilt of the eddy has interesting consequences for upwelling and downwelling within the eddy.

5.4.2 Patterns of upwelling and downwelling

Simple conceptual models of the vertical motion within CCEs predict upwelling at the centre (Fig. 5.10 A). Slightly more complex conceptual models of eddies predict upwelling in the centre and downwelling on the edges while the eddy is spinning up (Bakun, 2006) (Fig. 5.10 B). Patterns of upwelling in the RWS CCE do not fit these simple conceptual models. Rather, there is upwelling in the northern section of the eddy and downwelling in the southern section (Figs. 5.11 and 5.10 C). This pattern of upwelling/downwelling can be explained by the tilt of the eddy onto the continental shelf. A horizontal clockwise flow (on a Southern Hemisphere CCE) will gain a slight upward/downward component to the flow on an eddy that is tilting. In this case, a flow that is eastward on a non-tilting eddy will become eastward with a slight downward component in a Southern Hemisphere CCE whose surface tilts to the west (i.e the eddy presented

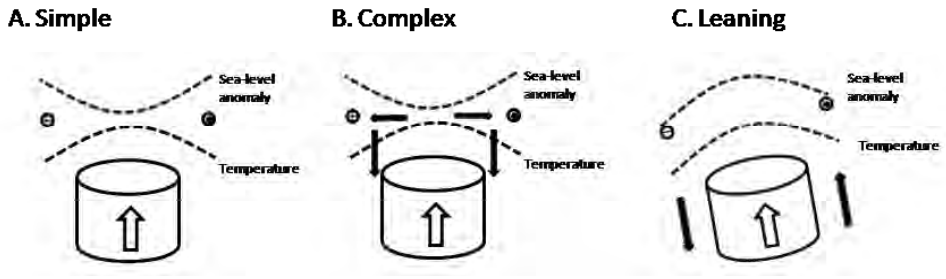

Figure 5.10: Schematic of movement within cold-core eddies for different models (simple, more complex and tilting). Arrows indicate direction of flow.

in this chapter). Similarly, a westward flow on a non-tilting eddy will become slightly upwelling as the eddy tilts to the west (Fig. 5.11).

This pattern of upwelling/downwelling due to the tilt of the eddy is reflected in the path of the particles as they travel around the eddy (Fig. 5.12). These particle paths are on a slant as they travel upwards on the south of the eddy but downwards on the north of the eddy. This tilt in the particle paths is greater at depth.

5.4.3 Northward flow on the continental shelf

A significant result of this chapter is that, depending on the winds, particle entrainment can come from the south. In the simulations presented here this was due to a northward flow on the continental shelf. This is a significant result as it means coastal species from far south of the eddy formation zone can be entrained into this eddy and others like it. In this section we look at how robust the model is at depicting this northward flow.

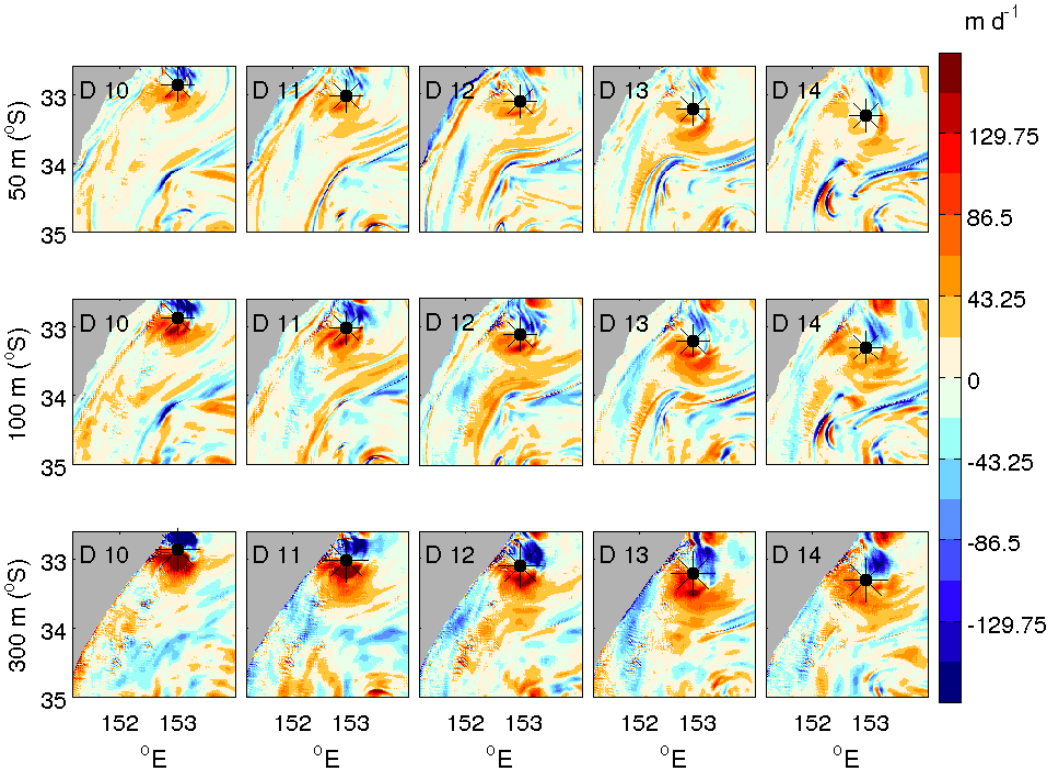

Figure 5.11: Vertical component of velocity in the RWS at 50 m (top row), 100 m (middle row) and 300 m (bottom row). Red indicated upward movement and blue indicates downward movement. The * indicates the eddy's centre as determined by sea-level height.

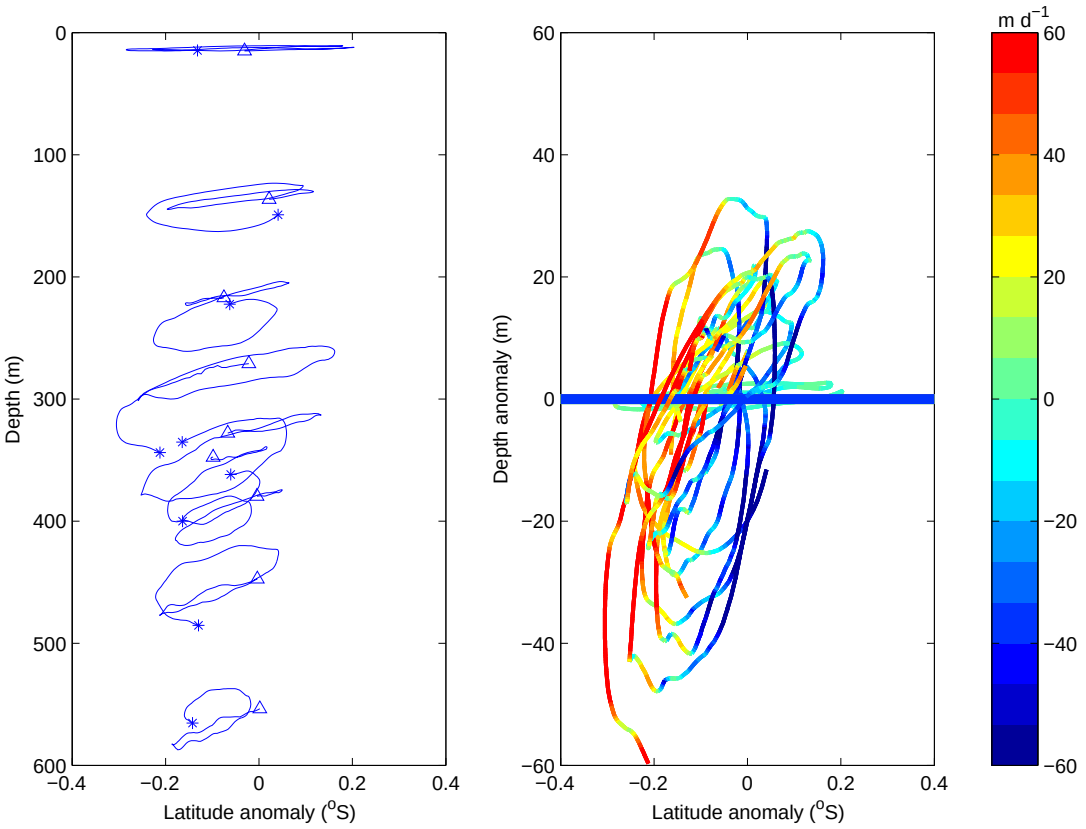

Figure 5.12: Left: Latitude versus depth of particles within the RWS eddy between model days 12 and 18. A * indicates the start of the track on day 12 and a Δ indicates the end of the track on day 18. The latitude shown is the latitude minus the eddy centre to remove the signal of the southward movement of the eddy. Right: the same as left except the average depth of each particle path has been subtracted from each depth point so that the deviation from the average is shown. Only a subset of particles are shown. Colour indicates the speed of vertical movement (blue means downward movement and red means upward movement.)

Model outputs of the meridional components of velocity are compared to mooring data from the continental shelf for the duration of the model runs (Fig. 5.13). Two moorings are used, SYD100 and SYD140, which are situated in 100 m of water and 140 m of water in a cross-shelf transect off Sydney (approx 34^{o}S) (Roughan and Morris, 2011). In the lead-up to the eddy's formation both the model and observations show a northward flow on the continental shelf (model day 5). The northward flow in the model begins 3 days prior to the northward flow in the observations, and ends 5 days afterwards. As such, water may not be entrained from as far south as that found in the model but, as the northwards flow did exist in the observations, it is likely that the eddy did entrain waters from the south.

Another feature of this northward flow that can be verified by observations is that of the depth of this northward flow. Velocities on the continental shelf and slope were obtained from a shipboard ADCP from a research cruise that coincided with the eddy formation (SS05/2009 from the 17-27 Oct 2009). In the model, the northward flow is evident on the continental shelf and slope. There is also evidence of this northward flow on the edge of the continental shelf and slope (down to 1000 m) in the velocity observations (Fig 5.14). As such, the deep reaching northward flow as seen in the model is a reproduction of a northward flow that can be verified by observations.

5.5 Summary

We used Lagrangian particle paths within the Regional Ocean Modelling System to determine source waters and regions of upwelling and downwelling within

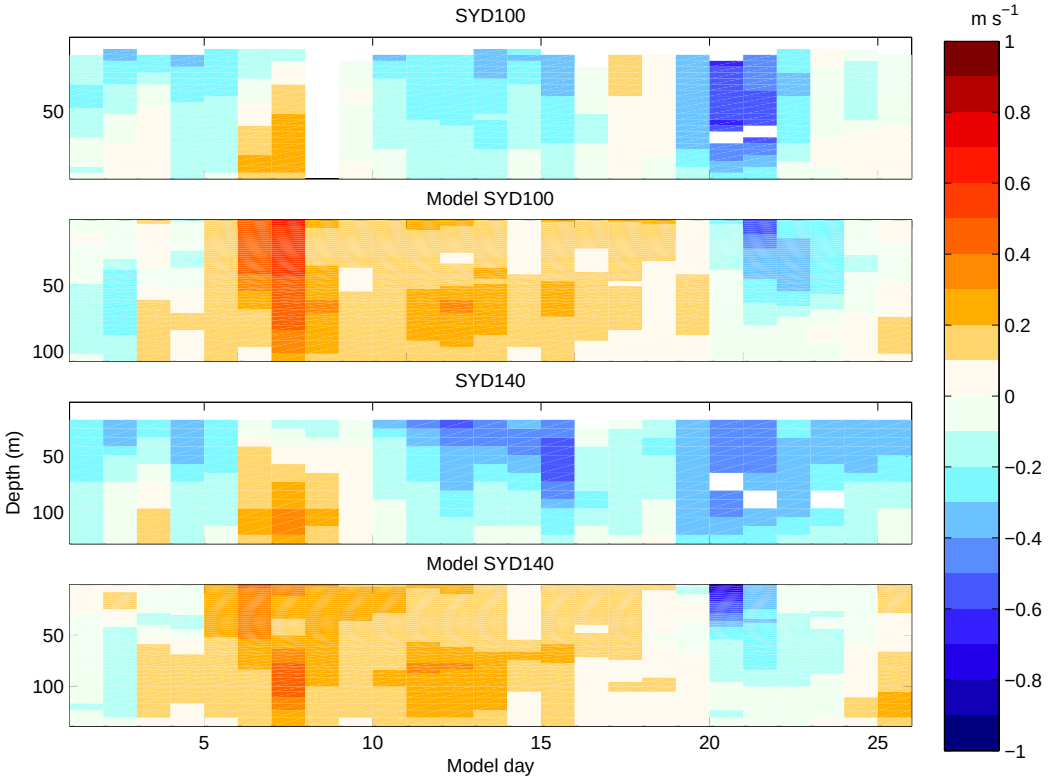

Figure 5.13: Observations of the north/south component of the flow (top and 3rd row) compared with model output (2nd and bottom row). These are the temporal change of velocity between days 1 and 26 at the location of the moorings SYD100 (top 2 rows) and SYD120 (bottom 2 rows). Red indicates a northward movement and blue indicates southward movement. All values are daily averages

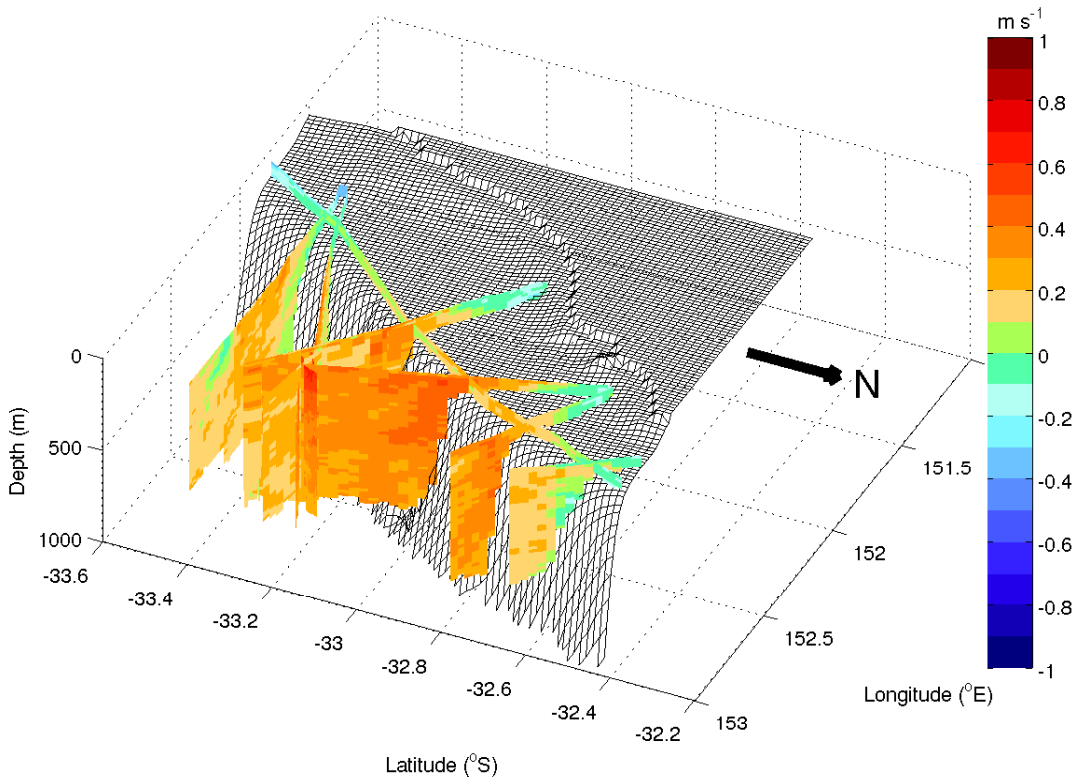

Figure 5.14: A 3D depiction of observations (from shipboard ADCP from the Southern Surveyor research cruise SS05/09) of the meridional component of velocity for the continental shelf and slope for the period from 17 to 27 October (17 October is model day 25). Red indicates a northward flow and blue indicates a southward flow.

a CCE that formed in October 2009. We found that, despite the predominantly southward flowing current, water can be entrained into the eddy from shelf regions south of the eddy. This was due to a northward flow on the continental shelf just prior to the eddy's formation. Altering the wind field to be upwelling favourable reversed the shelf flow and, hence, prevented entrainment of water from the south of the eddy. Entrainment of different source waters affected the T and S properties of the eddy. The upwelling wind scenario, which did not entrain water from the south, was missing distinctive T and S signatures. The tilt of the eddy onto the continental shelf was investigated and it was found that this created a distinct upwelling and downwelling pattern within the eddy. The northward flow within the model on the continental shelf and slope was shown to be robust by comparisons with observations of continental shelf and slope velocities.

Chapter 6

Plankton population dynamics in a Western Boundary Current cold-core eddy.

Abstract

Chapter 5 shows that continental shelf waters from a wide latitudinal range across the southeast Australian continental shelf are entrained into the October 2009 cold-core eddy (CCE). In this chapter a biological model is initialised to investigate if this entrainment will enhance biological production of continental shelf waters. Upwelling brings nutrients onto the continental shelf. A phytoplankton bloom forms in the upwelled water which is then entrained into the forming CCE. After entrainment the phytoplankton bloom increases in concentration followed by an increase in zooplankton concentration. As

the phytoplankton bloom, and subsequent zooplankton bloom, in the centre of the eddy is older than that on the peripherals the zooplankton numbers increase in the centre of the eddy first, consuming the phytoplankton. This results in a lower phytoplankton concentration in the eddy centre as compared to the eddy peripherals. These results show that CCEs do enhance the biological production of entrained waters.

6.1 Introduction

6.1.1 Biological modelling in the East Australian Current

Chapters 4 and 5 investigated the physical conditions surrounding the formation of the eddy. Continental shelf waters were entrained into the eddy but the effect of entrainment on biological processes cannot be obtained from only a study of physical processes. To aid the interpretation of the physical constraints on the biological processes a biological model is needed.

In the EAC region there have been a few biological modelling studies. Baird et al. (2006a,b) looked at plankton dynamics on the continental shelf and Macdonald et al. (2009) looked at how these plankton blooms affect carbon fluxes. Both studies were idealised and lacked the resolution to effectively capture submesoscale cold-core eddies (CCEs) such as that seen in Chapters 4 and 5. The realistic simulations of the CCE (Chapters 4 and 5), when coupled with a biological model, can give insights into the biological dynamics within EAC mesoscale CCEs.

A biological model is initialised within the higher resolution configuration (as described in Chapters 2 and 4) to further investigate biological implications in the CCE under realistic wind forcing (RWS). In particular, the effect of upwelling and entrainment into a cold-core eddy (CCE) on the ecosystem dynamics on the continental shelf off southeast Australia is examined. The biological model is initialised and run for a period coinciding with the simulations of the October 2009 CCE (Chapter 4). It is considered unnecessary to initialise the biological model coinciding with the October 2008 warm-core eddy (WCE; Chapter 3) as, in contrast, WCEs tend to be biologically unproductive. Furthermore, the WCE did not entrain continental shelf waters and, therefore, is unlikely to be important for continental shelf species.

6.1.2 The biological model

The biological model initialised is known as the Fennel model (Fennel et al., 2006). The Fennel et al. (2006) biological model is based on the Fasham et al. (1990) model. It has 7 state variables: phytoplankton, zooplankton, nitrate, ammonium, small detritus, large detritus and phytoplankton chlorophyll. An important addition to the Fasham et al. (1990) model is the addition of the state variable phytoplankton chlorophyll. It has units of mg chlorophyll m^{-3} and is a measurement of chlorophyll stored in the phytoplankton. In the Fennel et al. (2006) model, phytoplankton grow from the available nutrients (nitrate and ammonium). Phytoplankton are moved into the zooplankton group via grazing or into the small and large detrital groups via a mortality rate. Zooplankton also move into the detrital groups via a mortality rate. Detritus and a loss from

zooplankton due to inefficient grazing are transferred via a decay rate into the ammonium group. The ammonium group decays into the nitrate group.

In this Chapter the biological model configuration is described (Sec. 6.2). This model is then used in a case study of biological interactions in the CCE as described in Chapters 4 and 5. The surface and vertical biological reaction and entrainment of continental shelf waters are described in Sec. 6.3.1 and Sec. 6.3.2 respectively. The temporal change in biological tracers and how this affects the patterns of plankton on the eddy are discussed in Sec. 6.4.1.

6.2 Methods

6.2.1 The physical model

The ocean state of the October 2009 CCE is simulated using the Regional Ocean Modelling System (ROMS). A detailed description of the model's configuration for the EAC region can be found in Chapter 2 and a brief summary is included here. SynTS (Ridgway et al., 2008) is used to prescribe initial, boundary and climatology data. The Flather (1976) condition is used for the barotropic velocity components at the northern boundary. The baroclinic velocity field and the tracers on the northern boundary are nudged to external estimates at a timescale of 4 days. All other boundaries are radiative. NCEP 2.5-degree 6 hourly reanalysis data sets (Kalnay et al., 1996) and the NOAA/NCDC Blended 6-hourly 0.25-degree Sea Surface Winds data set (Zhang et al., 2006) are used to implement the Bulk flux method of Fairall et al. (1996) at the atmospheric boundary. The model is initialised on 18 September 2009 and has a 5-day spin-up.

More details on the forcings and initial conditions can be found in in Chapter 2. The biological model is initialised after the 5-day spin-up on model day 1. The grid used is the same as that used in Chapters 4 and 5.

6.2.2 Biological initial conditions

The initial nitrate (NO_3) conditions came from CSIRO's CARS climatology (Ridgway et al., 2002). Average October nitrate concentrations are used but modified so that, if the initial nitrate's mixed layer depth is shallower than the physical model's mixed layer depth, the nitrate's mixed layer depth is increased. This is to prevent the nitrocline from mixing into the mixed layer, (which can create a spurious phytoplankton bloom). All other variables are initialised with a small seeding population (0.01 mmol N m^{-3}). With the exception of the zooplankton half saturation constant and the zooplankton maximum growth rate the parameters used were the default (Fennel et al., 2006). The zooplankton half saturation constant and the zooplankton maximum growth rate have been increased to account for geographical differences in zooplankton processes. Short test show that this yields more realistic results. The parameters used in the model are shown in Table 6.1.

Symbol	Description	Units	Value
AttSW	Light attenuation due to seawater	m^{-1}	0.04
AttChl	Light attenuation by chlorophyll	(mg Chl m^2)$^{-1}$	0.02486
PARfrac	Fraction of shortwave radiation that is photosynthetically active	none	0.43
Vp0	Eppley temperature-limited growth parameter	none	1.0
I_{thNH4}	Radiation threshold for nitrification inhibition	Watt m^2	0.0095
D_{p5NH4}	Half-saturation radiation for nitrification inhibition	Watt m^2	0.1
NitriR	Nitrification rate: oxidation of NH4 to NO3	day^{-1}	0.05
K_{NO3}	Inverse half-saturation for phytoplankton NO3 uptake	(mmole N m^{-3})$^{-1}$	2.0
K_{NH4}	Inverse half-saturation for phytoplankton NH4 uptake	(mmole N m^{-3})$^{-1}$	2.0
K_{Phy}	Zooplankton half-saturation constant (squared) for ingestion	(mmole N m^{-3})^2	0.05
PhyIP	Phytoplankton, NH4 inhibition parameter	(mmole N)$^{-1}$	1.5
PhyIS	Phytoplankton, initial slope of P-I curve	mg C/(mg Chl Watts m^{-2} day)	0.025
PhyMin	Phytoplankton minimum threshold value	[mmole N m^{-3}	0.001
PhyMR	Phytoplankton mortality rate	day^{-1}	0.15
$ZooAE_N$	Zooplankton Nitrogen assimilation efficiency	none	0.75
ZooBM	Zooplankton Basal metabolism	none	0.1
ZooER	Zooplankton specific excretion rate	day^{-1}	0.1
ZooGR	Zooplankton maximum growth rate	day^{-1}	0.75
ZooMR	Zooplankton mortality rate	day^{-1}	0.025
LDeRRN	Large detritus remineralization rate N-fraction	day^{-1}	0.01
CoagR	Coagulation rate: aggregation rate of small detritus and phytoplankton	day^{-1}	0.005
DeRRN	Small detritus remineralization rate N-fraction	day^{-1}	0.03
wPhy	Vertical sinking velocity for phytoplankton	m day^{-1}	0.1
wLDet	Vertical sinking velocity for large detritus	m day^{-1}	1.0
wSDet	Vertical sinking velocity for small detritus	m day^{-1}	0.1

Table 6.1: Parameters used in the biological model.

6.2.3 Biological boundary conditions

In a similar manner to the physical model, biological open boundary conditions are specified on the northern, eastern and southern bounderies. The western boundary is land. Biological variables are nudged back to their initial conditions in the northern boundary and the eastern and southern boundaries have radiative conditions.

6.2.4 Nudging zone

In addition to the northern boundary condition there is a boundary nudging layer in the first 40 grid squares inwards from the northern boundary. In a similar manner to the physical model, the nudging timescale is 1 day^{-1} on the outer grid squares but tapers linearly to zero in the inner grid squares. This enables the model to be free running in the middle of the domain. This nudging removes spurious phytoplankton growth due to upwelling in the boundaries.

6.3 Results

6.3.1 Surface evolution of a plankton bloom

In the Fennel et al. (2006) model used here there are 2 nutrient classes: a nitrate class (NO_3) and an ammonium class (NH_4). Decaying detritus adds to the ammonium class which is nitrified to the nitrate class. Phytosynthetic growth is reliant on avaliable nutrients (NO_3 and NH_4) but phytoplankton grow prferrentially from the nitrate class so that the presence of ammonia as a nutrient will inhibit growth. At the time of the phytoplankton bloom (day 9) NH_4 concerntra-

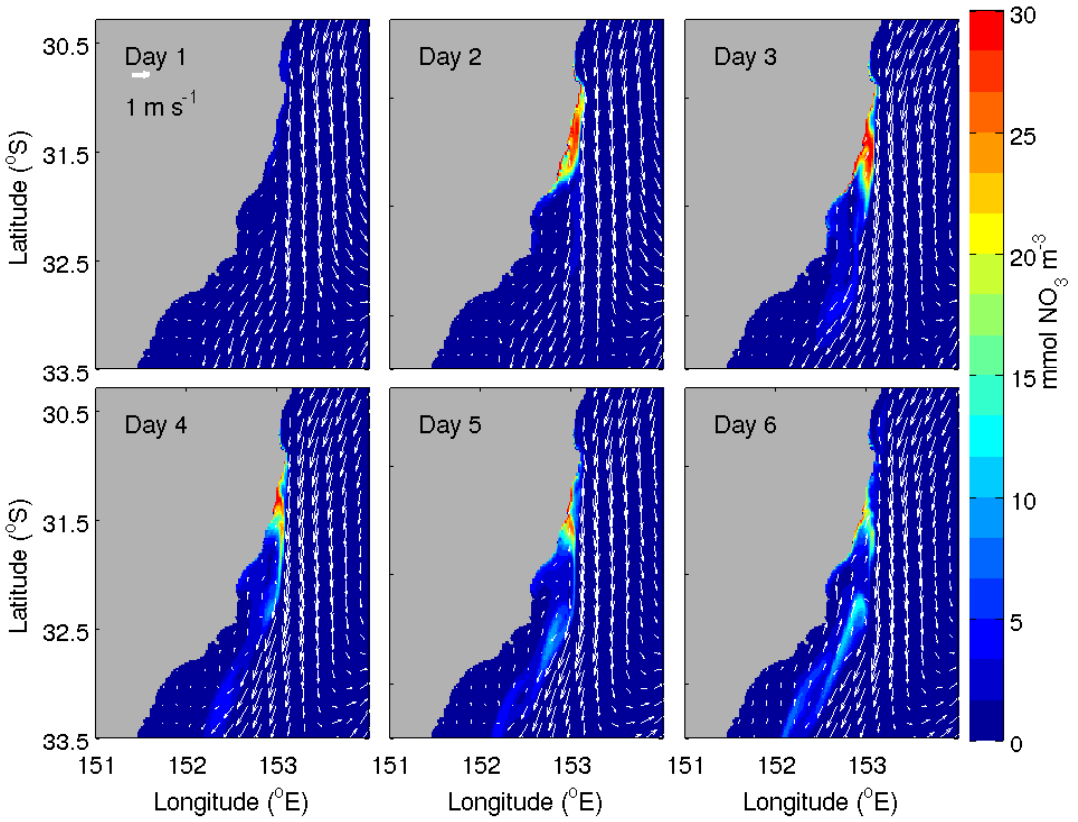

Figure 6.1: Sea surface nitrate for days 1-6. Arrows indicate current velocity.

tions are small (less than 0.01 mol N m^{-3}) so NO_3 concerntrations are examined here. Initially the surface fields are deplete of nitrate (Fig 6.1). The EAC drives upwelling onto the continental shelf and slope lifting up cool nutrient rich waters onto the continental shelf (Fig. 6.2). This is evident in the surface nitrate fields from day 2 in a localised area (31-31.5^{o}S). This plume of upwelled nitrate is advected south along the continental shelf by the EAC (Fig 6.1). More nitrate is upwelled at 31-31.5^{o}S to replace the advected nitrate and a long filament of upwelled nitrate forms along the continental shelf (Fig 6.3). This upwelled nitrate is advected off the continental shelf and is entrained into the forming eddy.

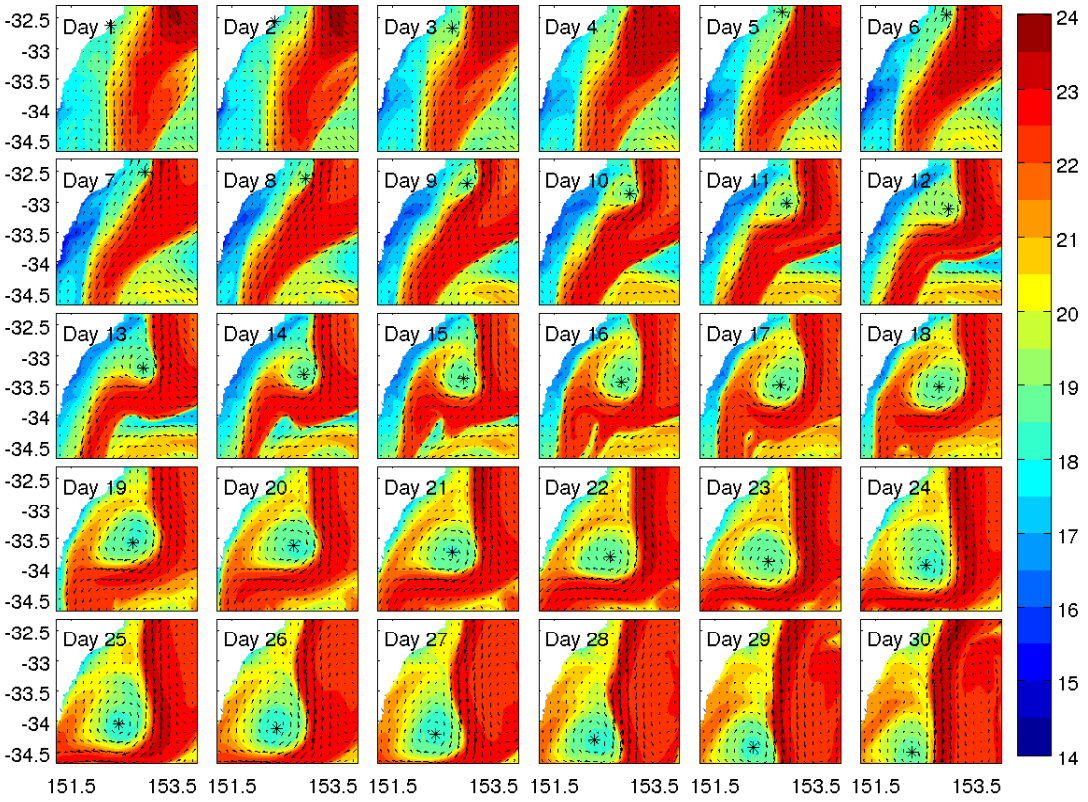

Figure 6.2: Sea surface temperature for days 1-30. Arrows indicate current velocity. The '*' indicates the eddy centre.

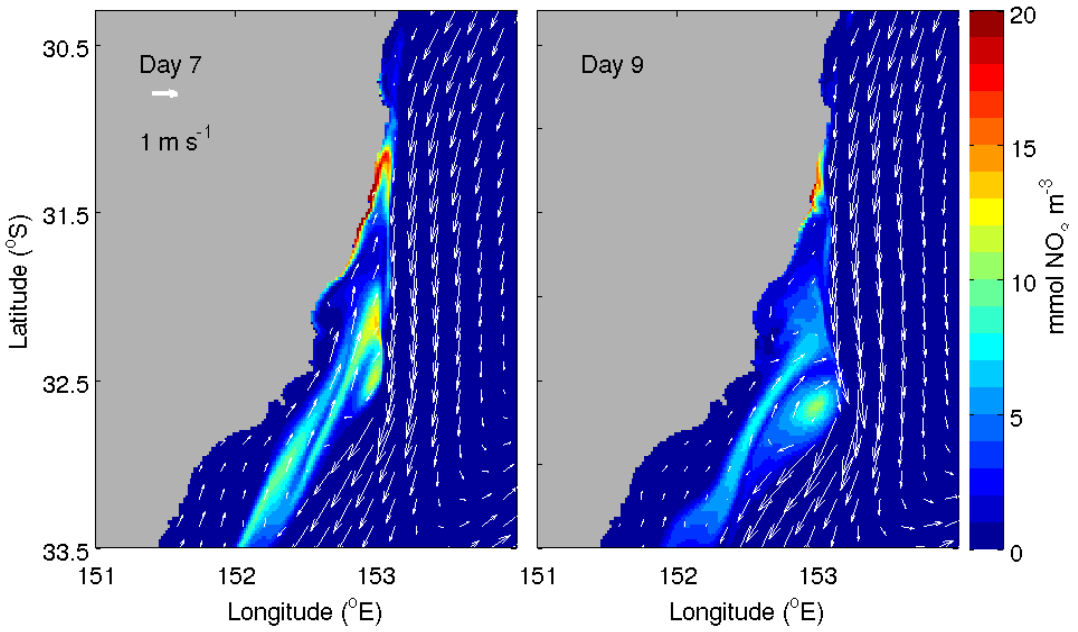

Figure 6.3: Sea surface nitrate for days 7-9. Arrows indicate current velocity.

Over time the eddy becomes larger as it entrains continental shelf waters. The eddy is connected to the continental shelf up till day 19, entraining the upwelled nitrate plume from 31-31.5°S (Fig 6.4). The nitrate concentration in the centre of the eddy is larger than that of the entrained water on the peripherals of the eddy. This increase in nitrate in the eddy centre is indicative of upwelling at the centre of the eddy. In this case the eddy is contributing nitrate to the entrained nitrate plume.

Phytoplankton growth in the region is limited by the available nitrogen. As such, when nitrogen is upwelled from depth, phytoplankton blooms often form. This is evident in the model from day 7 as a phytoplankton bloom forms along the continental shelf in the advected nitrate plume that was upwelled from day 2 at 31-31.5 °S (Fig 6.5). This continental shelf phytoplankton bloom increases

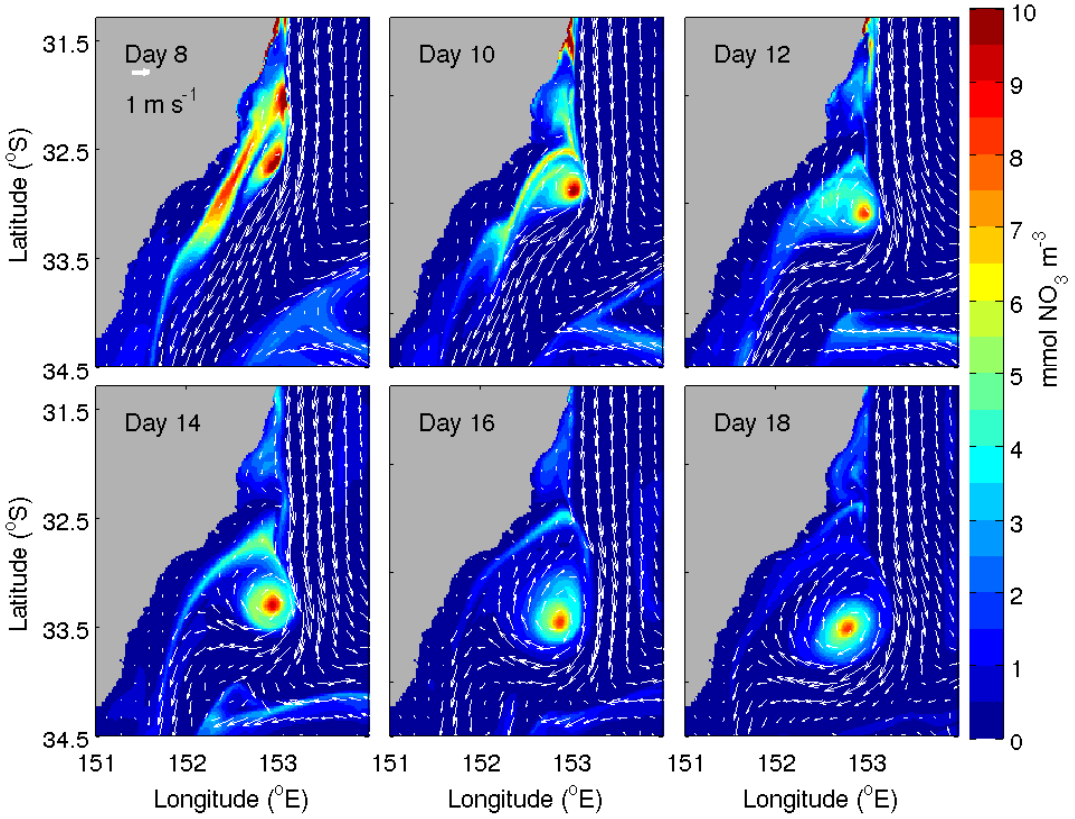

Figure 6.4: Sea surface nitrate for days 13-18. Arrows indicate current velocity.

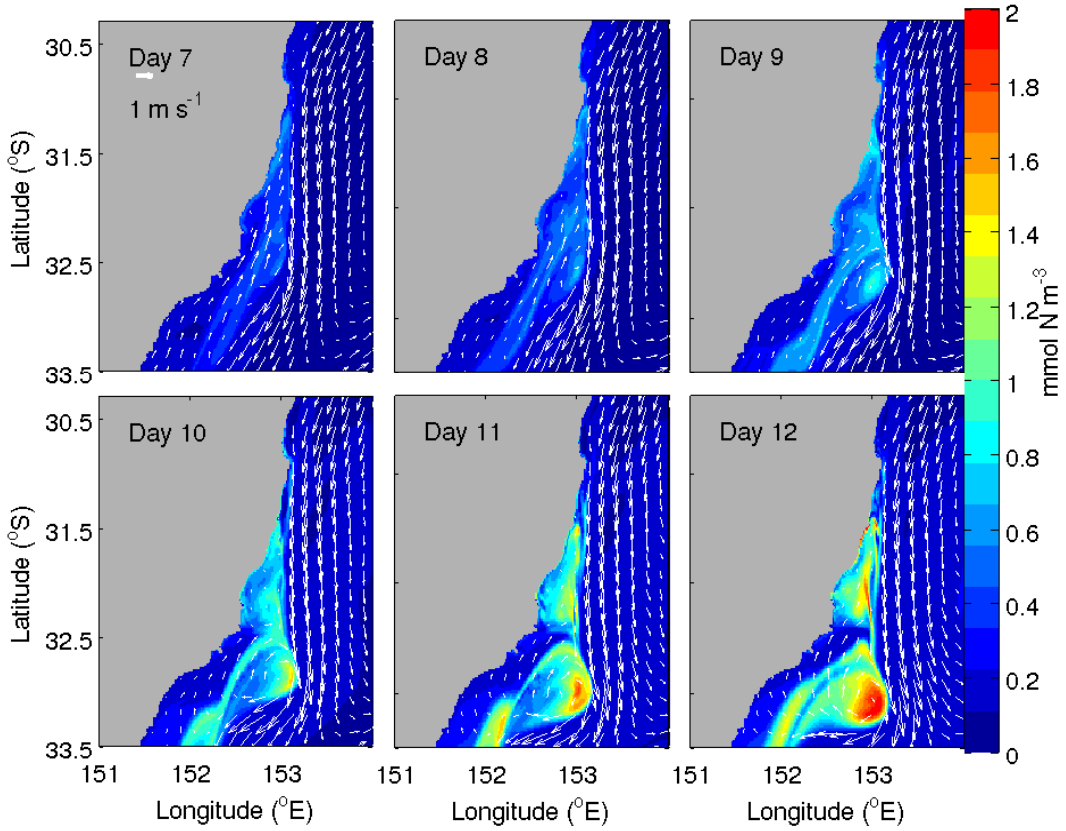

Figure 6.5: Sea surface phytoplankton for days 7-12. Arrows indicate current velocity.

significantly (from 1.4 to 2 mmol N m^{-3}) between days 11 to 12 (Fig 6.5). This increase is due to entrainment of the phytoplankton into the eddy and subsequent growth. The increased nitrate from upwelling in the centre of the eddy significantly enhances the growth of the entrained phytoplankton bloom.

From day 13 the phytoplankton concentrations in the centre of the eddy begin to decrease (Fig 6.6). This decrease is initially located in the centre of the eddy but later found around the eddy edge. By day 18 the phytoplankton concentrations in the centre have decreased significantly so that the phytoplankton concentration in the centre is less than that of the peripherals. Why this is the

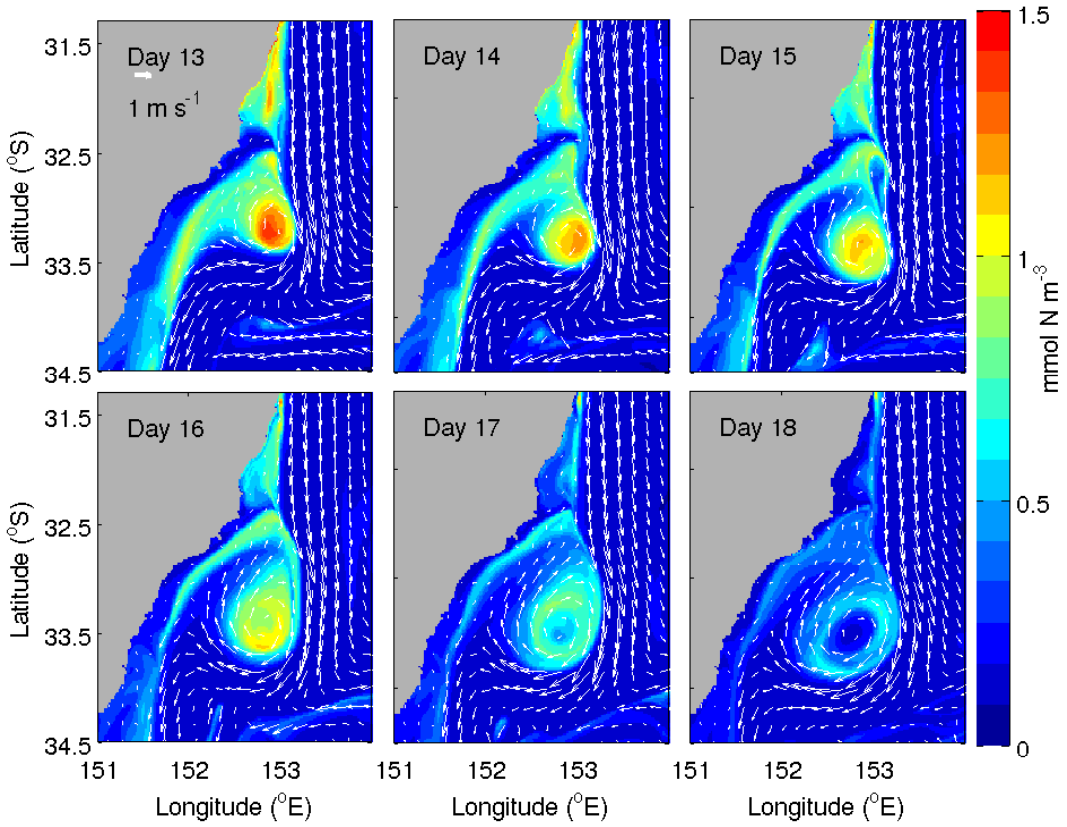

Figure 6.6: Sea surface phytoplankton for days 13-18. Arrows indicate current velocity.

case is the subject of the next few sections.

As zooplankton are consumers of phytoplankton, zooplankton blooms often follow phytoplankton blooms. In the biological model zooplankton do not assimilate all the available phytoplankton nitrogen so that the zooplankton blooms form with less nitrogen concentrations than the phytoplankton blooms. The zooplankton bloom that forms in the continental shelf upwelled plume is of a small concentration and area (Fig 6.7). The zooplankton bloom forms mainly in the eddy. For this eddy, entrainment into the eddy enhances higher level trophic production. From day 13 zooplankton concentrations increase within the eddy,

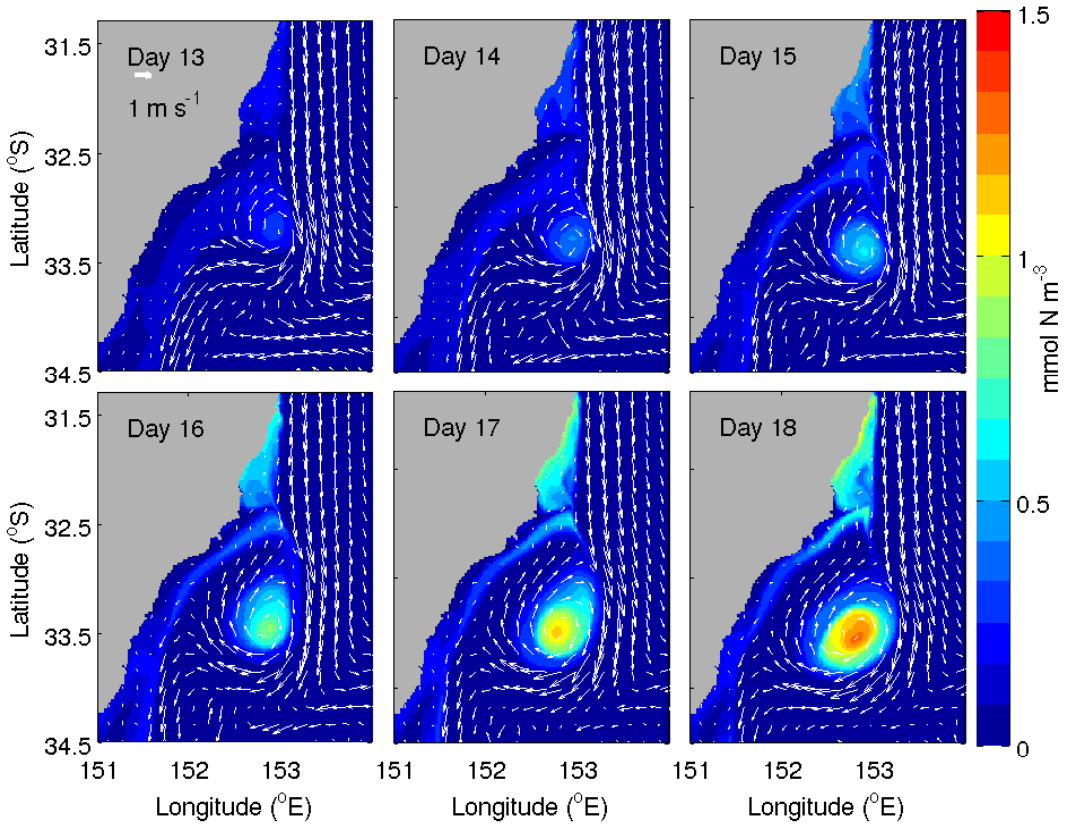

Figure 6.7: Sea surface zooplankton for days 13-18. Arrows indicate current velocity.

reaching a maximum by day 19 (Fig 6.8). This increase is in the eddy centre, coinciding with the decrease of phytoplankton in the centre of the eddy.

6.3.2 Vertical evolution of a plankton bloom

Evidence of nitrate upwelling into the eddy can also be seen in vertical transects (Fig. 6.9). As is normal for a CCE, nitrate from depth is uplifted. This uplifted nitrate tilts into the continental shelf due to the tilt of the eddy as discussed in Chapter 5. The uplifted nitrate has a higher concentration (>12 mmol N m^{-3}) than that of the nitrate in the entrained shelf waters (<1.6 mmol N m^{-3}). Up-

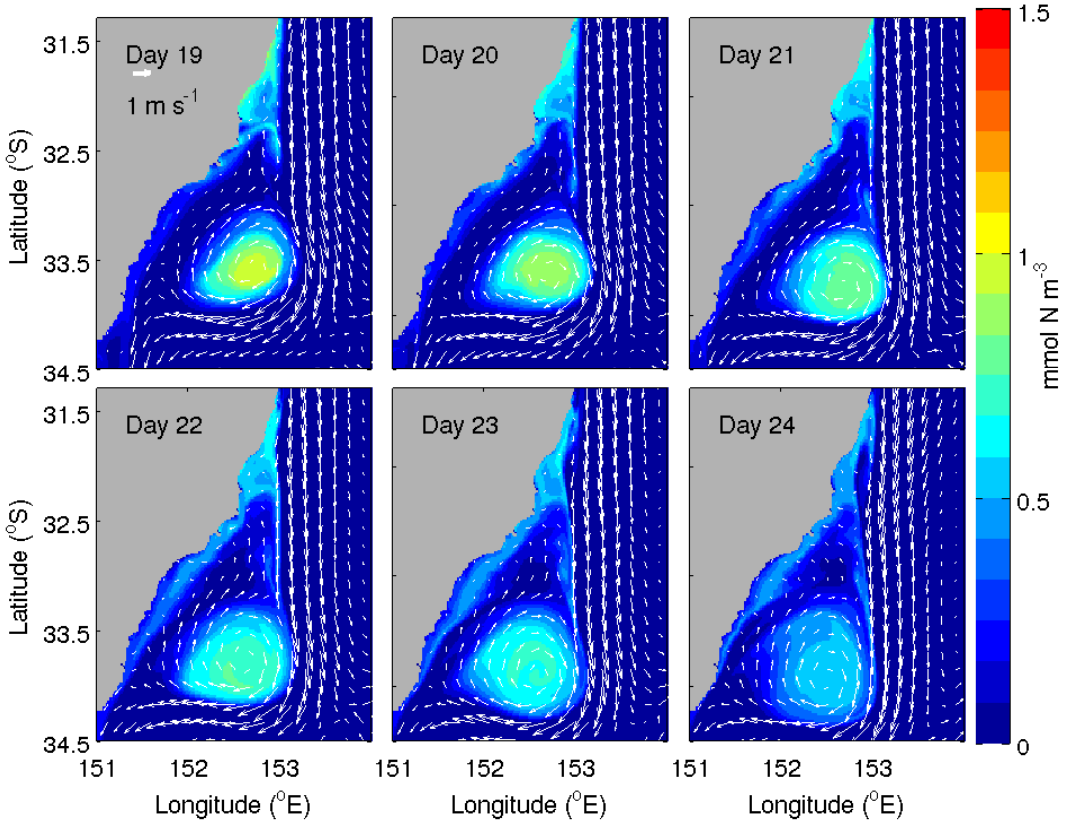

Figure 6.8: Sea surface zooplankton for days 19-24. Arrows indicate current velocity.

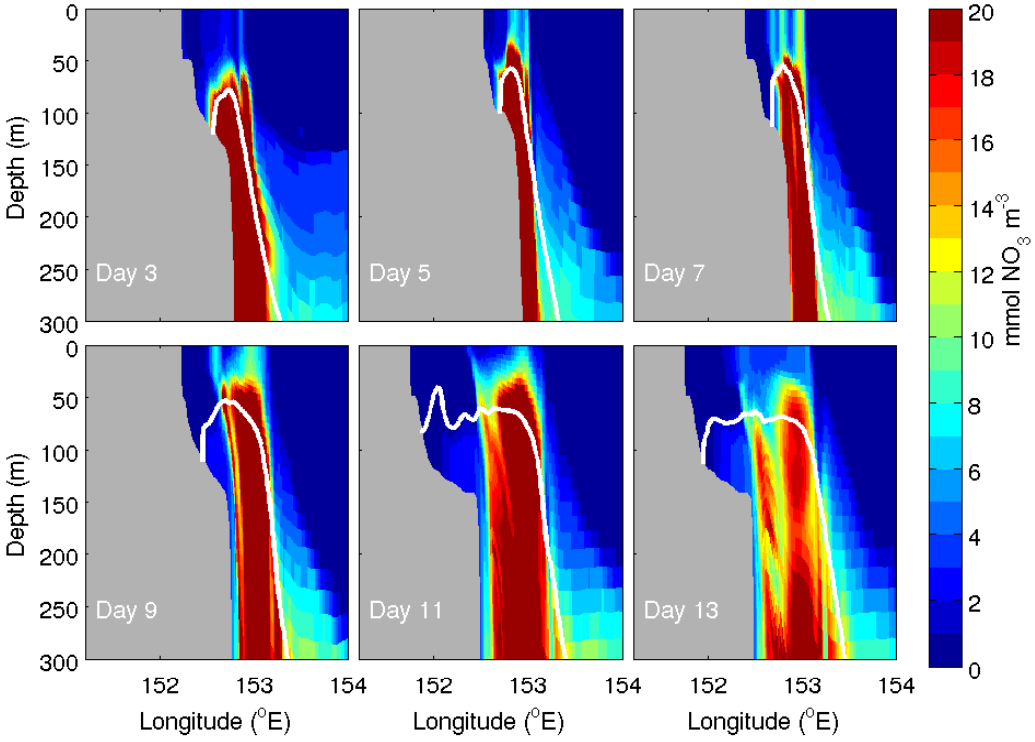

Figure 6.9: Vertical profile of nitrate through the centre of the eddy (as indicated by a * in Fig. 6.2) for every second day between days 3 and 13. The 16°C isotherm is shown in white.

lifted nitrate reaches a depth of 0-20 m in the eddy centre. From day 15, the uplift in the eddy centre is high enough in the water column to be mixed into the entrained surface waters (Fig. 6.10) resulting in the high phytoplankton biomass as seen in the centre of the eddy in Section 6.3.1.

For most of the eddy the phytoplankton and zooplankton bloom form in the surface 20 m (Fig. 6.11). This is above the depth where the upwelled nitrate reaches so that the bloom forms from entrained nitrate and nitrate that has been mixed up to the surface from the 20 m upwelled nitrate.

On the peripherals of the eddy the phytoplankton and zooplankton blooms

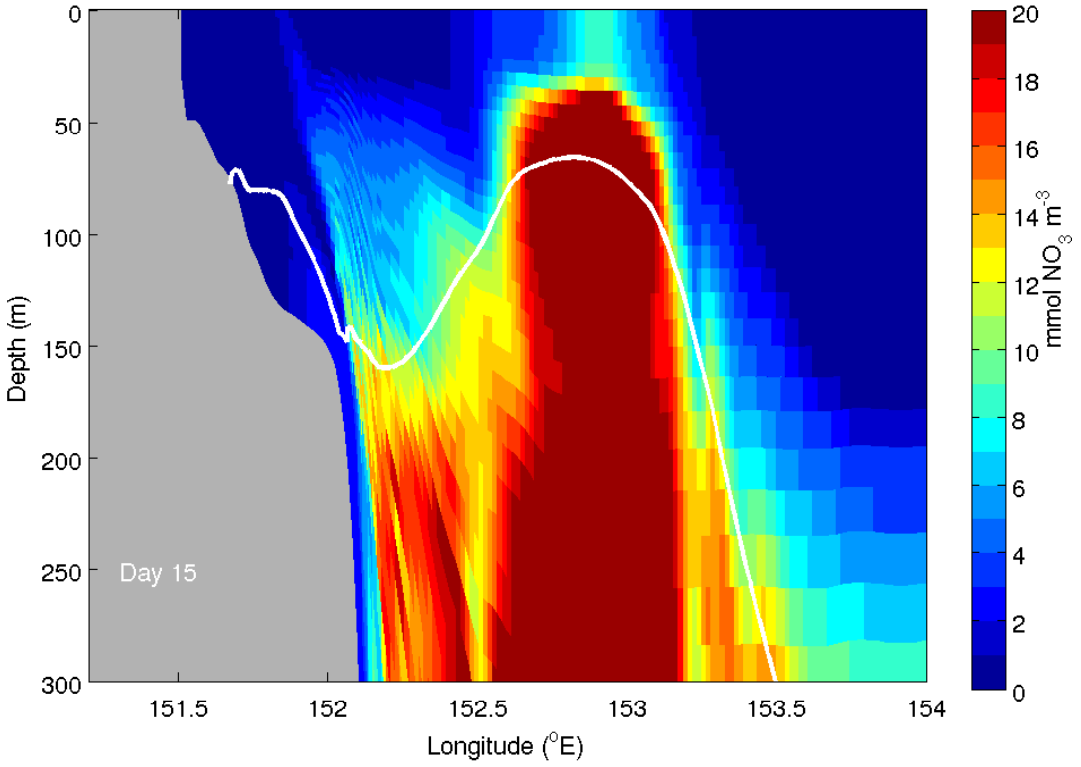

Figure 6.10: Vertical profile of nitrate through the centre (as indicated by a * in Fig. 6.2) of the eddy for day 15. The 16°C isotherm is shown in white.

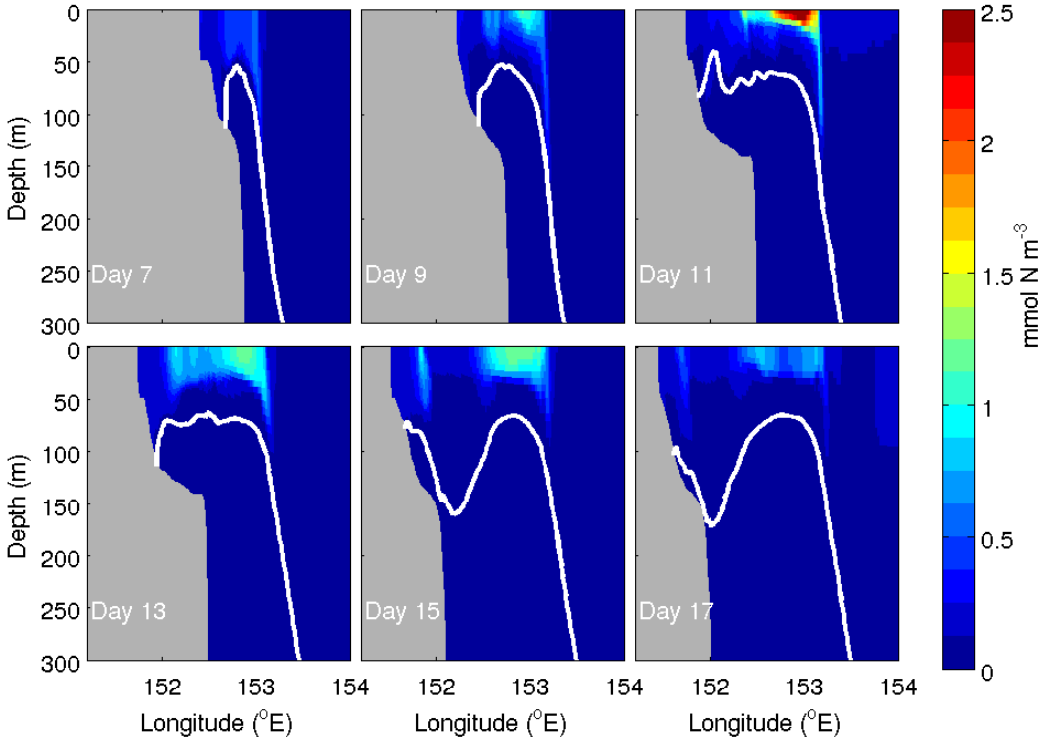

Figure 6.11: Vertical profile of phytoplankton through the centre (as indicated by a * in Fig. 6.2) of the eddy for every second day between days 7 and 17. The 16°C isotherm is shown in white.

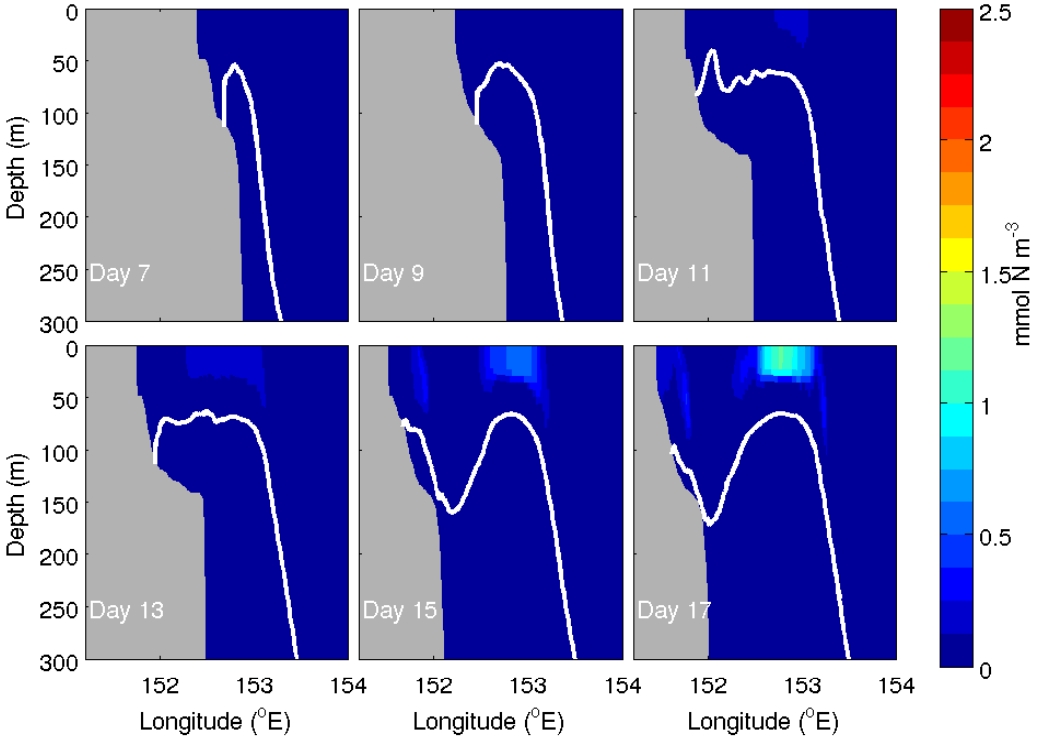

Figure 6.12: Vertical profile of zooplankton through the centre (as indicated by a * in Fig. 6.2) of the eddy for every second day between days 7 and 17. The 16°C isotherm is shown in white.

extend down to a depth of 150 m (Fig. 6.11 and 6.12). Sufficient light for phytoplankton production does not extend down to this depth (Fig 6.13), preventing growth of phytoplankton. Rather, the occurrence of phytoplankton and zooplankton at this depth is indicative of downwelling at the edges of the eddy pushing the phytoplankton and zooplankton down at depth.

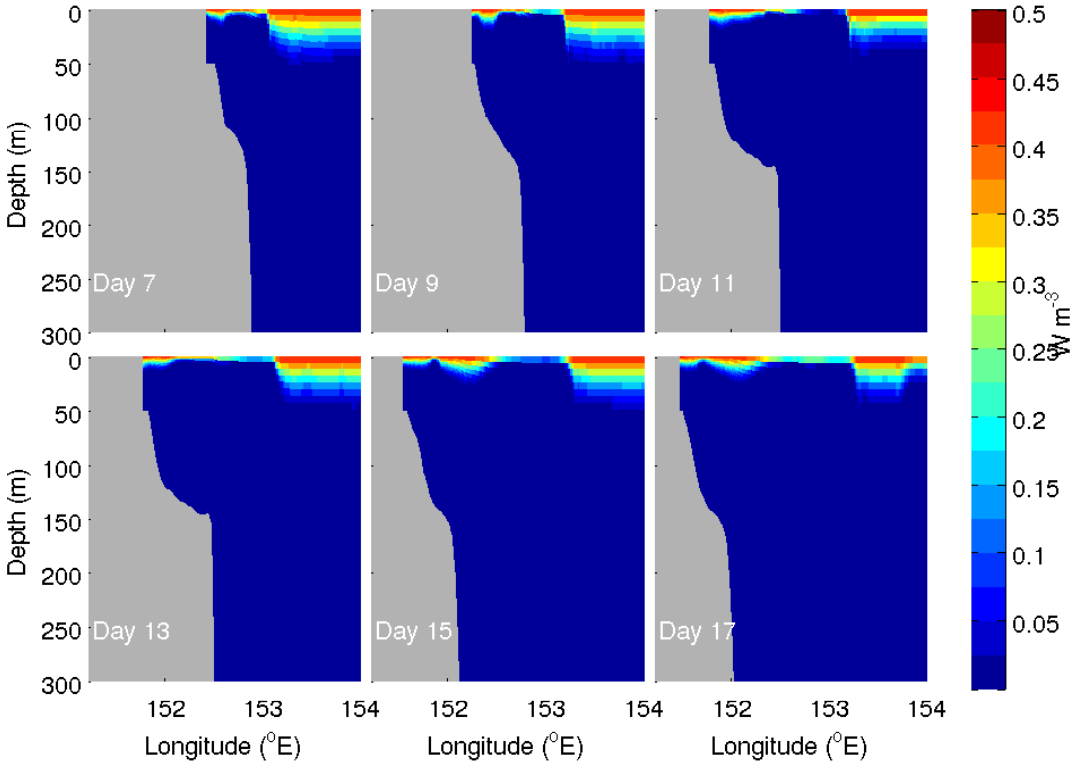

Figure 6.13: Vertical profile of photosynthetically available radiation (PAR) through the centre (as indicated by a * in Fig. 6.2) of the eddy for every second day between days 7 and 17. PAR was calculated using formula 5 from Fennel et al. (2006) and all parameters used are in Table 6.1.

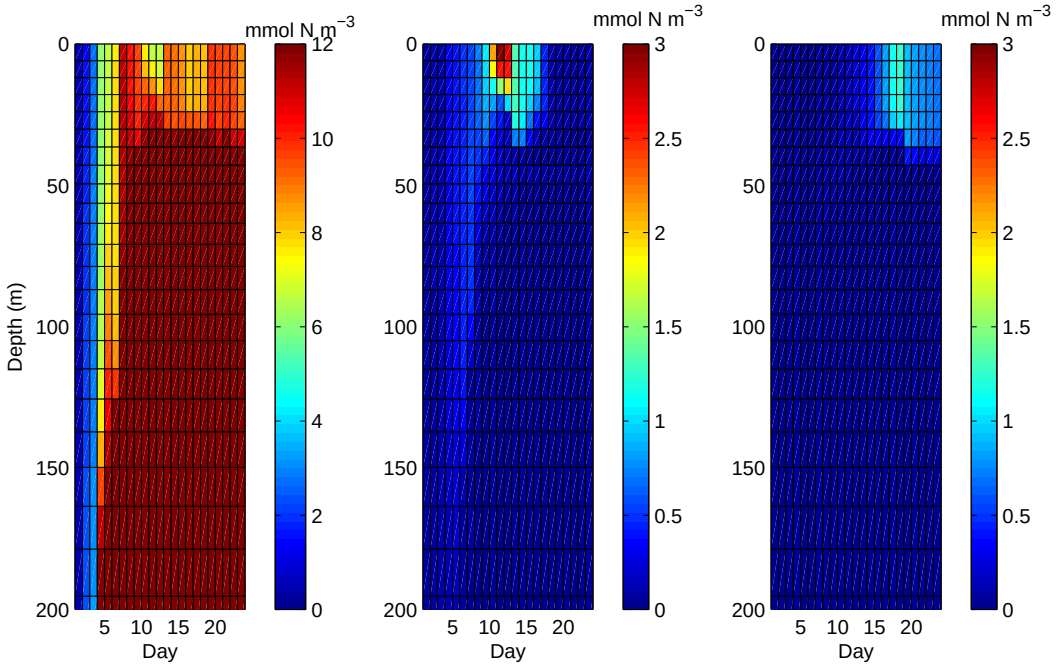

Figure 6.14: Evolution over time (x-axis) of nitrate (left), phytoplankton (middle) and zooplankton (right) concentrations (mmol N m^3) through the centre of the eddy.

6.4 Discussion

6.4.1 Temporal and spatial evolution

The temporal evolution of nitrate, phytoplankton and zooplankton follow a typical ocean ecosystem pattern after injection of a limiting factor such as nitrate into the system. In the centre of the eddy nitrate is upwelled, appearing in the surface waters (via mixing) by model day 8 (Fig. 6.14). A strong phytoplankton response can be seen from day 9 and a zooplankton response from day 13. This cycle is important in understanding why the phytoplankton die off from the centre of the eddy outwards. The pattern of phytoplankton biomass can be attributed to the stage in the lifecycle of the water bodies in the eddy.

Initially, the eddy is small but grows over time as it entrains coastal waters. The further from the centre of the eddy a body of water is, the less time it has been in the eddy. As such, the further from the eddy centre, the earlier the water body is in its lifecycle. At each radii out from the centre of the eddy (0 0.2^oE and 0.4^oE of the eddy have been chosen as examples in Fig. 6.15) the lifecycle (nitrogen peak followed by a phytoplankton peak and a zooplankton peak) is evident, albeit more delayed the further the water body is from the eddy centre. At the centre of the eddy, the peaks in nitrogen, phytoplankton and zooplankton occur on days 7, 11 and 18 respectively (Fig. 6.15). Further out from the eddy centre the peaks in nitrate are not so obvious. At 0.2^oE of the centre of the eddy, the peaks in phytoplankton and zooplankton occur on days 11 and 18 respectively. At 0.4^oE of the centre of the eddy, the peak in phytoplankton occurs on day 17. The peak in zooplankton does not occur as the simulation finishes before that time. The further out from the centre a water mass is, the less nutrients are available from upwelling in the eddy. As such, the peaks in nitrogen, phytoplankton and zooplankton become less with increasing radial distance from the eddy centre.

6.4.2 Subsurface chlorophyll maximum

In many parts of the ocean (including this study region) observations of chlorophyll can sometimes display a subsurface chlorophyll maximum. This vertical structure of chlorophyll is not reproduced in the model output presented here. Some fine-tuning of model parameters may assist in reproducing a subsurface chlorophyll maximum. In particular, detrital sinking and decay rates will

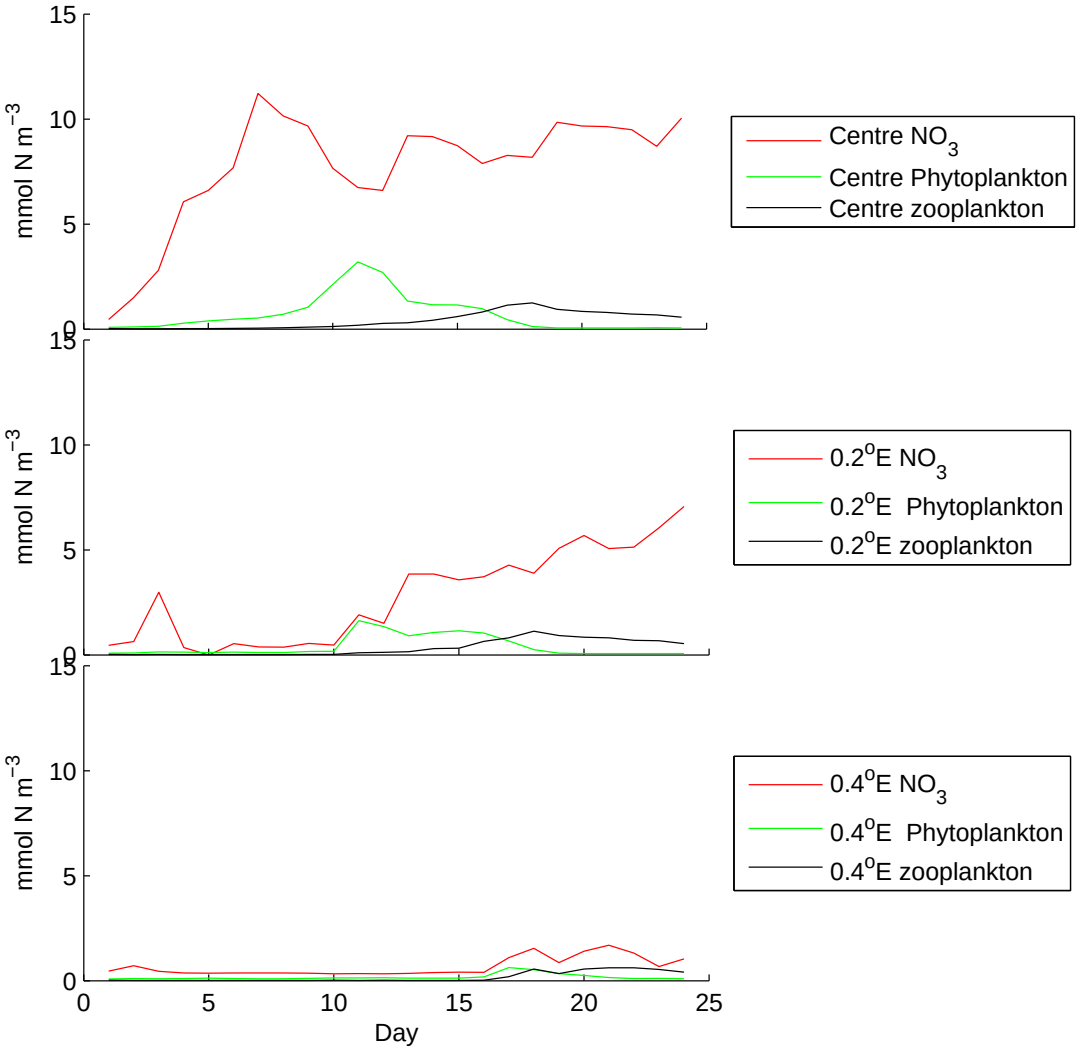

Figure 6.15: Evolution of sea surface nitrate (top), phytoplankton (middle) and zooplankton (bottom) in the centre of the eddy (red), 0.2^{o}E of the eddy centre (green) and 0.4^{o}E of the eddy centre (black).

change where nutrients are sitting within the water column. This will then alter where in the water column the phytoplankton will grow which will alter the vertical structure of chlorophyll.

6.5 Summary

A biological model was initialised within the high resolution configuration of ROMS. To assist in the interpretations of the biological reactions to the physical fields, a simulation was run to coincide with the realistic wind scenario's CCE (described in Chapter 4). Nitrate was upwelled onto the continental shelf and entrained into the eddy. Entrainment into the eddy enhanced biological growth in the continental shelf waters. The eddy grew as continental shelf waters were entrained into the eddy, adding extra rings throughout the simulation. This meant that the waters in the centre of the eddy had been in the eddy longer than the waters on the peripherals. As such, the phytoplankton bloom was at a later stage in the life cycle in the eddy centre as compared to the peripherals. These findings enhance the results of Chapter 5 by demonstrating that the CCE does enhance the biological production of entrained continental shelf waters.

Chapter 7

Summary and future work

The results presented here delve into some of the intricacies of the dynamics of eddies in the East Australian Current (EAC) region. The results help to answer questions regarding eddy formation, source waters and transfer of energy to eddies. In the past, modelling studies of the region have been of insufficient resolution, too idealised and reliant on data assimilation methods. This is the first modelling study to be able to address the dynamics of both warm-core eddies (WCEs) and cold-core eddies (CCEs) in the EAC bifurcation region. This chapter summarises the findings of the previous chapters, revisits the goals of this thesis and outlines potential for future work leading on from this thesis.

7.1 Summary

7.1.1 Chapter 2

In Chapter 2 the model and model configurations were presented. The Regional Ocean Modelling System (ROMS) was implemented and configured for the EAC separation region, located off southeast Australia. This grid was specifically designed to capture eddies in this region. The boundary conditions were specified along with the boundary nudging regime. The external sources of information fed into the model (for use in boundary and nudging conditions) were described.

7.1.2 Chapter 3

In Chapter 3 a case study of a WCE was performed for October 2008, coinciding with when the eddy was overwashed with EAC waters. Two distinct stages were identified: the first where the EAC encircled the eddy and the second where the EAC overwashed the eddy. The vorticity of the eddy was examined and it was shown that, during the EAC encircling stage, waters of cyclonic vorticity were shed from the eddy. A cyclonic barrier which was preventing the overwashing process was removed. The overwashing submerged the mixed layer of the original eddy, creating a two-layer system which formed a sub-surface maximum velocity at the interface of the two layers. It was found that the original eddy layer sunk 10-50 m. Overwashing occurred in the 8 days between the expulsion of cyclonic vorticity and the separation of the eddy from the EAC. A depth tracer which tracks horizontal movement, and a latitudinal tracer which tracks vertical

movement were introduced. These tracers can track movement of water parcels and reveal that original eddy waters sunk 20-90 m during the simulation. This sinking was confirmed by temperature and salinity profiles at the centre of the eddy.

7.1.3 Chapter 4

In Chapter 4 a case study of a CCE was performed for the period of time during its formation. A sensitivity analysis was also performed to ascertain which factors were important in the eddy formation. It was found that varying the wind forcing between northerly and southerly affected the density field and flow on the continental shelf. These conditions affected the location, size and isothermal uplift of the eddy. Surprisingly, the maximum uplift within the eddy occurred when there was downwelling winds due to a stronger northward flow on the continental shelf which drove greater velocity shear. Analysis of energy transformation showed the prevailing source of CCE eddy kinetic energy was from the EAC highlighting the importance of baroclinic and barotropic processes. The study also found that the curvature of the coastline and gradients in density from shelf to slope water were necessary for eddy formation.

7.1.4 Chapter 5

In Chapter 5 the CCE was investigated further. Lagrangian particle paths were seeded within the model to help investigate source waters into the eddy. The northward flow on the continental shelf and slope that was shown (in Chapter 4) to have relevance to the eddy's formation was also found to be important in

determining source waters into the eddy. When this northward flow was present waters entrained into the eddy came from north and far south of the eddy. When this northward flow was not present waters entrained into the eddy only come from north of the eddy. This affected the T and S properties of the eddy as, when the eddy didn't entrain particles from the south, it was missing distinct T and S signatures. The tilt of the eddy onto the continental shelf was also investigated. The tilt created a distinct upwelling/downwelling pattern within the eddy. The northward flow within the model on the continental shelf and slope was shown to be robust as it compared well with observations of continental shelf and slope velocities.

7.1.5 Chapter 6

In Chapter 6 the Fennel et al. (2006) biological model was tested for this configuration. The model was used to investigate the biological reaction of continental shelf waters after they were entrained off the shelf and into the cold-core eddy. It was found that entrainment into the eddy did enhance the biological production of the entrained waters. As they were entrained last, the waters of the outer rings of the eddy were at an earlier stage in the plankton bloom. As such, when the centre of the eddy was towards the end of the bloom, the outer edges of the eddy had a higher phytoplankton concentration.

7.2 Objectives

The objectives, as raised in Chapter 1, have been addressed as follows.

1. *To understand dynamics within an East Australian Current warm-core eddy, particularly when it is being overwashed by East Australian Current waters.*

   The dynamics within the WCE studied show some complex interactions with the EAC. Overwashing, a process where the EAC submerges the original eddy, is expected due to the density difference between the EAC and the eddy. A cyclonic barrier, however, can prevent overwashing. This cyclonic barrier also makes the eddy unstable as the density distribution is not at its lowest state of available potential energy and the eddy can expel water to the north. As soon as the cyclonic waters are expelled the EAC can wrap completely around the eddy and then overwash the eddy. Overwashing creates a two-layered system with a sub-surface maximum velocity at the interface of the EAC and the submerged WCE.

2. *To examine the dynamics within an East Australian Current cold-core eddy and suggest possible mechanisms for eddy formation.*

   A CCE forms on the boundary of the EAC and coastal waters. Eddies can lean across the continental shelf and then stand vertically. Temperature gradients, velocity shear and bathymetry all play a role in eddy formation. Both baroclinic and barotropic instabilities are involved in eddy formation. In the case study shown in this thesis, however, baroclinic instabilities play a larger role. A northward flow on the continental shelf and slope is

suspected to also contribute to eddy formation.

3. *To investigate the source waters for an East Australian Current cold-core eddy.*

   Waters can become entrained into CCEs from the continental shelf and slope from north and south of the eddy. When a northward flow is not present on the continental shelf and slope, water is not entrained from the south. Water from the continental slope is upwelled into the eddy. When a CCE leans onto the shelf there is also uplift in the south of the eddy which is counterbalanced by downwelling in the north.

4. *To test the Fennel et al. (2006) biological model for its suitability to perform studies on entrainment and upwelling into East Australian Current cold-core eddies.*

   The Fennel et al. (2006) biological model can be initialised within the EAC configuration of ROMS. The model can be used to investigate the biological reaction of waters after they are entrained into the eddy. Entrainment into the eddy enhances biological production.

7.3 Future work

The new configuration of the model developed for this study has the potential to address many more research areas than those presented in this thesis. In particular, the biological model presented in this thesis has potential for a wide variety of applications. Future work should include model validation through comparison to observations. It can then be used to add spatial and temporal data to a wide range of biological studies for the region. In addition to this, the Regional Ocean Modelling System (ROMS) has the capacity to model chemical interactions as well as the physical and biological ones addressed in this thesis.

Under climate change conditions the Tasman Sea is predicted to warm substantially and the EAC is expected to increase in velocity. As the results of Chapter 4 show, temperature gradients and the speed of the EAC affect the formation of CCEs. In light of these results, an interesting question that can be answered by the model is: *"How will CCE formation change under climate change conditions?"*. To answer this, multi-year simulations need to be performed using forcing from predicted future climatological conditions.

From this thesis, there are a couple of changes that can be made to field work strategies. Velocities (measured by ADCP) should be collected more often. These velocities can be used to determine if and how often the northward flow occurs. The results of this thesis show that water entrained into a cold-core eddy came from a wide range of latitudes. If drifters were placed on the continental shelf as a CCE forms then the source waters to an eddy can be known. The sampling strategy can then be made to target continental shelf waters that are entrained into the eddy, thus enabling collection of samples before and after

entrainment.

Bibliography

Baird, M., Suthers, I., Griffin, D., Hollings, B., Pattiaratchi, C., Everett, J., Roughan, M., Oubelkheir, K., Doblin, M., 2010. The effect of surface flooding on the physical-biogeochemical dynamics of a warm core eddy off southeast Australia. Deep Sea Research Part II: Topical Studies in Oceanography 58, 592–605.

Baird, M. E., Timko, P. G., Suthers, I. M., Middleton, J. H., 2006a. Coupled physical-biological modelling study of the East Australian Current with idealised wind forcing. Part I: Biological model intercomparison. J. Mar. Sys. 59, 249–270.

Baird, M. E., Timko, P. G., Suthers, I. M., Middleton, J. H., 2006b. Coupled physical-biological modelling study of the East Australian Current with idealised wind forcing: Part II. Biological dynamical analysis. Journal of Marine Systems 59, 271–291.

Bakun, A., 2006. Fronts and eddies as key structures in the habitat of marine fish larvae: opportunity, adaptive response and competitive advantage. Scientia Marina 70 (S2), 105–122.

Barkley, R., 1970. The Kuroshio Current. Sci. J 6, 54–60.

Bowen, M., Wilkin, J., Emery, W., 2005. Variability and forcing of the East Australian Current. Journal of geophysical research 110 (C3), C03019.

Brassington, G., Summons, N., Lumpkin, R., 2011. Observed and simulated Lagrangian and eddy characteristics of the East Australian Current and the Tasman Sea. Deep Sea Research Part II: Topical Studies in Oceanography 58, 559–573.

Budgell, W., 2005. Numerical simulation of ice-ocean variability in the Barents Sea region. Ocean Dynamics 55 (3-4), 370–387.

Capet, X., McWilliams, J., Molemaker, M., Shchepetkin, A., 2008. Mesoscale to submesoscale transition in the California Current system. Part II: Frontal processes. Journal of Physical Oceanography 38, 44–64.

Chapman, D., 1985. Numerical treatment of cross-shelf open boundaries in a barotropic coastal ocean model. Journal of Physical Oceanography 15 (8), 1060–1075.

Chapman, R., Nof, D., 1988. The sinking of warm-core rings. Journal of Physical Oceanography 18, 565–583.

Chelton, D. B., Schlax, M. G., Samelson, R. M., 2011. Global observations of nonlinear mesoscale eddies. Progress In Oceanography 91 (2), 167 – 216.

Church, J., 1987. East Australian Current adjacent to the Great Barrier Reef. Marine and Freshwater Research 38 (6), 671–683.

Colas, F., Capet, X., McWilliams, J., Shchepetkin, A., 2008. 1997-1998 El Niño off Peru: A numerical study. Progress in Oceanography 79 (2-4), 138–155.

Condie, S., 1995. Interactions between western boundary currents and shelf waters: A mechanism for coastal upwelling. Journal of Geophysical Research-Oceans 100 (C12).

Cresswell, G., 1983. Physical evolution of Tasman Sea eddy J. Marine and Freshwater Research 34, 495–513.

Cresswell, G. R., 1982. The Coalescence of Two East Australian Current Warm-Core Eddies. Science 215 (4529), 161–164.

Csanady, G., 1971. On the equilibrium shape of the thermocline in a shore zone. Journal of Physical Oceanography 1 (4), 263–270.

Csanady, G., 1977. Intermittent fullupwelling in Lake Ontario. Journal of Geophysical Research 82 (3), 397–419.

Csanady, G., 1979. The birth and death of a warm core ring. Journal of Geophysical Research: Oceans (1978–2012) 84 (C2), 777–780.

Deng, X., Griffin, D., Ridgway, K., Church, J., Featherstone, W., White, N., Cahill, M., 2010. Satellite altimetry for geodetic, oceanographic and climate studies in the Australian region.

Di Lorenzo, E., Schneider, N., Cobb, K., Franks, P., Chhak, K., Miller, A., Mcwilliams, J., Bograd, S., Arango, H., Curchitser, E., et al., 2008. North Pacific Gyre Oscillation links ocean climate and ecosystem change. Geophysical Research Letters 35, L08607.

Didden, N., Schott, F., Nov 15 1993. Eddies in the North Brazil Current retroflection region observed by GEOSAT altimetry. Journal of Geophysical Research-Oceans 98 (C11), 20121–20131.

Dietze, H., Matear, R., Moore, T., 2009. Nutrient supply to anticyclonic mesoscale eddies off western Australia estimated with artificial tracers released in a circulation model. Deep-Sea Research Part I 56, 1440–1448.

Dinniman, M., Klinck, J., Smith, W., et al., 2003. Cross-shelf exchange in a model of the Ross Sea circulation and biogeochemistry. Deep Sea Research Part II: Topical Studies in Oceanography 50 (22-26), 3103–3120.

Duncan, C., 1968. An eddy in the subtropical convergence southwest of South Africa. Journal of Geophysical Research 73 (2), 531–534.

Everett, J., Baird, M., Oke, P., Suthers, I., 2012. An avenue of eddies: Quantifying the biophysical properties of mesoscale eddies in the Tasman Sea. Geophysical Research Letters 39 (16), L16608.

Everett, J., Baird, M., Suthers, I., 2011. Three-dimensional structure of a swarm of the salp Thalia democratica within a cold-core eddy off southeast Australia. Journal of Geophysical Research 116, C12046.

Fairall, C., Bradley, E., Rogers, D., Edson, J., Young, G., et al., 1996. Bulk parameterization of air-sea fluxes for tropical ocean-global atmosphere coupled-ocean atmosphere response experiment. J. Geophys. Res 101 (C2), 3747–3764.

Fasham, M., Ducklow, H., McKelvie, S., 1990. A nitrogen-based model of plank-

ton dynamics in the oceanic mixed layer. Journal of Marine Research 48 (3), 591–639.

Fennel, K., Wilkin, J., Levin, J., Moisan, J., O'Reilly, J., Haidvogel, D., 2006. Nitrogen cycling in the Middle Atlantic Bight: Results from a three-dimensional model and implications for the North Atlantic nitrogen budget. Global Biogeochemical Cycles 20 (3), GB3007.

Fennel, K., Wilkin, J., Previdi, M., Najjar, R., 2008. Denitrification effects on air-sea CO2 flux in the coastal ocean: Simulations for the northwest North Atlantic. Geophys. Res. Lett 35, L24608.

Flather, R., 1976. A tidal model of the northwest European continental shelf. Mem. Soc. R. Sci. Liege 6 (10), 141–164.

Flierl, G., Mied, R., 1985. Frictionally induced circulations and spin down of a warm-core ring. Journal of Geophysical Research 90 (C5), 8917–8927.

Fuglister, F., Worthington, L., 1951. Some Results of a Multiple Ship Survey of the Gulf Stream. Tellus 3 (1), 1–14.

Godfrey, J., Cresswell, G., Boland, F., 1980a. Observations of low Richardson numbers and undercurrents near a front in the East Australian Current. Journal of Physical Oceanography 10, 301–307.

Godfrey, J., Cresswell, G., Golding, T., Pearce, A., Boyd, R., 1980b. The separation of the east Australian current. Journal of Physical Oceanography 10 (3), 430–440.

Hamon, B., 1965. The East Australian Current, 1960-1964. In: Deep Sea Research and Oceanographic Abstracts. Vol. 12. Elsevier, pp. 899–921.

Hayward, T., Mantyla, A., 1990. Physical, chemical and biological structure of a coastal eddy near Cape Mendocino. Journal of Marine Research 48, 825–850.

Henschke, N., Everett, J., Baird, M., Taylor, M., Suthers, I., 2011. Distribution of life history stages of the salp Thalia democratica in shelf waters during a spring bloom. Mar Ecol Prog Ser 430, 49–62.

Hitchcock, G. L., Langdon, C., Smayda, T., 1985. Seasonal variations in the phytoplankton biomass and productivity of a warm-core Gulf Stream ring. Deep Sea Research Part A. Oceanographic Research Papers 32 (11), 1287 – 1300.

Ikeda, M., Johannessen, J., Lygre, K., Sandven, S., 1989. A process study of mesoscale meanders and eddies in the Norvegian coastal current. Journal of physical oceanography 19, 20–35.

Jeffrey, S., Hallegraeff, G., 1987. Phytoplankton pigments, species and light climate in a complex warm-core eddy of the East Australian Current. Deep Sea Research Part A. Oceanographic Research Papers 34 (5-6), 649 – 673.

Jia, F., Wu, L., Qiu, B., 2011. Seasonal Modulation of Eddy Kinetic Energy and Its Formation Mechanism in the Southeast Indian Ocean. Journal of Physical Oceanography 41, 657–665.

Kahru, M., Mitchell, B., Gille, S., Hewes, C., Holm-Hansen, O., 2007. Eddies en-

hance biological production in the Weddell-Scotia Confluence of the Southern Ocean. Geophys. Res. Lett 34, L14603.

Kalnay, E., Kanamitsu, M., Kistler, R., Collins, W., Deaven, D., Gandin, L., Iredell, M., Saha, S., White, G., Woollen, J., et al., 1996. The NCEP/NCAR 40-Year Reanalysis Project. Bulletin of the American Meteorological Society 77 (3), 437–471.

Kasai, A., Kimura, S., Nakata, H., Okazaki, Y., 2002. Entrainment of coastal water into a frontal eddy of the Kuroshio and its biological significance. Journal of Marine Systems 37 (1-3), 185 – 198.

Kimura, S., Kasai, A., Nakata, H., Sugimoto, T., Simpson, J., Cheok, J., 1997. Biological productivity of meso-scale eddies caused by frontal disturbances in the Kuroshio. ICES Journal of Marine Science 54 (2), 179–192.

Lee, T., Yoder, J., Atkinson, L., 1991. Gulf Stream Frontal Eddy Influence on Productivity. Journal of Geophysical Research 96 (C12), 22–191.

Lima, I., Olson, D., Doney, S., 2002. Biological response to frontal dynamics and mesoscale variability in oligotrophic environments: Biological production and community structure. J. Geophys. Res 107 (3111).

Logerwell, E., Smith, P., 2001. Mesoscale eddies and survival of late stage Pacific sardine (Sardinops sagax) larvae. Fisheries Oceanography 10 (1), 13–25.

Lutjeharms, J., Penven, P., Roy, C., 2003. Modelling the shear edge eddies of the southern Agulhas Current. Continental Shelf Research 23 (11-13), 1099–1115.

Macdonald, H., Baird, M., Middleton, J., 2009. Effect of wind on continental shelf carbon fluxes off southeast Australia: A numerical model. J. Geophys. Res. 114, C05016.

Marchesiello, P., McWilliams, J., Shchepetkin, A., 2003. Equilibrium structure and dynamics of the California Current System. Journal of Physical Oceanography 33 (4), 753–783.

Marchesiello, P., Middleton, J., 2000. Modeling the East Australian Current in the Western Tasman Sea. Journal of Physical Oceanography 30, 2956–2971.

Mata, M., Wijffels, S., Church, J., Tomczak, M., 2006. Eddy shedding and energy conversions in the East Australian Current. Journal of Geophysical Research-Oceans 111.

McGillicuddy, D., Robinson, A., 1997. Eddy-induced nutrient supply and new production in the Sargasso Sea. Deep Sea Research Part I: Oceanographic Research Papers 44 (8), 1427 – 1450.

McGillicuddy, D. J., Anderson, L. A., Bates, N. R., Bibby, T., Buesseler, K. O., Carlson, C. A., Davis, C. S., Ewart, C., Falkowski, P. G., Goldthwait, S. A., Hansell, D. A., Jenkins, W. J., Johnson, R., Kosnyrev, V. K., Ledwell, J. R., Li, Q. P., Siegel, D. A., Steinberg, D. K., 2007. Eddy/Wind Interactions Stimulate Extraordinary Mid-Ocean Plankton Blooms. Science 316 (5827), 1021–1026.

Mellor, G., Ezer, T., Oey, L., 1994. The pressure gradient conundrum of sigma coordinate ocean models. Journal of Atmospheric and Oceanic Technology 11, 1126–1134.

Mellor, G., Yamada, T., 1982. Development of a turbulence closure model for geophysical fluid problems. Reviews of geophysics and space physics 20 (4), 851–875.

Middleton, J. F., 1988. Long shelf waves generated by a coastal flux. Journal of Geophysical Research 93 (C9), 10724–10.

Middleton, J. F., Leth, O. K., 2004. Wind-forced setup of upwelling, geographical origins, and numerical models: The role of bottom drag. Journal of Geophysical Research: Oceans (1978–2012) 109 (C12).

Minobe, S., Kuwano-Yoshida, A., Komori, N., Xie, S., Small, R., 2008. Influence of the Gulf Stream on the troposphere. Nature 452 (7184), 206–209.

Moore, A., Arango, H., Di Lorenzo, E., Miller, A., Cornuelle, B., 2009. An adjoint sensitivity analysis of the Southern California Current circulation and ecosystem. Journal of Physical Oceanography 39 (3), 702–720.

Nelson, D., McCarthy, J., Joyce, T., Ducklow, H., 1989. Enhanced near-surface nutrient availability and new production resulting from the frictional decay of a Gulf Stream warm-core ring. Deep Sea Research Part A. Oceanographic Research Papers 36 (5), 705–714.

Nilsson, C., Cresswell, G., 1980. The formation and evolution of East Australian current warm-core eddies. Progress In Oceanography 9 (3), 133 – 183.

Nof, D., Dewar, W., 1994. Alignment of lenses: laboratory and numerical experiments. Deep Sea Research Part I: Oceanographic Research Papers 41 (8), 1207–1229.

Oke, P., Griffin, D., 2010. The cold-core eddy and strong upwelling off the coast of New South Wales in early 2007. Deep Sea Research Part II: Topical Studies in Oceanography.

Oort, A., 1964. Computations of the eddy heat and density transports across the Gulf Stream. Tellus 16 (1), 55–63.

Parker, C. E., 1971. Gulf stream rings in the Sargasso Sea. Deep Sea Research and Oceanographic Abstracts 18 (10), 981 – 993.

Pearce, A., 1977. Some features of the upper 500 m of the Agulhas Current. Journal of Marine Research 35, 731–753.

Peliz, A., Dubert, J., Haidvogel, D., 2003. Subinertial response of a density-driven eastern boundary poleward current to wind forcing. Journal of Physical Oceanography 33 (8), 1633–1650.

Ridgway, K., Coleman, R., Bailey, R., Sutton, P., 2008. Decadal variability of East Australian Current transport inferred from repeated high-density XBT transects, a CTD survey and satellite altimetry. Journal of Geophysical Research 113 (C08039).

Ridgway, K., Dunn, J., 2003. Mesoscale structure of the mean East Australian Current System and its relationship with topography. Progress in Oceanography 56 (2), 189–222.

Ridgway, K., Dunn, J., Wilkin, J., 2002. Ocean interpolation by four-dimensional weighted least squares - Application to the waters around Australasia. Journal of atmospheric and oceanic technology 19 (9), 1357–1375.

Ridgway, K., Godfrey, J., 1997. Seasonal cycle of the East Australian Current. Journal of Geophysical Research-Oceans 102 (C10).

Rossby, T., 1987. On the energetics of the Gulf Stream at 73W. Journal of Marine Research 45 (1), 59–82.

Roughan, M., Macdonald, H., Baird, M., Glasby, T., 2011. Modelling coastal connectivity in a Western Boundary Current: Seasonal and inter-annual variability. Deep Sea Research Part II: Topical Studies in Oceanography 58 (5), 628–644.

Roughan, M., Middleton, J., 2002. A comparison of observed upwelling mechanisms off the east coast of Australia. Continental Shelf Research 22 (17), 2551–2572.

Roughan, M., Morris, B., sept. 2011. Using high-resolution ocean timeseries data to give context to long term hydrographic sampling off Port Hacking, NSW, Australia. In: OCEANS 2011. pp. 1 –4.

Roughan, M., Oke, P., Middleton, J., 2003. A Modeling Study of the Climatological Current Field and the Trajectories of Upwelled Particles in the East Australian Current. Journal of Physical Oceanography 33 (12), 2551–2564.

Rubio, A., Barnier, B., Jordà, G., Espino, M., Marsaleix, P., 2009. Origin and dynamics of mesoscale eddies in the Catalan Sea (NW Mediterranean): Insight from a numerical model study. Journal of Geophysical Research 114 (C6), C06009.

Shchepetkin, A., McWilliams, J., 2003. A method for computing horizontal pressure-gradient force in an oceanic model with a nonaligned vertical coordinate. J. Geophys. Res 108 (C3), 3090.

Shchepetkin, A., McWilliams, J., 2005. The regional oceanic modeling system (ROMS): a split-explicit, free-surface, topography-following-coordinate oceanic model. Ocean Modelling 9 (4), 347–404.

Sikiric, M., Janekovic, I., Kuzmic, M., 2009. A new approach to bathymetry smoothing in sigma-coordinate ocean models. Ocean Modelling 29 (2), 128–136.

Sponaugle, S., Lee, T., Kourafalou, V., Pinkard, D., 2005. Florida Current frontal eddies and the settlement of coral reef fishes. Limnology and Oceanography, 1033–1048.

Suthers, I., Everett, J., Roughan, M., Young, J., Oke, P., Condie, S., Hartog, J., Baird, M., Hassler, C., Brassington, G., Byrne, M., N.J., H., Malcolm, H., 2011. The strengthening East Australian Current, its eddies and biological effects-an introduction and overview. Deep Sea Research Part II: Topical Studies in Oceanography 58, 538–546.

Tilburg, C., Hurlburt, H., O'Brien, J., Shriver, J., 2001. The dynamics of the East Australian current system: the Tasman front, the East Auckland current, and the East Cape current. Journal of Physical Oceanography 31 (10), 2917–2943.

Tranter, D., Carpenter, D., Leech, G., 1986. The coastal enrichment effect of

the East Australian Current eddy field. Deep-Sea Research. 1986. 33 (11/12), 1705–1728.

Tranter, D., Leech, G., Vaudrey, D., 1982. Biological significance of surface flooding in warm-core ocean eddies. Nature 297, 572–574.

Tranter, D., Parker, R., Cresswell, G., 1980. Are warm-core eddies unproductive? Nature 284, 540–542.

Wilkin, J., Zhang, W., 2007. Modes of mesoscale sea surface height and temperature variability in the East Australian Current. Journal of Geophysical Research 112 (C01013).

Yang, Y., Liu, C.-T., Hu, J.-H., Koga, M., 1999. Taiwan Current (Kuroshio) and Impinging Eddies. Journal of Oceanography 55, 609–617.

Yaochu, Y., Jilan, S., 1988. The calculation of Kuroshio current structure in the East China Sea–early summer 1986. Progress In Oceanography 21 (3-4), 343 – 361.

Zhang, H., Reynolds, R., Bates, J., 2006. Blended and Gridded High Resolution Global Sea Surface Wind Speed and Climatology from Multiple Satellites: 1987- Present. EOS, Transactions, American Geophysical Union 87 (36).